I. CALCULATION OF VIBRATIONAL TRANSITION MOMENTS

II. PHOTOCHEMISTRY OF VIBRATIONALLY EXCITED HYDROGEN IODIDE

III. PHOTOCHEMISTRY OF IODINE MONOCHLORIDE IN HYDROGEN

Thesis by

Robert Henry Reiner

In Partial Fulfillment of the Requirements

For the Degree of

Doctor of Philosophy

California Institute of Technology

Pasadena, California

1977

(Submitted April 13, 1977)

To my parents

ACKNOWLEDGMENTS

First, I would like to thank my research advisor, Professor Aron Kuppermann for his support during the past five years. Several of the projects in this thesis would never have been completed without his advice and encouragement. I also thank him for allowing me considerable freedom in my research and for giving me the confidence to work independently.

Second, I would like to thank Professors Jack Beauchamp, Bill Goddard, Vince McKoy, Wilse Robinson and Ahmed Zewail for their interest and help in my research and career.

Third, I would like to acknowledge the friendship and professional interaction of Jackie Berg, Jon Burke, John Dwyer, Bob "Fats" Frueholz, Tom Orlowski, Ron Rianda, George Schatz, Jeff Sell, Kosuke Shobatake and Tom Slankas.

Fourth, I thank Adria McMillan for the outstanding job she has done as the Kuppermann group secretary.

Finally, I thank my parents, Mary and Bob, to whom this thesis is dedicated, for their many years of sacrifice on my behalf and for their patience awaiting my employment.

ABSTRACT

The text of this thesis is divided into three sections.

In Part I, semi-empirical calculations of vibrational transition moments in general and hydrogen halide transition moments in particular are investigated. Semi-empirical transition moments, calculated using traditional approximations for the electric dipole operator, M(R), are compared with the exact vibrational transition moments for two hypothetical molecules in paper 1. The comparisons indicate that applying boundary conditions to an approximate M(R) does not significantly improve the transition moments predicted by that M(R). In paper 2, the same hypothetical molecules are used to evaluate a new method of obtaining M(R) from spectroscopic data, using each rovibrational moment in the vibrational bands rather than just the band centers. This method allows one to obtain an additional term in the Taylor series expansion of M(R), which produces corresponding improvement in the predicted vibrational transition moments. This new method is used on the experimental results available for HI and HF in papers 3 and 4, respectively. Here the rovibrational transition moments are also used to verify and determine the signs of measured transition moments.

The reaction and vibrational relaxation of hydrogen iodide are discussed in Part II of this thesis (paper 5). Thermal and photochemical decomposition studies performed on HI yield the following results: (1) A small first-order component in the dark (thermal) reaction was detected in addition to the well-known second-order component. (2) The activation energy of the second-order reaction component between 660 and

710 K is 52.9 ± 2.8 kcal/mole as compared with the 44 kcal/mole previously reported. (3) While the rate of the HI decomposition was enhanced in the photochemical experiments, a kinetic analysis indicated that this enhancement was due to thermal heating rather than by the reaction of vibrationally excited HI. (4) Theoretical estimates of vibrational reaction and relaxation rates were made suggesting experimental conditions which could lead to observation of vibrational enhancement of this reaction.

The photochemistry of iodine monochloride in hydrogen is the subject of Part III. In paper 6, the quantum yield of HCl formation in mixtures of ICl and H_2 is remeasured. The results indicate that while earlier conclusions are qualitatively correct, the secondary reactions in the ICl-H_2 system are more complicated than previously envisioned. The reaction ratio of ICl to H_2 with Cl at 298.05 K is 1133 ± 69. This implies that the reported rate constant for the reaction: Cl + ICl → Cl_2 + I, determined by the photolysis of pure ICl is several orders of magnitude too small.

TABLE OF CONTENTS

PROPOSITIONS

INTRODUCTION

INTRODUCTION

The six papers in this thesis are the result of a five year investigation into the reaction of vibrationally excited molecules. Our initial purpose was to investigate the effect of vibrational energy on the reaction:

$$2HI \rightarrow H_2 + 2I \quad . \qquad (A)$$

Experimental and theoretical evidence led us to suspect that vibrational energy was very important in reaction (A) and that a significant increase in the reaction rate would occur as vibrational energy was supplied to hydrogen iodide.

The feasibility of observing (A) in the gas phase is dependent on our ability to produce a significant steady state population of vibrationally excited reactant $HI^{\dagger}(v)$. The population of $HI^{\dagger}(v)$ depends not only on experimental parameters such as light intensity and gas pressure, but also on molecular properties of HI such as the extinction coefficients of the vibrational transitions and the vibrational relaxation rate constants. Unfortunately, most of the properties of HI crucial to the success or failure of this experiment have not been investigated.

The most important of these properties is the extinction coefficient or strength of the vibrational transions. The strength of a vibrational transition is proportional to the square of the vibration transition moment, a quantity which in principle can be obtained from

ab initio calculations. In practice, however, ab initio calculations of transition moments are generally in poor agreement with available experimental results. Failure of ab initio calculations to yield reasonable vibrational transition moments has led previous investigators to use semi-empirical methods.

Initially we intended to use the standard semi-empirical procedure (fitting a Taylor series expansion of the dipole operator to measured transition moments) to estimate the desired vibrational transition moments of HI and then proceed with our feasibility study of reaction (A). However, we soon became aware of the limitations in previously used semi-empirical procedures for estimating transition moments. Because of the great importance of these moments in many areas of chemical dynamics and spectroscopy, we decided to detour from our investigation of reaction (A), to study in great detail the methodology of these semi-empirical calculations.

We examine semi-empirical procedures in papers 1-4. In paper 1, the self-consistency of procedures proposed by various authors is investigated using two "hypothetical" molecules. These "hypothetical" molecules have a known dipole operator which is used to generate experimental transition moments. We then use these generated transition moments to test the predictions of various order semi-empirical approximations. In paper 2, we propose a new semi-empirical method and test its self-consistency using the same two "hypothetical" molecules. In paper 3, this new semi-empirical procedure is applied to available

spectroscopic data on HI to calculate the vibrational transition moments of HI which were needed for our feasibility study of reaction (A). The vibrational transition moments of HF are similarly obtained as discussed in paper 4.

We finally return to the problem of vibrational excitation of reaction (A) in paper 5. In this paper, preliminary experiments measuring the importance of vibrational energy on reaction (A) are discussed. In these experiments a kinetic scheme, permitting the separation of the effects of thermal heating and vibrational enhancement in gas phase experiments, was developed and tested. Discrepancies in previous kinetic treatments of reaction (A) were also found and corrected. Unfortunately however, these experiments did not yield any information concerning vibration excitation on reaction (A). A feasibility study, completed in this paper, shows that while vibrational energy may be very important in (A), direct experimental observation of the effect would be quite difficult.

Our failure to observe vibrational excitation in reaction (A) led us to search for other possible reactions. One promising reaction is:

$$ICl + H_2 \rightarrow HCl + HI \quad . \qquad (B)$$

While investigating reaction (B) we discovered discrepancies in previously reported rate constants of secondary reactions in the $ICl - H_2$ system of between three and four orders of magnitude. In paper 6 we reinvestigated the photolysis of ICl in H_2 in order to correct these errors.

1. AN ACCURATE TEST OF ELECTRIC DIPOLE OPERATOR APPROXIMATIONS

An accurate test of electric dipole operator approximations*

Robert H. Reiner and Aron Kuppermann

Arthur Amos Noyes Laboratory of Chemical Physics,†
California Institute of Technology, Pasadena, California 91125

(Received)

ABSTRACT

Semi-empirical transition moments, calculated using approximations for M(R), the electric dipole operator, are compared with the exact moments for two hypothetical molecules. The comparisons indicate that (1) neither a Padé polynomial nor a modified wavefunction expansion predicts significantly better transition moments than a Taylor series approximation of the same order and (2) fewer parameters for M(R) are needed in an "HI-type" molecule than in an "HF-type" molecule.

---

* This work was supported in part by a contract (EY-76-S-03-0767) from the U. S. Energy Research and Development Administration. Report Code: CALT-767P4-144.

† Contribution No. 5390

1. INTRODUCTION

Various authors[1,2] have shown that the lack of information concerning the variation of the electric dipole operator, M(R), with internuclear distance R is the principal restriction to the calculation of accurate transition moments. Although M(R) is explicitly defined (under the conditions of validity of the Born-Oppenheimer approximation--see Sec. 2), ab initio calculations of M(R) do not yet predict accurate transition moments.[1,3] To date, only semi-empirical procedures have been used to estimate vibrational matrix elements of M(R) not measured experimentally.

These semi-empirical methods (Taylor series polynomial, Padé polynomial, and modified wavefunction expansion) have one important feature in common: an assumed form of M(R), fitted to measured transition moments, is used to calculate the remaining transition moments. Since there are usually less than four or five measured transition moments for any molecule, there has been little or no analysis of what Meredith and Smith[1] call the "approximation error"--"error introduced into the calculated matrix elements because the chosen dipole moment approximation does not correctly represent the real moment of the molecule."

In order to estimate the magnitude of the approximation error and to determine the relative benefit of using one assumed form of M(R) over another form, we have examined the behavior of M(R) and its vibrational matrix elements in HF and HI molecules having "hypothetical" M(R). The hypothetical M(R) were constructed to described, at least qualitatively, the expected behavior of the real (but unknown) M(R) for HF and HI.

For each molecule, transition moments between the ground vibrational state and upper vibrational states (vibrational quantum number $v \leq 9$) were computed using these constructed M(R). The lower transition moments (between three and five moments--depending on the order of the approximation used) were used to construct Taylor series,[1] Padé polynomial,[2] and modified wavefunction approximations to M(R) (see Sec. 4). The matrix elements of the approximations to M(R) were then compared with the transition moments of the original, hypothetical M(R). From these comparisons, we were able to assess the value of each approximation.

In the next section, we review the theory of semi-empirical transition moment calculations. The construction of hypothetical M(R) for HF and HI is discussed in Sec. 3, and the computational procedure used to obtain the transition moments is explained in Sec. 4. In Sec. 5, the transition moments computed from the exact hypothetical M(R) and various approximations to it are presented. The implications of these results to semi-empirical calculations are discussed in Sec. 6.

2. THEORY

In the framework of the electric dipole approximation, the strength, $S_{vJM}^{v'J'M'}$, of a transition from vibrotational state vJM to v'J'M' of a diatomic molecule in a $^1\Sigma$ electronic state is related to the transition dipole moment vector $\underset{\sim}{\mathcal{I}}_{vJM}^{v'J'M'}$ defined by

$$\underset{\sim}{\mathcal{I}}_{vJM}^{v'J'M'} \equiv \langle vJM | \underset{\sim}{\mu} | v'J'M' \rangle \tag{1}$$

$$= \int \Psi_{vJM}^{*}(\underset{\sim}{R}, \underset{\sim}{r})\, \underset{\sim}{\mu}\, (\underset{\sim}{R}, \underset{\sim}{r})\, \Psi_{v'J'M'}(\underset{\sim}{R}, \underset{\sim}{r}) d^3R d^3r. \tag{2}$$

In this expression, $\underset{\sim}{R}$ and $\underset{\sim}{r}$ refer to the sets of spin and center of mass space coordinates of the molecular nuclei and electrons, respectively, Ψ are the total electronic nuclear wavefunctions, and $\underset{\sim}{\mu}$ is the total electronic dipole moment operator (including electrons and nuclei).[4] For light polarized in the x direction and propagating in the z direction, for example, M and M' represent the projection of initial and final rotational angular momenta on the light propagation direction and $S_{vJM}^{v'J'M'}$ is proportional to the square of the absolute value of the x component of $\underset{\sim}{\mathcal{I}}_{vJM}^{v'J'M'}$.[5] For unpolarized light, propagating in the z direction, $S_{vJM}^{v'J'M'}$ is proportional to the sum of the squares of the absolute values of the x and y components of $\underset{\sim}{\mathcal{I}}_{vJM}^{v'J'M'}$. The constant of proportionality depends on the radiation density and the frequency of the transition.[6] The strength $S_{vJ}^{v'J'}$ of a given rotational line is obtained by summing $S_{vJM}^{v'J'M'}$ over all M' and averaging it over all M. The total band strength, $S_{v}^{v'}$ is defined as the sum of the strengths of all rotational components of the band.

Under conditions of validity of the Born-Oppenheimer approximation,[1] the determining factor which must be calculated in order to

obtain $S_v^{v'}$ is the vibrotational transition dipole moment[4]

$$M_v^{v'} \equiv \langle v, J | M(R) | v'J' \rangle \tag{3}$$

$$= \int \psi^*_{vJ}(R) M(R) \psi_{v'J'}(R) dR \quad , \tag{4}$$

where the ψ are the vibrotational wavefunctions which satisfy the radial Schrödinger equation

$$\frac{-\hbar^2}{2m} \frac{d^2\psi_{vJ}}{dR^2} + \left[V(R) + \frac{\hbar^2 J(J+1)}{2mR^2} \right] \psi_{vJ} = E_{vJ} \psi_{vJ} \tag{5}$$

and M(R) is the magnitude of the dipole moment vector[7] defined by

$$\underset{\sim}{M}(R) = \int \psi^*_{e\ell}(\underset{\sim}{R}, \underset{\sim}{r}) \underset{\sim}{\mu}(\underset{\sim}{R}, \underset{\sim}{r}) \psi_{e\ell}(\underset{\sim}{R}, \underset{\sim}{r}) d\underset{\sim}{r} \quad , \tag{6}$$

where $\psi_{e\ell}$ is the electronic wavefunction of the $^1\Sigma$ state being considered. Therefore, knowledge of M(R) and the vibrational wavefunctions $\psi_{vJ}(R)$ suffice to evaluate $S_{vJ}^{v'J'}$.

Evaluation of M(R) from first principles is in general a very difficult task, since it requires a detailed knowledge of the electronic wavefunctions as a function of internuclear distance. For this reason, one usually assumes a form of the functional dependence of M on R together with ψ_{vJ} obtained from numerical integration of Eq. (5) in order to calculate the band strengths.

Rather than compute wavefunctions and vibrotational transition moments for each rotational state in the vibrational band, we assume that in the centrifugal potential term in Eq. (5), R can be replaced by its equilibrium value for J = 0. The corresponding $\psi_{vJ}(R)$ is then essentially independent of J and the total nuclear energy becomes the sum of vibrational and rotational energies with no vibrational rotational coupling.

This simplification is a very good approximation. Herman et al.[8] have shown that it introduces into the J^{th} rotational transition moment a relative error of order $J \cdot B_e/\omega_e$, where B_e is the rotational constant at equilibrium nuclear separation, and ω_e is the vibrational constant at equilibrium position. For HI, $B_e/\omega_e \approx 0.003$. Calculations we performed on the first three vibrational bands show that this simplification produces less than 2 % error in the HI band strengths. Since this is much less than the error produced by extrapolation of M(R) to transitions of higher Δv, this simplification is entirely justified.

Within this approximation, computation of transition moments becomes a straightforward problem of determining $J = 0$ eigenfunctions of the potential V(R), which are then used in Eq. (3) to evaluate $\langle v|M(R)|v'\rangle$ for a particular choice of M(R).

3. CONSTRUCTION OF M(R)

The hypothetical M(R) constructed for HF was essentially that reported from the ab initio calculations of Lie.[3] These values for M(R) with the additional values, $M(0) = 0$ and $M(\infty) = 0$, were connected using a cubic spline procedure.[9] The resulting M(R) is shown in curve A of Fig. 1.

The M(R) used for HI was chosen in a more arbitrary manner since no ab initio calculations were available for this molecule. M(R) was chosen to have a physically reasonable shape given by

$$M(R) = A\, R^B \exp(-C\,R) \ , \tag{7}$$

where parameters A, B, and $C > 0$. Three additional constraints on A, B, and C were: (1) M(R) was decreasing for $R > 1.9$ a.u.; (2) $M(R) = 0$ for $R \geq 8.5$ a.u. [see Ref. 2, Eq.(12)]; and (3) the permanent dipole moment of HI, $M_0^0 = 0.164$ a.u.,

$$M_0^0 \equiv \langle 0 | M(R) | 0 \rangle \ . \tag{8}$$

With these additional constraints, the constructed M(R) qualitatively mimics the behavior of the real M(R) for HI.[10] The values of A, B, and C used in Eq.(7) are 0.4172, 1.1740, and 0.7336, respectively (all dimensions are in atomic units). This constructed M(R) is shown in curve A of Fig. 2.

4. COMPUTATION PROCEDURE

4.1. Potential Energy Curves

For HF, the RKR potential shown in Fig. 1, previously described in Ref. 1, was used. For HI, the vibrational constants ω_e, $\omega_e x_e$, $\omega_e y_e$, and $\omega_e z_e$ determined from infrared absorption experiments to the first four vibrationally excited states of the ground electronic state[11,12] were used to calculate the positions of the next five vibrational energy levels using the approximate expression

$$E_v = \omega_e(v + \tfrac{1}{2}) - \omega_e x_e(v + \tfrac{1}{2})^2 + \omega_e y_e(v + \tfrac{1}{2})^3 - \omega_e z_e(v + \tfrac{1}{2})^4. \quad (9)$$

The RKR procedure of McClintock, Demtröder, and Zare[13] was then used to determine the classical turning points for each eigenvalue. The smoothed potential curve drawn through these points using a cubic spline method[9] is shown in Fig. 2.

4.2. Wavefunctions

Equation (5) was integrated for both potentials by the finite difference method.[14] The resulting matrix equations were solved using the Givens-Householder method.[15] The integration procedure was checked by comparing the eigenvalues used to generate the RKR potential with those calculated from Eq.(5) using that potential. They agree to within 0.2%.

5. RESULTS

5.1. Hydrogen Fluoride

In column two of Table I, the transition moments, M_0^v, between the ground and v^{th} vibrational state of HF are listed for the M(R) constructed in Sec. 3 and shown in curve A of Fig. 1.

Using the values of M_0^0 through M_0^3, a third-order Taylor series expansion of M(R) was constructed, as described in Sec. 3.1 of Ref. 1. The resulting cubic polynomial is curve B in Fig. 1. The transition moments obtained using this approximation to M(R) are given in column three.

In a similar manner, quartic and quintic Taylor series representations of M(R) were obtained using M_0^4 and M_0^5, respectively. The quartic polynomial shown in curve C of Fig. 1 yielded the transition moments reported in column four of Table I. The quintic polynomial is shown in curve D. Its corresponding matrix elements are given in column five.

The danger of using a truncated Taylor series expansion for M(R) to compute transition moments beyond the data base has been discussed previously.[1,16] In order to eliminate the unphysical divergence in the Taylor series representation of M(R) as $R \to \infty$ and hence produce a more accurate M(R), Herbelin and Emanuel have suggested using a Padé representation of M(R).[2] In the Padé method, M(R) is represented by the ratio of two quadratic polynomials which satisfy the boundary condition $M(\infty) = 0$. The parameters used in the Padé approximation are obtained from the five coefficients of the fourth-order Taylor series. Using the method described in Sec. II.C of Ref. 2, we obtain the Padé approximation for M(R) shown in curve E. The transition moments

obtained using curve E are listed in column six.

The rationale in using the Padé representation of M(R) was that any additional physical constraints imposed on an approximate M(R) make it a more accurate M(R); a more accurate M(R) should predict more accurate transition moments.

For the same reason the following "modified wavefunction expansion" of M(R) was proposed An M(R) corresponding to the known transition moments may be obtained using the wavefunction expansion method of Trischka and Salwen.[16] This method consists in expanding $M(R)|0\rangle$ in terms of vibrational wavefunctions $|v\rangle$. Assuming these functions form a complete set, we may use the identity

$$|M(R)|0\rangle = \sum_v |v\rangle\langle v|M(R)|0\rangle \qquad (10)$$

from which we obtain

$$M(R) = \frac{1}{|0\rangle} \sum_v M_0^v |v\rangle \ . \qquad (11)$$

Equation (11) is rigorous for a complete basis set which includes contributions from the continuum. When the sum in Eq.(11) is truncated at v_{max}, the resulting M_0^v for $v > v_{max}$ vanish identically. Therefore, such a truncated version of Eq.(20) cannot be used for predicting values of M_0^v. It does, however, generate an M(R) curve from values of M_0^v. As seen in Fig. 13 of Ref 1, this M(R) is reasonable for R in the range of 1.0 to about 3.2 a.u. The spike at 3.3 a.u. is due to the truncation of Eq.(11) at $v_{max} = 9$. We can eliminate this unphysical spike by smoothly connecting the M(R) at 3.0 a.u. to the point M(5.42) = 0 (beyond which distance the interaction between the H and F atoms can be neglected, as discussed in Ref.2) using a cubic spline[9] and making M vanish thereafter.

We also smoothly connect M(1.2) with M(0) = 0 by a similar spline method. The resulting curve is the modified wavefunction expansion of M(R). Although it is more difficult to compute and does not have an analytic form, like the Padé polynomial, it has several advantages: (1) it can be parameterized to any order; (2) it has physically realistic behavior for all R; and (3) it exhibits no physical singularities sometimes present in the Padé method.

Using the transition moments calculated from the fifth-order Taylor series (column five), a fifth-order modified wavefunction of M(R) is calculated using the procedure just described. The resulting M(R) is shown in curve F. In column seven of Table I the matrix elements of curve F are listed.

5.2. Hydrogen Iodide

Analogous results were obtained for HI for the hypothetical operator described by Eq.(1) and shown in curve A of Fig. 2. The transition moments for this operator are given in column two of Table II. Curves B, C, and D are the respective cubic, quartic, and quintic Taylor series approximations to this M(R). The corresponding transition moments are given in columns three, four, and five of Table II. Curve E of Fig. 2 is the fourth-order Padé approximation and curve F is the fourth-order (not fifth-order as in HF) modified wavefunction expansion of M(R) for HI. The matrix elements of E and F are listed in columns six and seven of Table II.

6. DISCUSSION AND CONCLUSIONS

6.1. Effects of Boundary Conditions on M(R)

We see in Figs. 1 and 2 that between 0 and 8 bohr, curves E and F are better approximations to curve A than curves C and D. However, since we are interested in M(R) only to predict transition moments, the behavior of M(R) is important only in the region where the corresponding vibrational wavefunctions are nonzero. Since direct comparison of the M(R) is somewhat deceptive, we evaluate the various semi-empirical procedures using the transition moments listed in Tables I and II.

Comparing the Taylor series and the Padé approximations with the exact results, we see that the additional physical constraint present in the Padé polynomial does not consistently or substantially improve the predicted transition moments. In fact, because of the circuitous and approximate route via intermediate Taylor series expansions that was used (and which was introduced for numerical convenience in the determination of the coefficient without excessive evaluations of transition moment integrals), the transition moments used to generate the Padé polynomial (M_0^v, $v \leq 4$) are not always reproduced.

This same conclusion is true for the modified wavefunction expansion. The matrix elements of a modified wavefunction expansion of M(R) are no more accurate than a Taylor series polynomial of the same order. This is true for the fifth-order HF expansion given in Table I, the fourth-order HI expansion shown in Table II, and for other order expansions calculated for both molecules but not presented.

The failure of the boundary condition criteria to improve transition moment calculations appears to be a general result. Forcing M(R)

to be zero at large R or at zero apparently has little or no effect on the behavior of M(R) in the crucial regions of Figs. 1 and 2 where the vibrational wavefunctions are nonzero.

6.2. Number of Terms in M(R) Needed to Predict Transition Moments

The key question in predicting transition moments using a series expansion for M(R) is: How many terms in M(R) are needed? Of course, the Taylor series expansion of M(R) is identical to M(R) if an infinite number of terms are used. And, obviously, we can obtain an M(R) which predicts the first n transition moments using n terms. But unless we can predict the first n transition moments using less than n terms, semi-empirical calculations are useless.

The number of terms necessary depends on the accuracy of the prediction desired and on the behavior of M(R) for the particular molecule studied. From Tables I and II we see that while a quintic polynomial for HF predicts M_0^v for $v > 5$ having an average relative error of 1.7, the quintic polynomial for HI predicts an average relative error of 0.02. Even the HI quartic polynomial gives an average relative error of only 0.24 for the same transition moments.

The difference in behavior of these two molecules is due to the difference of the importance of the higher derivatives of M(R) in the unshaded regions. To use a Taylor series to accurately describe an M(R) having a maximum some distance from R_e, many derivatives of M(R) at R_e are needed. For a molecule having an M(R) similar to curve A in either figure, fewer coefficients of M(R) are needed if R_e is significantly to the right of the maximum in M(R) than when R_e is on the left of the maximum. The reason for this is that when R_e is significantly

right of the maximum all the vibrational wavefunctions are zero near this maximum in M(R). This is not true when R_e is to the left of the maximum because the shape of the internuclear potential requires that the higher vibrational wavefunctions will eventually sample M(R) about its maximum.

While present ab initio calculations for real molecules do not predict accurate transition moments, they do describe the qualitative shape of M(R). This provides the experimentalist with an estimate of the number of coefficients needed for accurate semi-empirical calculations. For example, the failure of the cubic and quartic approximations in Table I to reproduce the transition moments of the Lie M(R) suggests that similar disagreement can be expected when cubic and quartic approximations are used on the experimental results of HF.

In the case of HI, we may be guardedly optimistic. A quartic or higher polynomial may predict reasonable transition moments. However, since no ab initio calculations exist, the transition moments so predicted should be used with caution.

TABLE I. HF transition dipole moments, M_0^v (in atomic units).

Moment	Exact	Approximation				
		Taylor Cubic	Taylor Quartic	Taylor Quintic	Padé Fourth Order	Mod. Wfn. Exp. Fifth Order
M_0^0	0.718	0.718	0.718	0.718	0.718	0.718
M_0^1	0.423(-1)	0.423(-1)	0.423(-1)	0.423(-1)	0.426(-1)	0.423(-1)
M_0^2	-0.605(-2)	-0.605(-2)	-0.605(-2)	-0.605(-2)	-0.580(-2)	-0.605(-2)
M_0^3	-0.163(-2)	-0.163(-2)	-0.163(-2)	-0.163(-2)	-0.790(-3)	-0.164(-2)
M_0^4	0.835(-3)	0.100(-2)	0.835(-3)	0.835(-3)	0.850(-3)	0.820(-3)
M_0^5	0.130(-3)	-0.456(-3)	-0.343(-3)	0.130(-3)	-0.336(-3)	0.100(-3)
M_0^6	-0.323(-3)	0.208(-3)	0.145(-3)	-0.295(-3)	0.754(-4)	-0.306(-3)
M_0^7	0.180(-3)	-0.993(-4)	-0.656(-4)	0.239(-3)	0.559(-5)	0.242(-3)
M_0^8	-0.268(-4)	0.505(-4)	0.321(-4)	-0.162(-3)	-0.174(-4)	-0.146(-3)
M_0^9	-0.454(-4)	-0.273(-4)	-0.169(-4)	0.105(-3)	-0.118(-4)	0.715(-4)

TABLE II. HI transition dipole moments, M_0^v (in atomic units).

Moment	Exact	Approximation				
		Taylor Cubic	Taylor Quartic	Taylor Quintic	Padé Fourth Order	Mod. Wfn. Exp. Fourth Order
M_0^0	0.164	0.164	0.164	0.164	0.164	0.164
M_0^1	-0.930(-2)	-0.930(-2)	-0.930(-2)	-0.930(-2)	-0.930(-2)	-0.930(-2)
M_0^2	0.908(-3)	0.908(-3)	0.908(-3)	0.908(-3)	0.908(-3)	0.908(-3)
M_0^3	-0.108(-3)	-0.108(-3)	-0.108(-3)	-0.108(-2)	-0.108(-3)	-0.108(-3)
M_0^4	0.124(-4)	0.169(-4)	0.124(-4)	0.124(-4)	0.126(-4)	0.125(-4)
M_0^5	-0.352(-6)	-0.340(-5)	-0.643(-6)	-0.352(-6)	-0.649(-6)	-0.661(-6)
M_0^6	-0.800(-6)	0.796(-6)	-0.544(-6)	-0.787(-6)	-0.544(-6)	-0.538(-6)
M_0^7	0.657(-6)	-0.135(-6)	0.494(-6)	0.643(-6)	0.483(-6)	0.505(-6)
M_0^8	-0.450(-6)	-0.551(-7)	-0.355(-6)	-0.439(-6)	-0.341(-6)	-0.388(-6)
M_0^9	0.287(-6)	0.860(-7)	0.233(-6)	0.280(-6)	0.221(-6)	0.201(-6)

REFERENCES

1. R. E. Meredith and F. G. Smith, J. Quant. Spectrosc. Radiat. Transfer 13, 89 (1973).
2. J. M. Herbelin and G. Emanuel, J. Chem. Phys. 60, 689 (1974).
3. G. C. Lie, J. Chem. Phys. 60, 2991 (1974).
4. I. N. Levine, Molecular Spectroscopy (John Wiley and Sons, Inc., New York, NY, 1975), Sec. 4.4.
5. Reference 4, pp. 120-122.
6. G. Herzberg, Spectra of Diatomic Molecules (D. Van Nostrand, Inc., Princeton, NJ, 1950), 2nd Ed., pp. 19-21.
7. Reference 4, pp. 62-63.
8. R. Herman, R. W. Rothery, and R. J. Rubin, J. Mol. Spectrosc. 2, 369 (1958).
9. J. H. Ahlberg, E. N. Wilson, and J. N. Walsh, The Theory of Splines and Their Applications (Academic Press, NY, 1967).
10. W. Benesch, J. Chem. Phys. 39, 1048 (1963).
11. L. A. Pugh and K. M. Rao, J. Mol. Spectrosc. 37, 373 (1971).
12. C. Haeusler, C. Meyer, and P. Barchewitz, J. Phys. 25, 961 (1964).
13. M. McClintock, W. Demtröder, and R. N. Zare, J. Chem. Phys. 51, 5509 (1969).
14. D. G. Truhlar, J. Comput. Phys. 10, 123 (1973).
15. B. Carnahan, H. A. Luther, and J. O. Wilkes, Applied Numerical Methods (John Wiley and Sons, NY, 1969), p. 267.
16. J. Trischka and H. Salwen, J. Chem. Phys. 31, 218 (1959).

FIGURE CAPTIONS

FIG. 1. HF hypothetical dipole operator, M(R), and approximations as a function of internuclear distance, R. Shown are the constructed M(R), A, and the following approximations: B, cubic Taylor series; C, quartic Taylor series; D, quintic Taylor series; E, Padé polynomial; F, fifth-order modified wavefunction expansion. The arrow into the abscissa at 1.732 bohr labeled R_e indicates the equilibrium internuclear separation. The RKR potential for HF together with eigenvalues and eigenfunctions is the inset.

FIG. 2. HI hypothetical dipole operator, M(R), and approximations as a function of internuclear distance R. The labels for M(R) are the same as those used in Fig. 1 except here F is the fourth-order modified wavefunction expansion of M(R). The arrow at 3.04 bohr indicates the equilibrium internuclear separation. The RKR potential for HI is the inset.

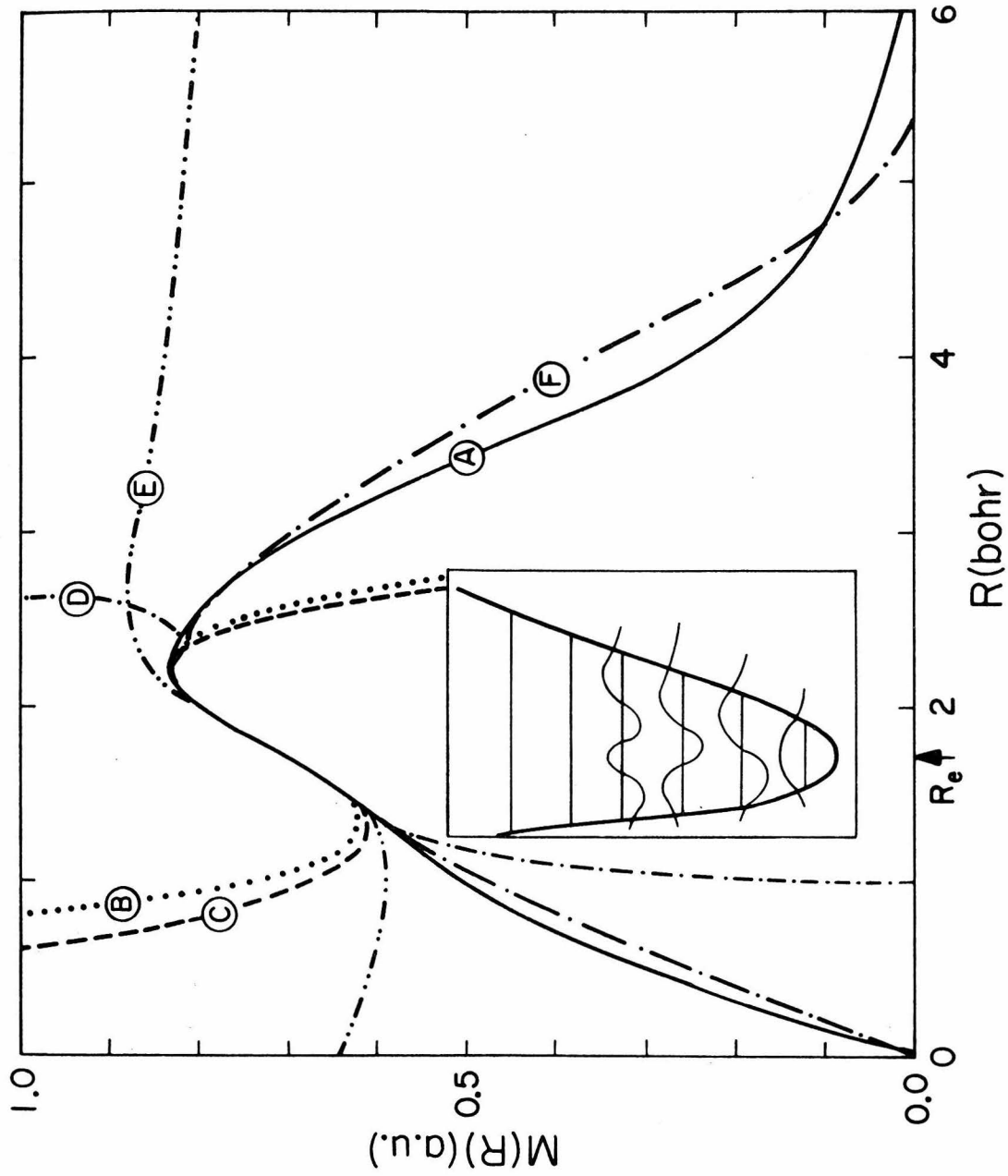

Figure 1.

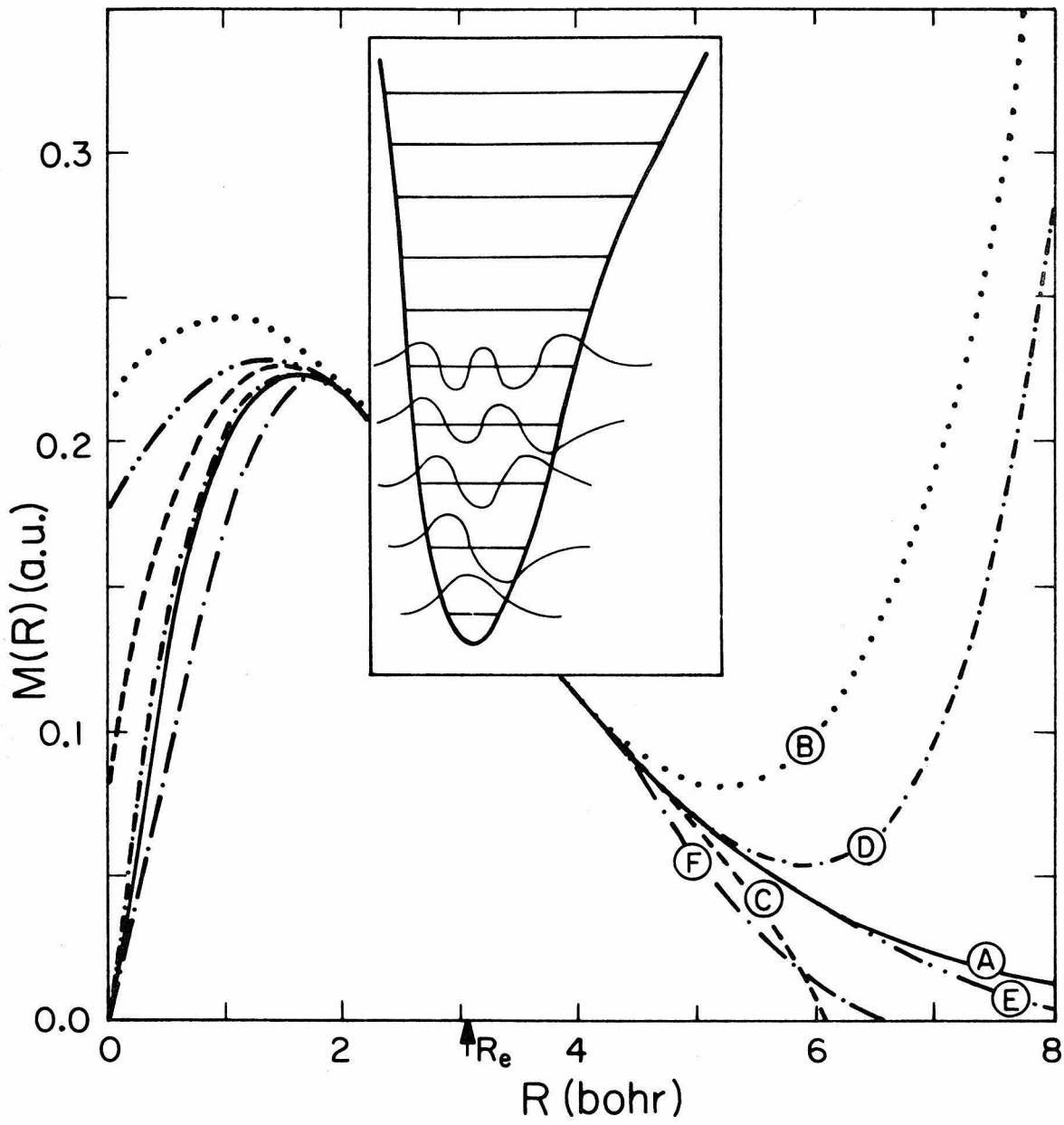

Figure 2.

2. APPROXIMATING DIPOLE MOMENT OPERATORS USING ROVIBRATIONAL TRANSITION MOMENTS

Approximating dipole moment operators using rovibrational transition moments*

Robert H. Reiner and Aron Kuppermann

Arthur Amos Noyes Laboratory of Chemical Physics,† California Institute of Technology, Pasadena, California 91125

(Received)

ABSTRACT

Additional terms in a Taylor series expansion of the transition dipole moment operator, M(R), may be obtained by fitting M(R) to each rovibrational transition moment in the vibrational band rather than to the total band strength. Vibrational transition moments calculated in this manner are compared with exact moments for two hypothetical molecules. The comparisons indicate that one additional term in the Taylor series expansion may be obtained using all rovibrational moments.

---

* This work was supported in part by a contract (EY-76-S-03-0767) from the U.S. Energy Research and Development Administration. Report Code: CALT-767P4- .

† Contribution No.

1. INTRODUCTION

In previous semi-empirical calculations of transition moments, approximations to the dipole moment operator, M(R), have been determined using the nonrotating vibrational matrix elements.[1-3] Rotation-vibration interaction has only been used to resolve ambiguities in the signs of the transition moments.[4,5] This is primarily due to the historic difficulty in obtaining accurate rovibrational matrix elements.[5] With the advent of high-speed computers, exact rovibrational wavefunctions are now easily obtained by numerical integration of the radial Schrödinger equation [Eq.(5), Ref. 6][2,6] making it possible to fit M(R) to all rovibrational transition moments, $M_{0,J}^{v,J'}$ in the v^{th} vibrational band, rather than just the center of the band M_0^v (equivalently $M_{0,0}^{v,0}$).

The conventional method of approximating M(R) is by a Taylor series expansion about R_e, the equilibrium internuclear separation. Using v nonrotating transition moments, one obtains the first v coefficients in the Taylor series by solving a set of v equations [see Eq.(28), Ref. 2]. However, if M(R) is fitted to all the $M_{0,J}^{v,J'}$ in the first v vibrational bands, we have an overdetermined system of linear equations, since there are many rovibrational lines in each vibrational band.

There are two distinct advantages in using all the $M_{0,J}^{v,J'}$ instead of just the M_0^v's. First, if there is experimental uncertainty in the individual rovibrational moments, then a least squares determination of the v Taylor series coefficients, made using the rovibrational moments, produces a more reliable dipole operator having a known uncertainty. Second, this overdetermined system of equations allows us to fit a Taylor series of order greater than v to the first v vibrational

bands. In a typical hydrogen halide, for example, more than 50 rovibrational lines have been measured in the first three vibrational bands of the molecule. This would allow one to determine up to a 50th-order Taylor series approximation for M(R).

Of course, it would be ridiculous to use these 50 transition moments to construct a 50-term Taylor series for M(R) since the data are not accurate enough for such a determination. In order to determine the appropriate number of additional terms (if any) that can be obtained from a least squares treatment of the rovibrational moments, we have employed the same "hypothetical" HF and HI molecules used in a previous paper.[6]

For each molecule, rovibrational transition moments between the ground and upper vibrational states ($v \leq 9$) were computed using the constructed M(R). Twenty rovibrational matrix elements in each of the first three vibrational bands were used to construct various order Taylor series approximations to M(R) using the least squares solution of the linear equations. Vibrotational matrix elements of these Taylor series approximations are compared with those calculated using conventional Taylor series and with the matrix elements of the original, hypothetical M(R).

In the next two sections the construction of the hypothetical M(R) and the computational procedure are reviewed. In Sec. 4 the results are presented. Their implications to semi-empirical calculations of transition moments are discussed in Sec. 5.

2. CONSTRUCTION OF M(R)

The hypothetical M(R) were constructed to, at least qualitatively, describe the expected behavior of the real (but unknown) M(R) for HF and HI. The M(R) constructed for HF, shown in Fig. 1 of Ref. 6 (curve A), was essentially that calculated by Lie.[7] The M(R) used for HI, shown in Fig. 2 of Ref. 6 (curve A) was chosen to have a physically reasonable shape given by

$$M(R) = A R^{B} \exp(-CR), \qquad (1)$$

where A, B, and C are 0.4172, 1.174, and 0.7336, respectively (all dimensions are in atomic units).

3. COMPUTATIONAL PROCEDURE

The computational procedure was identical to that described in Sec. 4 of Ref. 6 with one exception. In the present work the centrifugal term was retained in the radial Schrödinger equation [Eq.(5), Ref. 6]. The RKR potentials for HF and HI previously described were used in this equation. The resultant rovibrational wavefunctions were obtained using the Givens-Householder method (Sec. 4.2, Ref. 6).

4. RESULTS

4.1. Hydrogen fluoride

In column two of Table I, the nonrotating transition moments, M_0^v, between the ground and v^{th} vibrational state of HF are listed for the constructed M(R).

The transition moments calculated using the conventional cubic, quartic, and quintic Taylor series approximations to M(R) are listed in columns three, four, and five, respectively. These are the same Taylor series approximations of M(R) calculated previously, using the nonrotating transition moments (see Sec. 5.1 and Table I of Ref. 6).

The least squares quartic fit to rovibrational transition moments is performed using the sixty rovibrational transitions in the first three vibrational bands of HF together with the permanent dipole moment of the molecule. This set of 61 linear equations in five unknowns is similar to that used in Ref. 2 except that Eq. (28) of that reference now becomes

$$\langle v, J' | M(R) | 0, J \rangle = \sum_{i=0}^{4} M_i \langle v, J' | (R - R_e)^i | 0, J \rangle \qquad (2)$$

for each rovibrational transition $(0, J \rightarrow v, J')$. The unknown coefficients of the Taylor series approximation (the M_i's) are determined using a least squares multiple regression on the 61 Eq. (2)'s.[8] This quartic Taylor series approximation of M(R) is used to calculate the M_0^v's given in column six of Table I.

A quintic Taylor series is determined analogously, solving the set of 61 linear equations in five unknowns [index i now has an upper limit of five in Eq. (2)]. Vibrational transition moments of this Taylor series are listed in column nine.

We can mimic the uncertainty in experimental measurement by introducing statistical error into the rovibrational moments of the original, hypothetical M(R). A quartic least squares fit to rovibrational moments having an average fluctuation of 1% yields the M_0^v's in column seven. A similar quartic fit to rovibrational moments having 10% uncertainty produces the M_0^v listed in column eight of Table I.

In addition to determining how accurately the nonrotating transition moments are predicted, we may also examine how well the various Taylor series approximations reproduce the original rovibrational moments. In Figs. 1a and 1b, the rotational correction factors, $F_0^v(m)$

$$F_v^{v'} \equiv \frac{|\langle v, J|M(R)|v', J'\rangle|^2}{|\langle v, 0|M(R)|v', 0\rangle|^2} , \tag{3}$$

where

$$m = \begin{cases} J + 1 \text{ for R branch transitions} \\ -J \text{ for P branch transitions} \end{cases} \tag{4}$$

are shown as a function of m, for the original, constructed M(R). The circles are the $F_0^1(m)$, the squares, $F_0^2(m)$, and the triangles, $F_0^3(m)$. The conventional Taylor series approximations (cubic, quartic, and quintic) and the least squares rovibrational Taylor series approximations (quartic and quintic) predict rotational correction factors for the first vibrational band (solid line) and second vibrational band (dashed line) which are identical to those of the original M(R) (Fig. 1a). However, in the third vibrational band (Fig. 1b) significantly different rotational correction factors are predicted by the conventional cubic (dashed line), quartic (solid line), and quintic (dotted line) Taylor series approximations of M(R). Rotational correction factors predicted by both the

quartic and quintic rovibrational Taylor series are not perceptively different from those of the conventional quartic Taylor series (solid line).

4.2. Hydrogen iodide

Analogous results were obtained for a hydrogen iodide molecule having an M(R) described by Eq.(1). The vibrational transition moments of this hypothetical HI molecule are given in column two of Table II. The transition moments of the conventional cubic, quartic, and quintic Taylor series approximations of M(R) are listed in columns three, four, and five, respectively. The least squares quartic fit to the 60 rovibrational lines of the three vibrational bands of HI produces the moments in column six of Table II. The results of similar quartic fits using rovibrational lines having 1% and 10% random errors yields the transition moments in columns seven and eight, respectively. The transition moments in column nine are the result of a quintic fit to the 60 rovibrational moments in the first three bands.

In Figs. 2a and 2b, the rotational correction factors of the constructed M(R) [Eq.(1)] are displayed for the first vibrational band (circles), the second vibrational band (squares), and the third vibrational band (triangles). As in the HF case, all Taylor series approximations yield the original rotational correction factors for the first vibrational band (solid line) and the second vibrational band (dashed lines). Unlike the HF situation, all Taylor series approximations in HI predict almost the same rotational correction factors (solid line, Fig. 2b). The only visible disagreement between the original correction factors and those determined by the Taylor series approximation was that displayed by

the conventional cubic approximation (dashed line).

5. DISCUSSION

The most striking result displayed in Tables I and II is that the quartic rovibrational Taylor series (column six) and the quartic conventional Taylor series (column four) predict the same transition moments. Since the conventional quartic series requires knowledge of M_0^4 while the quartic rovibrational series does not, one addition term in the Taylor series expansion is obtained by using all the rovibrational moments.

Attempting to obtain a second additional term by fitting the rovibrational moments to a quintic Taylor series is not successful. In HF, the quintic (column nine) and quartic (column six) Taylor series predict the same M_0^V's. In HI, the quintic results are not as good as the quartic results.

An explanation for this failure may be seen in Figs. 1 and 2. In the first and second vibrational bands of both molecules, a cubic Taylor series is sufficient to determine the rovibrational behavior. In the third vibrational band, the quartic Taylor series is an improvement over the cubic Taylor series. This improvement is drastic in HF and less significant, but perceptible, in HI. However, a quintic rovibrational Taylor series does not alter any rotational correction factors predicted by the quartic fit. Therefore we should not expect the quintic to predict vibrational transition moments more accurately than the quartic. In fact, the vibrational moments predicted by the quintic are less accurate than those of the quartic approximation. This result is typical of least

squares approximations in general and is the reason why the order of an approximation should be no greater than is justified by its ability to fit the data.[9] Since the two quintic Taylor series yield no better rovibrational moments than the quartic, there is no purpose in using them.

An accurate Taylor series may be obtained even when large fluctuations are present in the rovibrational moments. In HF, the quartic determined from rovibrational moments having 10% uncertainty (column eight, Table I), although not as accurate as the exact quartic, still predicts better transition moments than the exact cubic approximation (column three). The 10% quartic in HI is not as good as the exact cubic, but the 1% quartic (column seven, Table II) is significantly better than this cubic. Hydrogen iodide is more sensitive to rovibrational fluctuations than HF because the difference between the cubic and quartic rotational correction factors is larger in HF than in HI. That is, more accurate data are needed to distinguish the dashed and dotted lines in Fig. 2b than are needed in Fig. 1b. Again, common sense must be used when fitting Taylor series to the rovibrational moments. When the uncertainty in the moments is larger than the change produced by using a higher-order approximation, it is pointless to use the higher-order approximation.

Another interesting aspect of Figs. 1b and 2b is that while the quartic Taylor series yields the exact $F_0^3(m)$ for HI, a conventional quintic Taylor series is needed to reproduce the $F_0^3(m)$ of HF. This means that for HI, M(R) is accurately described by a quartic approximation in the region of R sampled by all rovibrational wavefunctions, $|v,J\rangle$, where $v \leq 3$ and $-10 \leq J \leq 10$, while an addition term is necessary

for the M(R) of HF in the analogous region of R. This is another manifestation of the general result obtained previously,[6] that more terms are needed to describe the M(R) of an "HF-type" molecule to the same degree of accuracy as an "HI-type" molecule.

TABLE I. Vibrational transition moments of HF (in atomic units).

Moment	Approximation							
	Exact	Cubic	Quartic	Quintic	Exact Rovib. Quartic	1% Rovib. Quartic	10% Rovib. Quartic	Rovib. Quintic
M_0^0	0.718	--	--	--	--	--	--	--
M_0^1	0.423(-1)	--	--	--	--	0.422(-1)	0.420(-1)	--
M_0^2	-0.605(-2)	--	--	--	--	-0.605(-2)	-0.606(-2)	--
M_0^3	-0.16 (-2)	--	--	--	--	-0.164(-2)	-0.164(-2)	--
M_0^4	0.853(-3)	0.100(-2)	--	--	0.807(-3)	0.825(-3)	0.868(-3)	0.804(-3)
M_0^5	0.130(-3)	-0.456(-3)	-0.343(-3)	--	-0.323(-3)	-0.335(-3)	-0.363(-3)	-0.432(-3)
M_0^6	-0.323(-3)	0.208(-3)	0.145(-3)	-0.295(-3)	0.134(-3)	0.140(-3)	0.156(-3)	0.236(-3)
M_0^7	0.180(-3)	-0.993(-4)	-0.656(-4)	0.239(-3)	-0.598(-4)	-0.630(-4)	-0.715(-4)	-0.131(-3)
M_0^8	-0.268(-4)	0.505(-4)	0.321(-4)	-0.162(-3)	0.288(-4)	0.307(-4)	0.353(-4)	0.742(-4)
M_0^9	-0.454(-4)	-0.273(-4)	-0.169(-4)	0.105(-3)	-0.151(-4)	-0.161(-4)	-0.187(-4)	-0.435(-4)

TABLE II. Vibrational transition moments of HI (in atomic units).

Moment	Approximation							
	Exact	Cubic	Quartic	Quintic	Exact Rovib. Quartic	1% Rovib. Quartic	10% Rovib. Quartic	Rovib. Quintic
M_0^0	0.164	--	--	--	--	--	--	--
M_0^1	-0.930(-2)	--	--	--	--	-0.928(-2)	-0.936(-2)	--
M_0^2	0.908(-3)	--	--	--	--	0.906(-3)	0.910(-3)	--
M_0^3	-0.108(-3)	--	--	--	--	-0.108(-3)	-0.106(-3)	--
M_0^4	0.124(-4)	0.169(-4)	--	--	0.123(-4)	0.124(-4)	-0.141(-4)	0.161(-4)
M_0^5	-0.352(-6)	-0.340(-5)	-0.643(-6)	--	-0.586(-6)	-0.664(-6)	0.153(-4)	0.300(-4)
M_0^6	-0.800(-6)	0.796(-6)	-0.544(-6)	-0.787(-6)	-0.572(-6)	-0.533(-6)	-0.827(-5)	-0.270(-4)
M_0^7	0.657(-6)	-0.135(-6)	0.494(-6)	0.643(-6)	0.507(-6)	0.488(-6)	0.411(-5)	0.169(-4)
M_0^8	-0.450(-6)	-0.551(-7)	-0.355(-6)	-0.439(-6)	-0.361(-6)	-0.352(-6)	-0.209(-5)	-0.965(-6)
M_0^9	0.287(-6)	0.860(-7)	0.233(-6)	0.280(-6)	0.236(-6)	0.232(-6)	0.108(-5)	0.538(-5)

REFERENCES

1. W. S. Benedict, R. Herman, G. E. Moore, and S. Silvermann, J. Chem. Phys. 26, 1671 (1957).
2. R. E. Meredith and F. G. Smith, J. Quant. Spectrosc. Radiat. Transfer 13, 89 (1973).
3. J. M. Herbelin and G. Emanuel, J. Chem. Phys. 60, 689 (1974).
4. R. L. Spellicy, R. E. Meredith, and F. G. Smith, J. Chem. Phys. 57, 5119 (1972).
5. R. Herman, R. W. Rothery, and R. J. Rubin, J. Mol. Spectrosc. 2, 369 (1958).
6. R. H. Reiner and A. Kuppermann, J. Chem. Phys., submitted for publication.
7. G. C. Lie, J. Chem. Phys. 60, 2991 (1974).
8. B. Carnahan, H. A. Luther, and J. O. Wilkes, Applied Numerical Methods (John Wiley and Sons, New York, 1969), p. 573.
9. Ibid., p. 576.

FIGURE CAPTIONS

FIG. 1(a). Rotational correction factors F(m) as a function of rotational index m for the first and second vibrational bands of HF. Circles, ● , are exact results for the first vibrational band; squares, ■ , are the exact results for the second vibrational band. All Taylor series approximations used in the first band are the solid line; Taylor series approximations in the second band are the dashed line.

FIG. 1(b). Rotational correction factors F(m) as a function of rotational index m for the third vibrational band of HF. Triangles, ▲ , are exact results. The cubic Taylor series approximation is the dashed line; both the conventional and the rovibrational quartic are the solid line; the conventional Taylor series quintic is the dotted line.

FIG. 2(a). Rotational correction factors F(m) as a function of rotational index m for the first and second vibrational bands of HI. Circles, ● , are exact results for the first vibrational band; squares, ■ , are the exact results for the second vibrational band. All Taylor series approximations used in the first band yield the solid line; Taylor series approximations used in the second band yield the dashed line.

FIG. 2(b). Rotational correction factors F(m) as a function of rotational index m for the third vibrational band of HI. Triangles, ▲ , are exact results; cubic Taylor series approximation is the dashed line; all other Taylor series approximations yield the solid line.

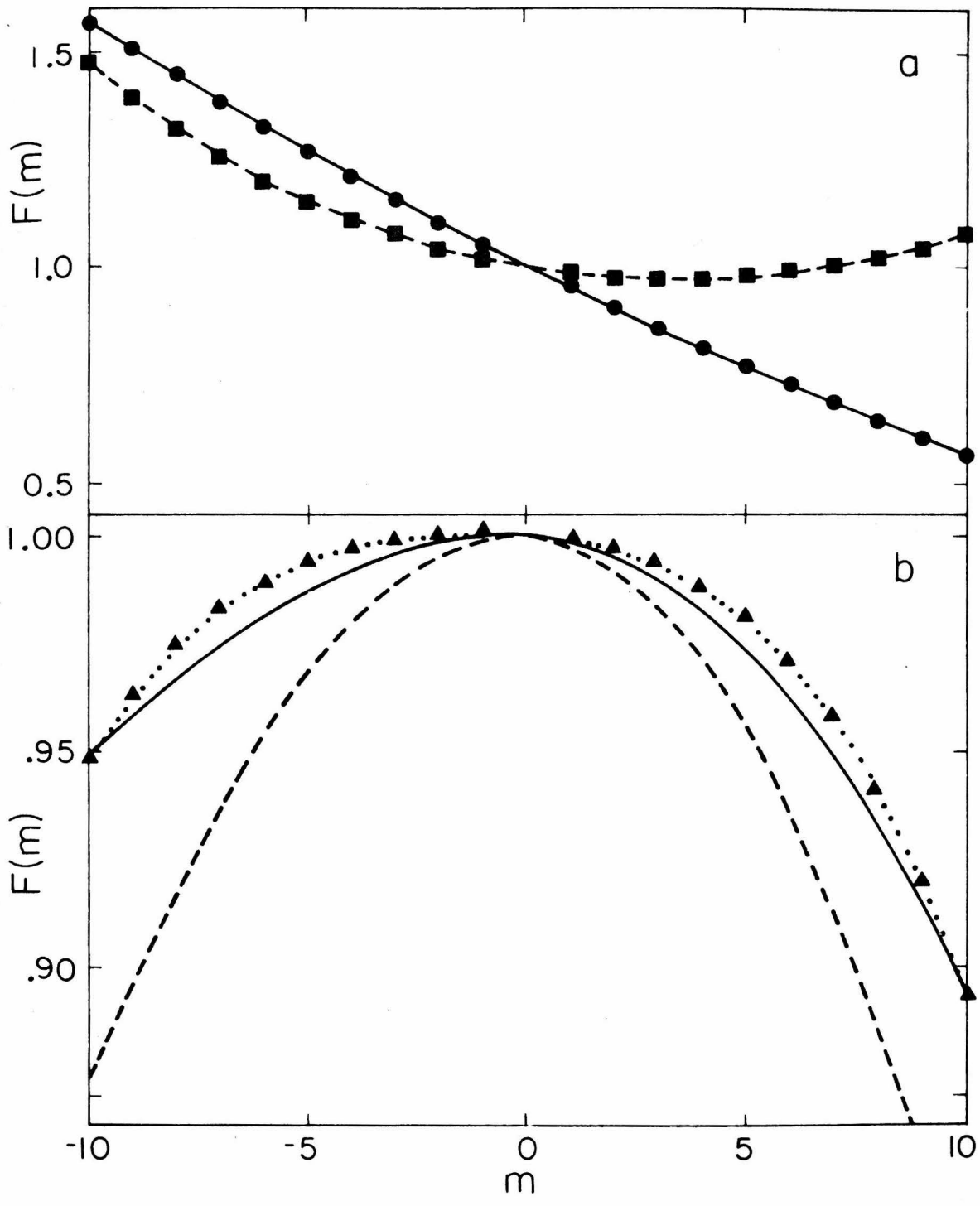

Figure 1.

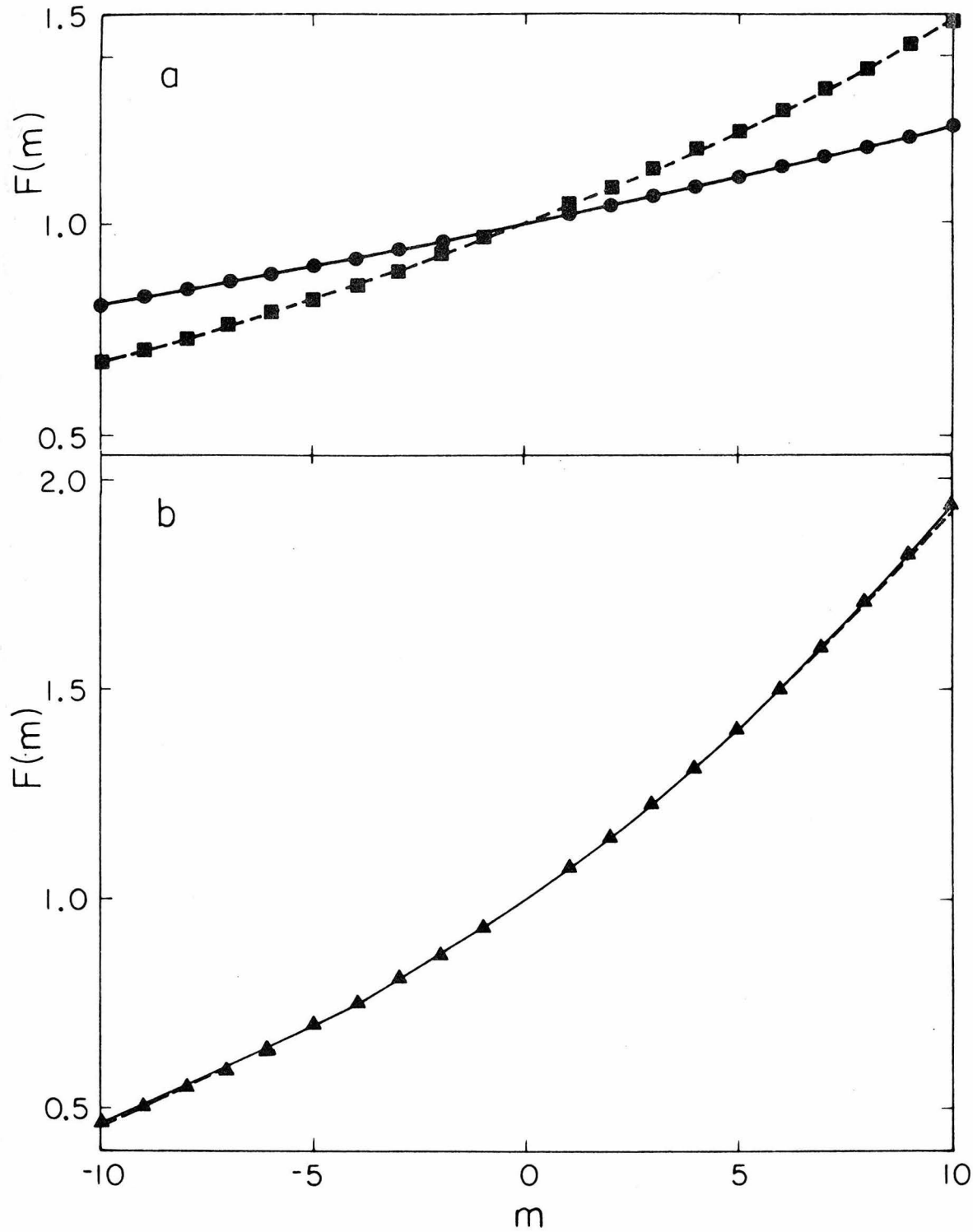

Figure 2.

3. VIBRATION-ROTATION INTERACTION IN THE FIRST THREE VIBRATIONAL BANDS OF HI

VIBRATION-ROTATION INTERACTION IN FIRST THREE VIBRATIONAL BANDS OF HI*

Robert H. REINER and Aron KUPPERMANN

Arthur Amos Noyes Laboratory of Chemical Physics,†
California Institute of Technology, Pasadena, California 91125, USA

Received

HI rovibrational wavefunctions obtained from numerical integration of the radial Schrödinger equation, together with line strengths measured in the first three vibrational bands, were used to determine the signs and magnitudes of the transition dipole moments of these bands. The transition moments obtained were $\langle 0|M(R)|1\rangle = -1.54 \times 10^{-3}$ (a.u.), $\langle 0|M(R)|2\rangle = 7.21 \times 10^{-4}$ (a.u.), and $\langle 0|M(R)|3\rangle = -4.43 \times 10^{-4}$ (a.u.). A quartic Taylor series expansion of the dipole moment operator, M(R), was obtained by fitting M(R) to the rovibrational matrix elements. Transition moments between ground and upper levels of HI(4-9) and DI(0-9) predicted using this operator are in good agreement with those determined using nonrotating vibrational matrix elements.

---

* This work was supported in part by a contract (EY-76-S-03-0767) from the U.S. Energy Research and Development Administration.
Report Code: CALT-767P4-
† Contribution No.

1. Introduction

In a previous paper [1], we found that an improved Taylor series approximation of the transition dipole moment operator, M(R), may be obtained by fitting M(R) to individual rovibrational transition moments in the vibrational bands rather than fitting M(R) to the transition moment of the band center. We now use this method to fit an M(R) to experimental results available for HI. This M(R) is then used to predict other transition moments in HI and DI.

Since the measured band strengths are proportional to the square of the vibrational moments, there exists an uncertainty in the sign of the measured moments. The sign ambiguity may be resolved by measurement of the individual rotational lines in each vibrational band [2, 3]. Simply explained, the rotational-vibrational coupling produced by the centrifugal term in the radial Schrödinger equation {eq. (5) of ref. [4]} causes a stretching of the molecule. Different rotational states in a particular vibrational band therefore effectively "sample" M(R) at internuclear distances different from R_e. Thus, only one of the two choices for the sign of the rotationless transition moment, M_0^v, correctly predicts the remaining rovibrational transition moments, $M_{0,J}^{v,J'}$.

Measurements of the fundamental and first overtone bands of HI by Ameer and Benesch [5, 6] definitely established that $M_0^1 < 0$ and tentatively established that $M_0^2 > 0$. In this work, infrared measurements of Haeusler [7, 8] were used to verify Benesch's assignment of M_0^2, to assign $M_0^3 < 0$, and tentatively to assign $M_0^4 > 0$. A Taylor series expansion of M(R) to fourth order in $(R-R_e)$ has been found which fits the fifty measured rovibrational transition moments in the first three vibrational bands.

The remaining transition moments in HI(4-9) and DI were calculated using this M(R).

2. Computational Procedures

Taylor series approximations were fitted to the experimental results by solving the necessary linear equations using the procedures described earlier [1, 4]. The matrix elements for HI were evaluated using the rovibrational wavefunctions determined previously.

For DI, the vibrational constants, ω_e, $\omega_e x_e$, and $\omega_e y_e$ determined from infrared absorption experiments [9], were used to calculate the positions of the next six vibrational energy levels and the corresponding RKR potential using the procedure explained in Section 4.1 of ref. [4]. This potential is displayed in table 1. The rovibrational wavefunctions of DI were then obtained by integration of the radial Schrödinger equation {eq.(5), ref.[4]} using this internuclear potential and the procedure described in Section 4.2 of ref. [4].

3. Results

3.1. Sign determination of the matrix elements

In fig. 1 the variation of the rotational correction factors $F_0^1(m)$

$$F_v^{v'}(m) \equiv \frac{|\langle v, J|M(R)|v', J'\rangle|^2}{|\langle v, 0|M(R)|v', 0'\rangle|^2} \qquad (1)$$

where

$$m = \begin{cases} J+1 & \text{for R branch transitions} \\ -J & \text{for P branch transitions} \end{cases} \qquad (2)$$

are shown for the lines m = -6 to m = +7 for the fundamental band of HI. The experimental data are from ref. [5]. The designations [(+ - +)] in

this and subsequent figures refer to the signs used for M_0^1, M_0^2, M_0^3, ... The number of symbols used in the designation is the same as the order used in the Taylor series expansion of M(R)

$$M(R) = M_0 + M_1(R - R_e) + M_2(R - R_e)^2 + \ldots, \quad (3)$$

i.e., all higher coefficients in eq.(3) were set equal to zero. Thus, in fig. 1, the curve designated (- +) was that calculated assuming

$$M(R) = M_0 + M_1(R - R_e) + M_2(R - R_e) \quad (4)$$

for $M_0^1 = -1.57 \times 10^{-3}$(a.u.) and $M_0^2 = +7.07 \times 10^{-4}$(a.u.).

Figure 1 clearly shows that $M_0^1 < 0$. $M_0^2 > 0$ fits the experimental data slightly better than $M_0^2 < 0$, but neither fit the R branch lines well. Benesch [10] also noted this discrepancy and has suggested that it may be due to errors introduced by the truncation of the Taylor series expansion of M(R). We have calculated $F_0^1(m)$ using M(R) with terms to fourth order in $(R - R_e)$ and have found that the curves shown in fig. 1 converged after second order terms in $(R - R_e)$. Evidently the disparity between calculation and experiment for $m > 4$ is due either to some systematic error in the measurement of the rotational lines for $m > 4$ (possible) or the RKR potential does not describe the HI molecule accurately near $v = 0$ and 1 (not probable).

In fig. 2, the experimental data of Benesch [6] (open circles) are shown together with the variation of $F_0^2(m)$ calculated using Benesch's value of M_0^2. Rotational correction factors for the first overtone, $F_0^2(m)$, were calculated using terms in M(R) to fourth order in $(R - R_e)$. Terms higher than third order in $(R - R_e)$ did not visibly change $F_0^2(m)$ and are not displayed. It is clear from this figure that there is too much scatter

in Benesch's overtone data to establish convincingly the sign of M_0^2.

In fig. 3, the experimental results of Haeusler [7] are shown together with the variation of $F_0^2(m)$ calculated using Haeusler's value of M_0^2. The procedure used in the preceding paragraph is repeated. The excellent agreement between experiment and calculation shows that $M_0^2 > 0$ as Benesch speculated.

In addition to different $F_0^2(m)$, Haeusler and Benesch also obtain slightly different values of $|M_0^2|$ as well. We use Haeusler's value of $M_0^2 = 7.07 \times 10^{-3}$(a.u.) rather than Benesch's value of $M_0^2 = 8.06 \times 10^{-3}$ (a.u.) since Haeusler obtained the expected behavior of the rotational correction factors.

In fig. 4, we similarly analyze results for the second overtone of HI [8]. It is clear that $M_0^3 < 0$. Using the experimental conditions reported by Haeusler and Meyer [11] we make an order of magnitude estimate of $|M_0^4| \sim 1.84 \times 10^{-4}$ a.u. in order to calculate a fourth order Taylor series for M(R). Choosing $M_0^4 > 0$ gives much better agreement with experimental results than choosing $M_0^4 < 0$. Here we must be cautious, however. Curve (-+-+) depends on $|M_0^4|$ and that is not accurately known. The shaded regions about curves (-+-+) and (-+--) show how much these curves change as $|M_0^4|$ varies between reasonable limits established using ref. [11]. In spite of these fluctuations of F_0^3, which depend on $|M_0^4|$, $M_0^4 > 0$ gives consistently better agreement for the $0 \rightarrow 3$ rotational lines than does $M_0^4 < 0$.

3.2. Least squares optimization of Taylor series coefficients

A least squares determination of M_i (i = 0-4) was made using the data shown in figs. 1, 3, and 4, and $M_0^0 = 0.1653$ a.u. [4]. Using these

fifty transition moments we obtained the following Taylor series coefficients: $M_0 = 0.1651$ (a.u.), $M_1 = -0.9882 \times 10^{-2}$ (a.u.), $M_2 = 0.2374 \times 10^{-1}$ (a.u.), $M_3 = -0.2059 \times 10^{-1}$ (a.u.), and $M_4 = -0.1588 \times 10^{-2}$ (a.u.). Systematically discarding all experimental F factors that were greater than 3σ away from the calculated values of $F_0^V(m)$ (five values discarded) we obtained a second set of Taylor coefficients: $M_0 = 0.1651$ (a.u.), $M_1 = -0.8647 \times 10^{-2}$ (a.u.), $M_2 = 0.1914 \times 10^{-1}$ (a.u.), $M_3 = -0.3848 \times 10^{-1}$ (a.u.), and $M_4 = 0.2646 \times 10^{-1}$ (a.u.). The second set of coefficients was used to compute M(R).

The transition moments between the ground and higher vibrational states calculated using this rovibrational quartic Taylor series are listed in column 2 of table 2. For comparison, cubic and quartic (using our crude estimate of M_0^4) Taylor series obtained using the nonrotating vibrational transition moments are listed in columns 3 and 4 of this table. The matrix elements of the quartic rovibrational M(R) for all vibrational states with $v \leq 9$ are given in table 3.

3.3. Deuterium iodide transition moments

Within the accuracy of the Born-Oppenheimer approximation, the M(R) of HI and DI are identical. Using the DI vibrational wavefunctions together with the quartic rovibrational series approximation for M(R) we obtain the transition moments shown in column 5 of table 2. Transition moments of the cubic rotationless Taylor series are listed in column 6 for comparison. Matrix elements of the quartic rovibrational M(R) for all DI vibrational states with $v \leq 9$ are given in table 4.

4. Discussion

Previous analysis of rovibrational approximations of M(R) indicated that an additional term in the Taylor series was obtained using this method [1]. We see in table 2 that the rovibrational approximation predicts a value of M_0^4 comparable to our experimental estimate. Since this crude estimate may easily be a factor of three high or low, this good agreement is, in itself, not remarkable. However, the close agreement among the transition moments predicted by the cubic Taylor series, the estimated quartic Taylor series, and the rovibrational quartic Taylor series is consistent with a characteristic of "HI-type" molecules noted earlier: only three or four terms are needed to describe the transition moment of a molecule in which M(R) is monotonic in the region sampled by its vibrational wavefunctions [4].

Table 1

RKR potential for the $X\ ^1\Sigma^+$ state of deuterium iodide [a]

V	Energy (cm^{-1})	R_{min} (Å)	R_{max} (Å)
0	814.854	1.5149866	1.7197242
1	2,414.613	1.4549892	1.8133063
2	2,974.214	1.4175974	1.8851497
3	5,493.380	1.3893926	1.9487227
4	6,971.837	1.3665060	2.0079483
5	8,409.308	1.3471790	2.0646443
6	9,805.518	1.3304368	2.1198501
7	11,160.192	1.3156727	2.1742433
8	12,473.055	1.3024780	2.2283106
9	13,743.831	1.2905614	2.2824296
10	14,972.244	1.2797056	2.3369133
11	16,158.020	1.2697425	2.3920361
12	17,300.883	1.2605377	2.4480514
13	18,400.557	1.2519807	2.5052036
14	19,456.767	1.2439779	2.5637371
15	20,469.238	1.2364481	2.6239049

[a] Spectroscopic constants determined by Hurlock et al. [9]. The method is described in Section 4.1 of ref. [4].

Table 2

Vibrational transition moments of HI and DI (in atomic units)

Moment	HI			DI	
	Quartic Rovibration	Cubic Taylor	Quartic Taylor	Quartic Rovibration	Cubic Taylor
M_0^0	0.165	0.165	0.165	0.165	0.165
M_0^1	-0.154(-2)	-0.158(-2)	-0.158(-2)	-0.126(-2)	-0.131(-2)
M_0^2	0.721(-3)	0.708(-3)	0.708(-3)	0.531(-3)	0.550(-3)
M_0^3	-0.443(-3)	-0.433(-3)	-0.433(-3)	-0.289(-3)	-0.269(-3)
M_0^4	0.242(-3)	0.153(-3)	0.184(-3)	0.130(-3)	0.172(-3)
M_0^5	-0.107(-3)	-0.535(-4)	-0.724(-4)	-0.478(-4)	-0.232(-4)
M_0^6	0.455(-4)	0.193(-4)	0.289(-4)	0.171(-4)	0.724(-5)
M_0^7	-0.199(-4)	-0.795(-5)	-0.124(-4)	-0.627(-5)	-0.243(-5)
M_0^8	0.909(-5)	0.338(-5)	0.552(-5)	0.241(-5)	0.873(-6)
M_0^9	-0.432(-5)	-0.151(-5)	-0.213(-5)	-0.967(-6)	-0.334(-6)

Table 3

HI vibrational matrix elments, $\langle v|M(R)|v'\rangle$, using quartic rovibrational approximation for M(R) (atomic units)

v / v'	0	1	2	3	4	5	6	7	8	9
0	0.165									
1	-0.154(-2)	0.166								
2	0.721(-2)	-0.234(-2)	0.166							
3	-0.443(-3)	0.118(-2)	-0.295(-2)	0.166						
4	0.242(-3)	-0.751(-3)	0.165(-2)	-0.329(-2)	0.166					
5	-0.107(-3)	0.490(-3)	-0.982(-3)	0.226(-2)	-0.320(-2)	0.167				
6	0.455(-4)	-0.245(-3)	0.762(-3)	-0.112(-2)	0.309(-2)	-0.243(-2)	0.169			
7	-0.199(-4)	0.115(-3)	-0.426(-3)	0.103(-2)	-0.114(-3)	0.428(-2)	-0.618(-3)	0.172		
8	0.909(-5)	-0.544(-4)	0.218(-3)	-0.643(-3)	0.126(-2)	-0.105(-2)	0.600(-2)	0.272(-2)	0.177	
9	-0.432(-5)	0.264(-4)	-0.111(-3)	0.357(-3)	-0.879(-3)	0.143(-2)	-0.898(-3)	0.841(-2)	0.827(-2)	0.186

Table 4

DI vibrational matrix elements, $\langle v|M(R)|v'\rangle$, using quartic rovibrational approximation for M(R) (atomic units)

v	0	1	2	3	4	5	6	7	8	9
v'										
0	0.165									
1	-0.126(-2)	0.165								
2	0.531(-3)	-0.190(-2)	0.166							
3	-0.289(-3)	0.868(-3)	-0.244(-2)	0.166						
4	0.130(-3)	-0.519(-3)	0.118(-2)	-0.288(-2)	0.166					
5	-0.478(-4)	0.273(-3)	-0.730(-3)	0.151(-2)	-0.319(-2)	0.166				
6	0.171(-4)	-0.112(-3)	0.442(-3)	-0.907(-3)	0.188(-2)	-0.334(-2)	0.166			
7	-0.627(-5)	0.438(-4)	-0.201(-3)	0.627(-3)	-0.104(-2)	0.234(-2)	-0.324(-2)	0.167		
8	0.241(-5)	-0.173(-4)	0.847(-4)	-0.312(-3)	0.818(-3)	-0.112(-2)	0.292(-2)	-0.280(-2)	0.168	
9	-0.967(-6)	0.706(-5)	-0.357(-4)	0.141(-3)	-0.444(-3)	0.101(-2)	-0.115(-2)	0.367(-2)	-0.192(-2)	0.169

References

[1] R. H. Reiner and A. Kuppermann, J. Chem. Phys., to be submitted for publication.

[2] W. Benesch, J. Mol. Spectrosc. 15 (1965) 140.

[3] R. E. Meredith and F. C. Smith, J. Quant. Spectrosc. Radiat. Transfer 13 (1973) 89.

[4] R. H. Reiner and A. Kuppermann, J. Chem. Phys., to be submitted for publication.

[5] G. Ameer and W. Benesch, J. Chem. Phys. 37 (1962) 2699.

[6] W. Benesch, J. Chem. Phys. 39 (1963) 1048.

[7] C. Haeusler, Ph.D. Thesis, The University of Paris, March 1975.

[8] C. Haeusler and C. Meyer, Compt. Rend. 258 (1964) 5383.

[9] S. C. Hurlock, R. M. Alexander, K. N. Rao and N. Dreska, J. Mol. Spectrosc. 37 (1971) 373.

[10] W. Benesch, J. Chem. Phys. 40 (1964) 422.

[11] C. Haeusler, C. Meyer, and P. Barchewitz, J. Phys. 25 (1964) 561.

Figure Captions

Fig. 1. Rotational correction factors $F_0^1(m)$ as a function of rotational index m for the fundamental vibrational band of HI. Open circles are the measurements of Ameer and Benesch [5]. The lines are the calculated behavior of the F factors using different order Taylor series approximations for M(R). The designations +, - refer to the signs assumed for the transition moments of the appropriate order.

Fig. 2. Rotational correction factors $F_0^2(m)$ as a function of rotational index m for the first vibrational overtone of HI. Open circles are the measurements of Benesch [6]. The curves are calculated behavior of the F factors using different order Taylor series approximations for M(R). The designation scheme used is identical to that used in fig. 1.

Fig. 3. Rotational correction factors $F_0^2(m)$ as a function of rotational index m for the first vibrational overtone of HI. Solid squares and error bars are the measurements of Haeusler [7]. The curves are the same ones used in fig. 2.

Fig. 4. Rotational correction factors $F_0^3(m)$ as a function of rotational index m for the second vibrational overtone of HI. Solid circles and error bars are the measurements of Haeusler and Meyer [8]. The curves are calculated behavior of the F factors using different order Taylor series approximations for M(R). The shaded regions about curves (-+-+) and (-+--) show the effect the uncertainty in $|M_0^4|$ has on the calculated F factors.

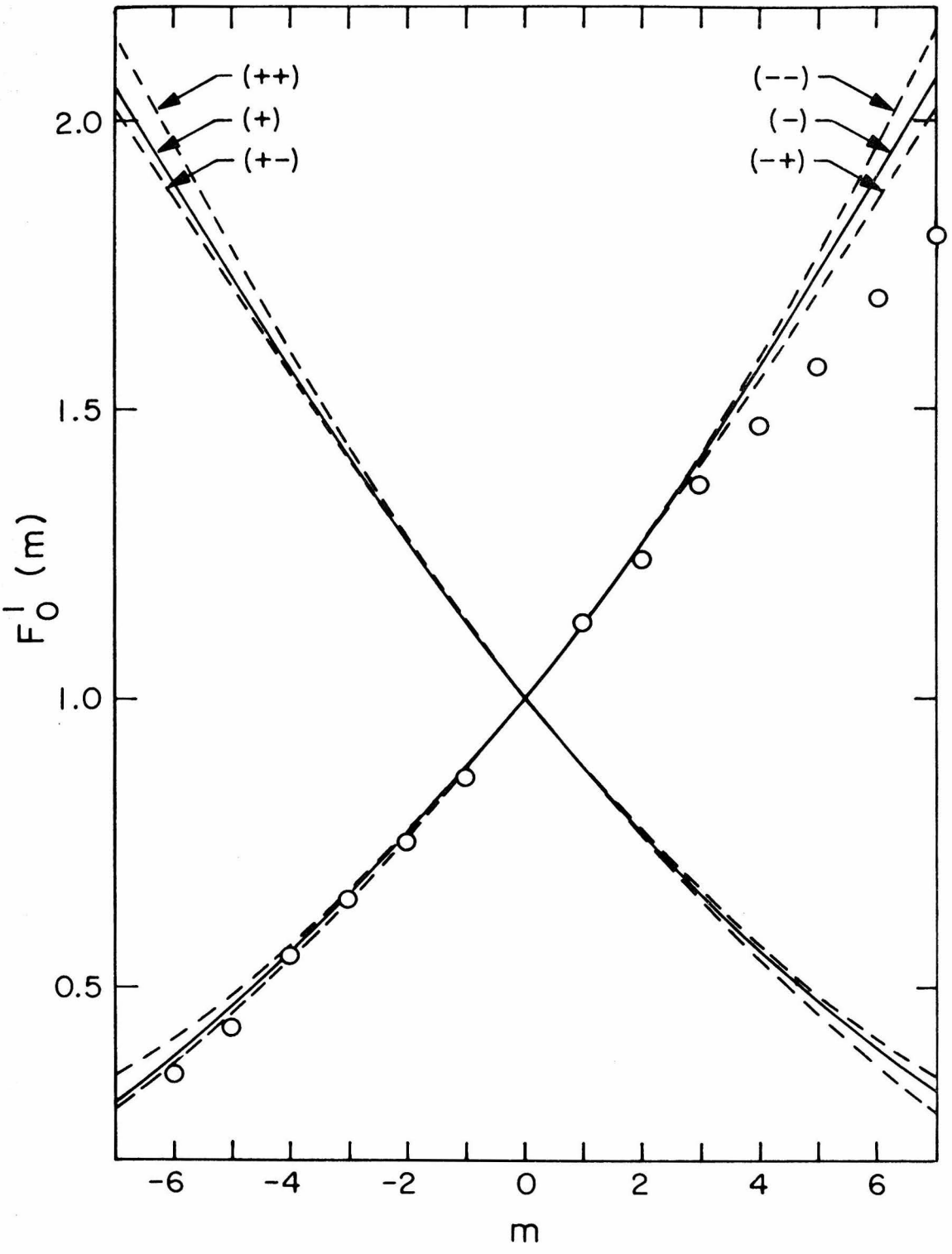

Figure 1.

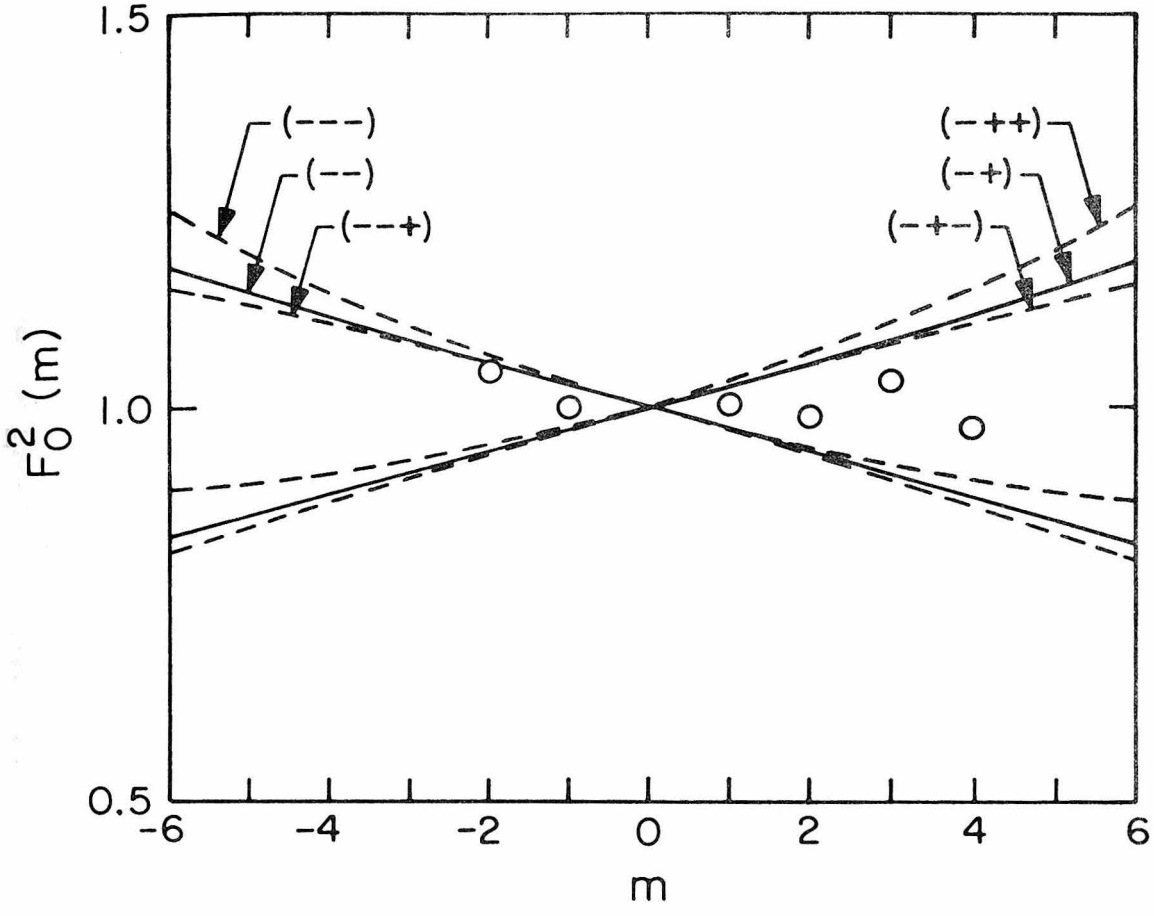

Figure 2.

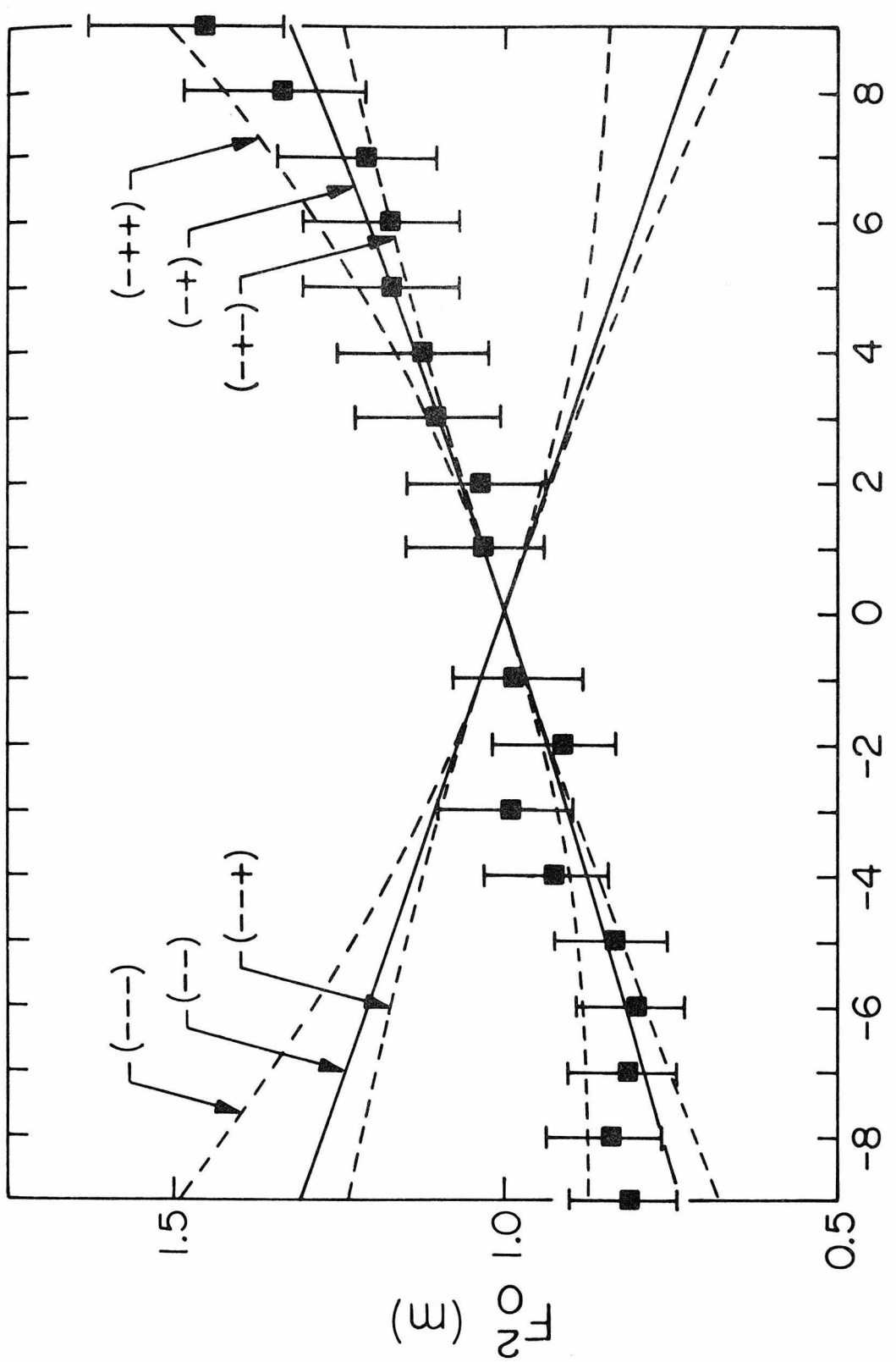

Figure 3.

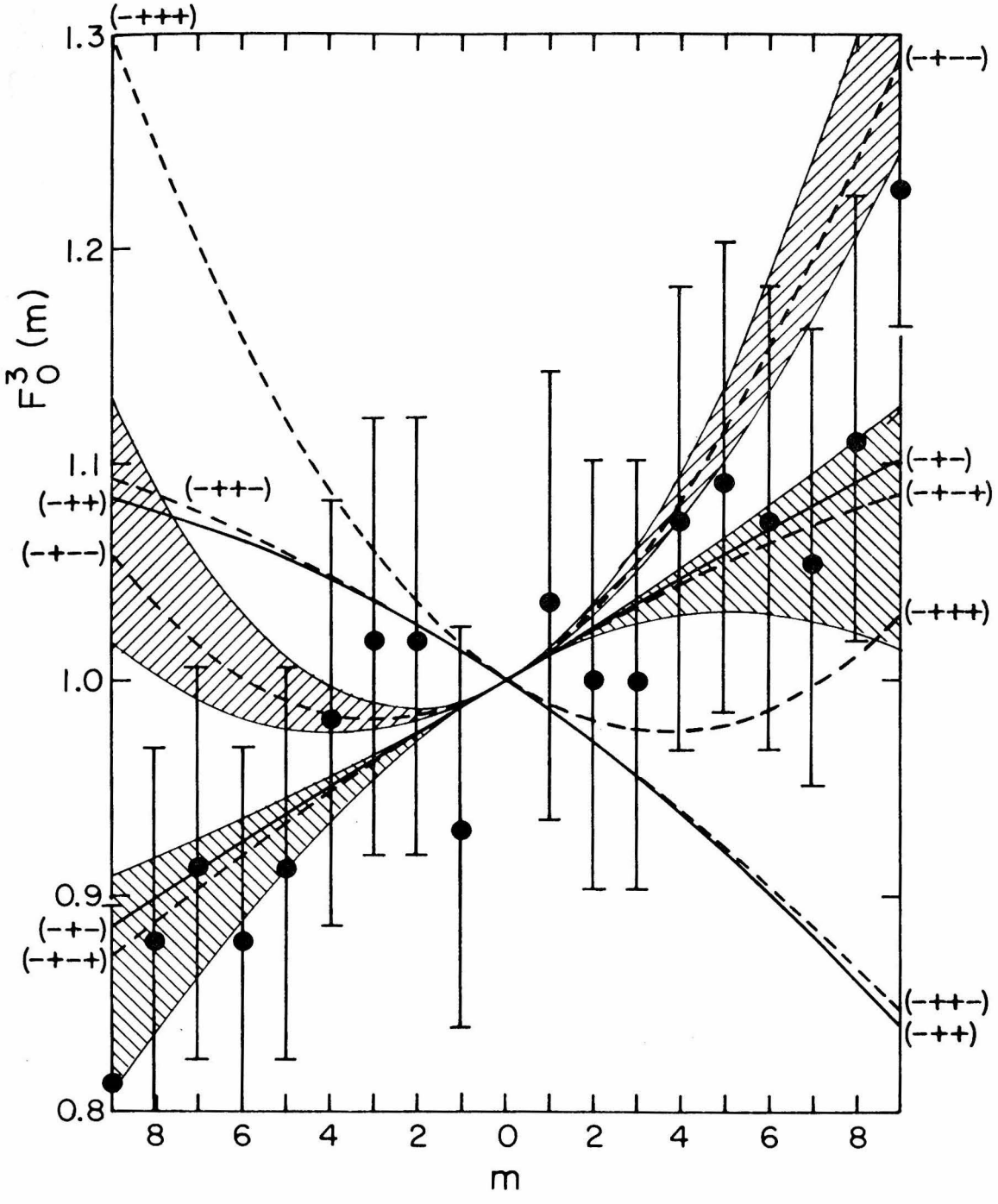

Figure 4.

4. VIBRATION-ROTATION INTERACTION IN THE FOURTH AND FIFTH VIBRATIONAL BANDS OF HF

VIBRATION-ROTATION INTERACTION IN THE FOURTH AND FIFTH VIBRATIONAL BANDS OF HF*

Robert H. REINER and Aron KUPPERMANN

Arthur Amos Noyes Laboratory of Chemical Physics,† California Institute of Technology, Pasadena, California 91125

(Received)

ABSTRACT

HF rovibrational wavefunctions, obtained from numerical integration of the radial Schrödinger equation, together with line strengths measured in the third and fourth vibrational overtones, were used to determine the signs and magnitudes of the transition dipole moments of these bands. The transition moments obtained were $\langle 0|M(R)|4\rangle = -1.36 \times 10^{-4}$(a.u.) and $\langle 0|M(R)|5\rangle = 3.33 \times 10^{-5}$(a.u.). A quintic Taylor series expansion of the dipole moment operator, M(R), was obtained by fitting M(R) to the rovibrational matrix elements of the first five vibrational bands. Transition moments between ground and upper levels of HF (6-9) and DF (0-9) predicted using this M(R) do not agree with those estimated previously using lower-order nonrotating Taylor series approximations.

---

* This work was supported in part by a contract (EY-76-S-03-0767) from the U.S. Energy Research and Development Administration. Report Code: CALT-767P4- .

† Contribution No.

1. Introduction

Meredith and Smith [1] determined the signs and magnitudes of the first three vibrational transition moments of HF. Using these moments, they constructed a cubic Taylor series approximation for the transition dipole moment operator, M(R), and used this approximation of M(R) to estimate the remaining moments. Recently Rimpel [2] measured the magnitudes of the fourth and fifth vibrational transition moments, M_0^4 and M_0^5, and found them to be in poor agreement with the results predicted by Meredith and Smith.

The failure of Meredith and Smith's cubic Taylor series approximation to describe accurately M(R) for HF is not surprising. In a previous paper, we predicted that a fifth- or sixth-order Taylor series expansion of M(R) would be necessary to adequately estimate the signs and magnitudes of the first nine vibrational transition moments in an "HF-type" molecule [3].

In this work, we resolve the sign ambiguity of M_0^4 and M_0^5 employing the rovibrational band analysis used previously [1, 4]. Knowing the proper signs for transition moments, a fifth-order Taylor series expansion of M(R) is found which fits the 57 measured rovibrational moments in the first five vibrational bands of HF. The remaining transition moments for HF (6-9) and DF (1-9) are calculated using this M(R) and compared with those calculated previously.

2. Computational Procedures

Taylor series approximations were fitted to the experimental results by solving the necessary linear equations using the procedures described earlier [4]. The matrix elements for HF were evaluated using the rovibrational wavefunctions determined previously [3].

For DF, the vibrational constants, ω_e and $\omega_e x_e$, determined from infrared absorption experiments [5], were used to calculate the positions of the next seven vibrational energy levels and the corresponding RKR potential using the procedure explained in Section 4.1 of ref. [3]. This potential is displayed in table 1. The rovibrational wavefunctions of DF were then obtained by integration of the radial Schrödinger equation {eq.(5) of ref.[3]} using this internuclear potential and the procedure described in Section 4.2 of ref.[3].

3. Results

3.1 Sign determination of the matrix elements

In figs. 1-5 the absolute values of the rovibrational transition moments $|M_{0,J}^{v,J'}|$ are shown as a function of the rotational index, m {see eq.(2) of ref.[4]}, for the first five vibrational bands of HF. The experimental results for the fundamental band are from [6], the first overtone from [7], the second overtone from [8], and the third and fourth overtones from [2].

Analysis of the first three vibrational bands by Meredith and Smith has established that $M_0^1 > 0$, $M_0^2 < 0$, and $M_0^3 > 0$. Using Rimpel's value for $|M_0^4| = 1.37 \times 10^{-4}$ (a.u.), we construct two quartic Taylor series approximations for M(R), one for each choice of sign of M_0^4. In figs. 3 and 4 we see that choosing $M_0^4 < 0$ (dashed line) seems to fit the experimental rovibrational moments better than choosing $M_0^4 > 0$ (dotted line). Because of the scatter in the experimental results, the sign choice is not as obvious as in earlier work with HI [4] but as shown in table 2, choosing $M_0^4 < 0$ minimizes the variance of $M_{0J}^{vJ'}$,

$$\sigma^2(M_{0J}^{vJ'}) = \sum (M_{0,J_{calc}}^{v,J'} - M_{0,J_{exp}}^{v,J'})^2.$$

Using Rimpel's value for $|M_0^5| = 3.46 \times 10^{-5}$ (a.u.) and $M_0^4 = -1.37 \times 10^{-4}$ (a.u.) determined in the preceding paragraph, we now construct two quintic Taylor series approximations for M(R). In fig. 5 we see that choosing $M_0^5 > 0$ (dashed line) fits the rovibrational moments in the fifth vibrational band of HF better than $M_0^5 < 0$ (dotted line). The effect of changing the sign of M_0^5 on the rovibrational moments in the

fourth and fifth vibrational bands is shown quantitatively in table 2. Clearly $M_0^5 > 0$.

3.2 Least squares optimization of Taylor series coefficients

Now that the signs and magnitudes of the 57 rovibrational transition moments in the first five vibrational bands of HF have been determined, the rovibrational Taylor series expansion of M(R) may be calculated. Previously we were able to obtain one additional term in the Taylor series expansion by using the rovibrational fitting procedure if the experimental rovibrational moments were accurate [9]. However, we see that the experimental uncertainty in rovibrational moments in the third and fourth overtones is too large to justify using a sixth-order Taylor series. Instead, the 57 rovibrational moments and $M_0^0 = 0.7156$ (a.u.) [1] are fitted to a quintic Taylor series which has the following coefficients: $M_0 = 0.7072$ (a.u.), $M_1 = 0.3091$ (a.u.), $M_2 = -2.394 \times 10^{-2}$ (a.u.), $M_3 = -8.530 \times 10^{-2}$ (a.u.), $M_4 = -1.813 \times 10^{-2}$ (a.u.), and $M_5 = -3.008 \times 10^{-2}$ (a.u.). Systematically discarding all experimental rovibrational transition moments that were greater than 3σ away from the calculated values of $M_{0,J}^{V,J'}$ (two values discarded), we obtained a second set of Taylor coefficients: $M_0 = 0.7064$ (a.u.), $M_1 = 0.3167$ (a.u.), $M_2 = -8.261 \times 10^3$ (a.u.), $M_3 = -7.251 \times 10^{-2}$ (a.u.), $M_4 = -1.067 \times 10^{-2}$ (a.u.), and $M_5 = -2.555 \times 10^{-2}$ (a.u.). The second set of coefficients was used to compute M(R). In figs. 1-5 it is evident that the rovibrational quintic Taylor series yields much better rovibrational moments than the nonrotating quintic Taylor series.

The transition moments between the ground and higher vibrational states of HF calculated using this rovibrational quintic Taylor series are listed in column 2 of table 3. For comparison, transition moments calculated using the nonrotating quintic Taylor series obtained by Rimpel [2] and the nonrotating cubic Taylor series are listed in columns 3 and 4 of this table. The matrix elements of the quartic rovibrational M(R) for all vibrational states with $v \leq 9$ are given in table 4.

3.3 Deuterium fluoride transition moments

Within the accuracy of the Born-Oppenheimer approximation, the M(R) of HF and DF are identical. Using the DI vibrational wavefunctions together with the quintic rovibrational series approximation for M(R), we obtain the transition moments shown in column 5 of table 3. Transition moments of the cubic rotationless Taylor series are listed in column 6 for comparison. Matrix elements of the quintic rovibrational M(R) for all DI vibrational states with $v \leq 9$ are given in table 5.

4. Discussion

The results displayed in table 3 are in striking contrast to those reported previously for HI [4]. In that paper we found that all Taylor series approximations for M(R) of third order or greater predicted approximately the same vibrational transition moments. The reason for this was that in HI the vibrational wavefunctions of interest sampled a region where M(R) was monotonic. A reasonable approximation of M(R) could be obtained with a cubic Taylor series. However, in table 3 we see significant differences between transition moments predicted by the cubic and quintic Taylor series. The reason for this constrast is that M(R) for HF is not monotonic in the region of R sampled by its vibrational wavefunctions. Instead, M(R) passes through a maximum at a distance far from R_e but still sampled by the vibrational wavefunctions. As a result, higher-order terms in the Taylor series expansion of M(R) are needed to describe M(R).

In the case of our "hypothetical" HF molecule [3], the quintic Taylor series was the lowest-order approximation which yielded the correct transition moment signs for $v \leq 8$ and reasonable magnitudes for $v \leq 7$. It is quite possible that more terms are needed to estimate transition moments for $v \leq 9$ for the real HF and DF molecules. The results in tables 4 and 5 should, therefore, be used with caution.

References

[1] R. E. Meredith and F. C. Smith, J. Quant. Spectrosc. Radiat. Transfer 13 (1973) 89.

[2] G. Rimpel, Z. Naturforsch. A 29 (1974) 588.

[3] R. H. Reiner and A. Kuppermann, manuscript in preparation.

[4] R. H. Reiner and A. Kuppermann, J. Chem. Phys., submitted for publication.

[5] R. N. Spanbauer, K.-N. Rao and L. M. Jones, J. Mol. Spectrosc. 16 (1965) 100.

[6] R. J. Lovell and W. F. Herget, J. Opt. Soc. Am. 52 (1962) 1374.

[7] R. E. Meredith, J. Quant. Spectrosc. Radiat. Transfer 12 (1972) 485.

[8] R. L. Spelling, R. E. Meredith and F. G. Smith, J. Chem. Phys. 57 (1972) 5119.

[9] R. H. Reiner and A. Kuppermann, manuscript in preparation.

Table 1

RKR potential for the $X\ ^1\Sigma^+$ state of deuterium fluoride[a)]

V	Energy (cm^{-1})	R_{min} (Å)	R_{max} (Å)
0	1,487.656	0.8457380	1.0039274
1	4,394.326	0.8012675	1.0788637
2	7,209.474	0.7741317	1.1373553
3	9,933.100	0.7540182	1.1897751
4	12,565.204	0.7379627	1.2391538
5	15,105.786	0.7246217	1.2869081
6	17,554.846	0.7132533	1.3338613
7	19,912.384	0.7033974	1.3805638
8	22,178.400	0.6947459	1.4274248
9	24,352.894	0.6870802	1.4747765
10	26,435.866	0.6802387	1.5229084
11	28,427.316	0.6740972	1.5720902
12	30,327.244	0.6685575	1.6225857
13	32,135.650	0.6635396	1.6746654
14	33,852.534	0.6589768	1.7286162
15	35,477.896	0.6548115	1.7847527

a) Spectroscopic constants determined by Spanbauer and Rao [5]. The method is described in Section 4.1 of ref. [3].

Table 2

Sign determination of M_0^4 and M_0^4

Order of M(R)	Vibrational Transition	M_0^4	M_0^5	$\sigma^2(M_{0J}^{vJ'})$ (variance) (arbitrary units)
4	0 → 3	-		0.534
4	0 → 3	+		1.51
4	0 → 4	-		7.89
4	0 → 4	+		27.9
5	0 → 4	-	+	8.37
5	0 → 4	-	-	13.2
5	0 → 5	-	+	1.14
5	0 → 5	-	-	5.17

Table 3

Vibrational transition moments of HF and DF (in atomic units)

Moment	HF			DF	
	Quintic Rovibrational	Quintic [2] Taylor	Cubic [1] Taylor	Quintic Rovibrational	Cubic [1] Taylor
M_0^0	0.715	0.716	0.716	0.713	0.713
M_0^1	0.387(-1)	0.388(-1)	0.388(-1)	0.331(-1)	0.331(-1)
M_0^2	-0.489(-2)	-0.493(-2)	-0.493(-2)	-0.345(-2)	-0.348(-2)
M_0^3	0.647(-3)	0.641(-3)	0.641(-3)	0.382(-3)	0.369(-3)
M_0^4	-0.136(-3)	-0.137(-3)	-0.966(-4)	-0.681(-4)	-0.501(-4)
M_0^5	0.333(-4)	0.346(-4)	0.131(-4)	0.149(-4)	0.880(-5)
M_0^6	-0.879(-5)	-0.954(-5)	0.178(-7)	-0.357(-5)	-0.194(-5)
M_0^7	0.211(-5)	0.250(-5)	-0.138(-5)	0.739(-6)	0.377(-6)
M_0^8	-0.341(-7)	-0.241(-6)	0.103(-5)	-0.432(-7)	-0.327(-8)
M_0^9	-0.577(-6)	-0.465(-6)	-0.665(-6)	-0.569(-8)	0.216(-7)

Table 4

HF vibrational matrix elements $\langle v|M(R)|v'\rangle$ using quintic rovibrational approximation for M(R) (atomic units)

v	0	1	2	3	4	5	6	7	8	9
v′										
0	0.715									
1	0.387(-1)	0.733								
2	-0.489(-2)	0.540(-1)	0.751							
3	0.647(-3)	-0.890(-2)	0.647(-1)	0.767						
4	-0.136(-3)	0.133(-2)	-0.133(-1)	0.722(-1)	0.782					
5	0.333(-4)	-0.317(-3)	0.214(-2)	-0.182(-1)	0.768(-1)	0.794				
6	-0.879(-5)	0.857(-4)	-0.564(-3)	0.311(-2)	-0.238(-1)	0.782(-1)	0.804			
7	0.211(-5)	-0.235(-4)	0.173(-3)	-0.888(-3)	0.424(-2)	-0.303(-1)	0.758(-1)	0.809		
8	-0.341(-7)	0.623(-5)	-0.553(-4)	0.297(-3)	-0.128(-2)	0.555(-2)	-0.379(-1)	0.686(-1)	0.807	
9	-0.577(-6)	-0.151(-5)	0.173(-4)	-0.104(-3)	0.461(-3)	-0.176(-2)	0.709(-3)	-0.468(-1)	0.553(-1)	0.797

Table 5

DF vibrational matrix elements $\langle v|M(R)|v'\rangle$ using quintic rovibrational approximation for M(R) (atomic units)

v	0	1	2	3	4	5	6	7	8	9
v'										
0	0.713									
1	0.331(-1)	0.726								
2	-0.345(-2)	0.464(-1)	0.739							
3	0.382(-3)	-0.623(-2)	0.562(-1)	0.752						
4	-0.681(-4)	0.793(-3)	-0.919(-2)	0.638(-1)	0.764					
5	0.149(-4)	-0.159(-3)	0.130(-1)	-0.124(-1)	0.698(-1)	0.776				
6	-0.357(-5)	0.376(-4)	-0.289(-3)	0.191(-2)	-0.159(-1)	0.741(-1)	0.787			
7	0.739(-6)	-0.101(-4)	0.774(-4)	-0.463(-3)	0.262(-2)	-0.198(-1)	0.768(-1)	0.796		
8	-0.432(-7)	0.328(-5)	-0.233(-4)	0.134(-3)	-0.680(-3)	0.344(-2)	-0.242(-1)	0.777(-1)	0.804	
9	-0.569(-8)	-0.140(-5)	0.774(-5)	-0.426(-4)	0.212(-3)	-0.950(-3)	0.440(-2)	-0.290(-1)	0.764(-1)	0.809

Figure Captions

Fig. 1. Magnitude of rovibrational transition moments as a function of rotational index m for the fundamental band of HF. Open circles are the measurements of Lovell and Herget [6]. The solid line is the calculated behavior of the rovibrational moments using both the qunitic Taylor series and the quintic rovibrational Taylor series.

Fig. 2. Magnitude of rovibrational transition moments as a function of rotational index m for the first vibrational overtone of HF. Open circles are the measurements of Meredith [7]. The solid line is the behavior predicted by the quintic rovibrational series and the dashed line represents the behavior predicted by the quintic nonrotational Taylor series.

Fig. 3. Magnitude of rovibrational transition moments as a function of rotational index m for the second vibrational overtone of HF. Open circles are the measurements of Spelling, Meredith and Smith [8]. The dashed line is the behavior predicted by a quartic Taylor series assuming $M_0^4 < 0$, and the dotted line is the behavior predicted choosing $M_0^4 > 0$. The solid line is the quintic rovibrational Taylor series result.

Fig. 4. Magnitude of rovibrational transition moments as a function of rotational index m for the third vibrational overtone of HF. Open circles are the measurements of Rimpel [2]. The dashed line is the behavior predicted by a quartic Taylor series assuming $M_0^4 < 0$, and the dotted line is the behavior predicted using $M_0^4 > 0$. The solid line is the quintic rovibrational Taylor series result.

Fig. 5. Magnitude of rotational transition moments as a function of rotational index m for the fourth vibrational overtone of HF. Open circles are the measurements of Rimpel [2]. The dashed line is the

behavior predicted by a quintic Taylor series assuming $M_0^5 > 0$. The dotted line is the behavior predicted assuming $M_0^5 < 0$. The solid line is the rovibrational quintic result.

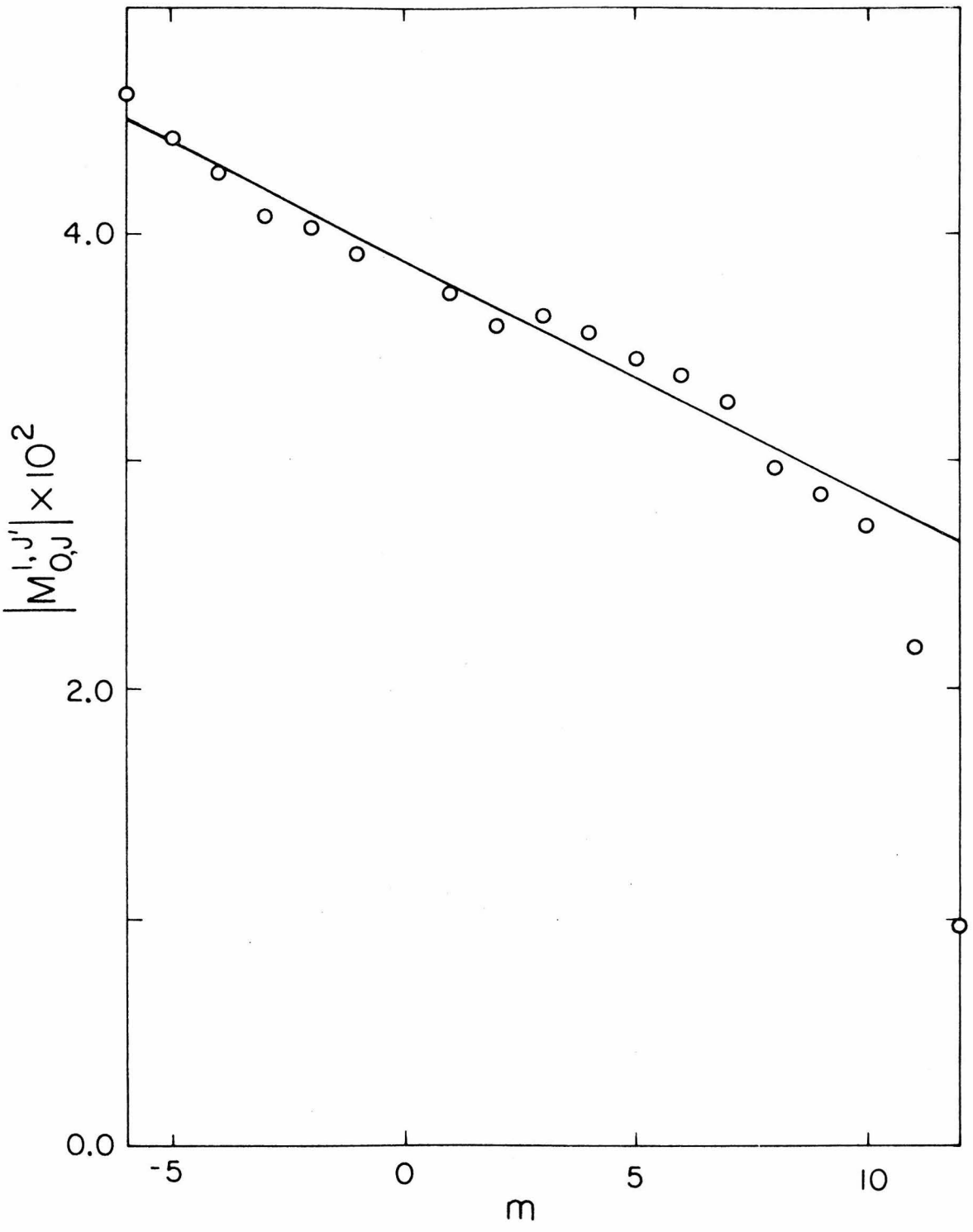

Figure 1.

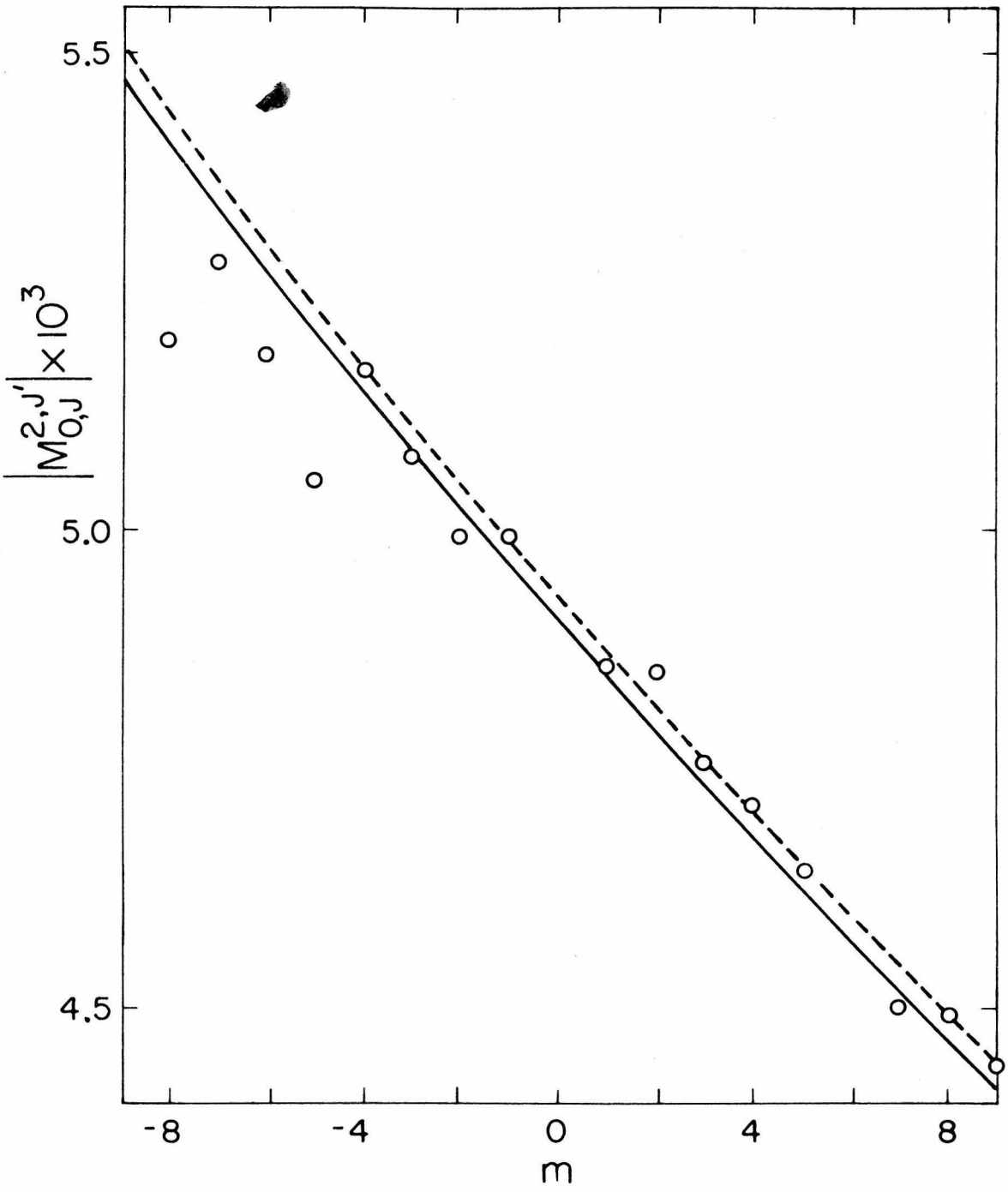

Figure 2.

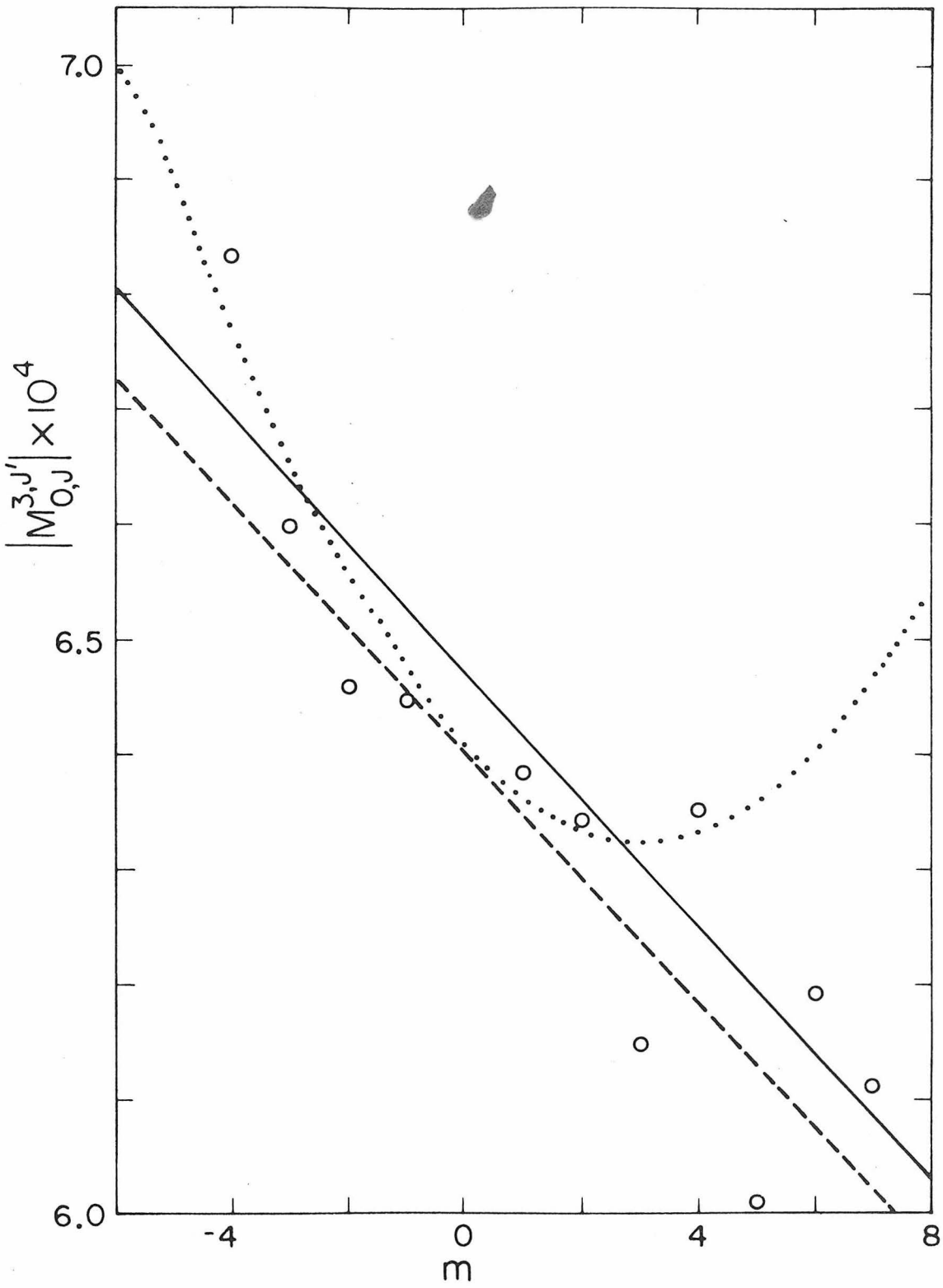

Figure 3.

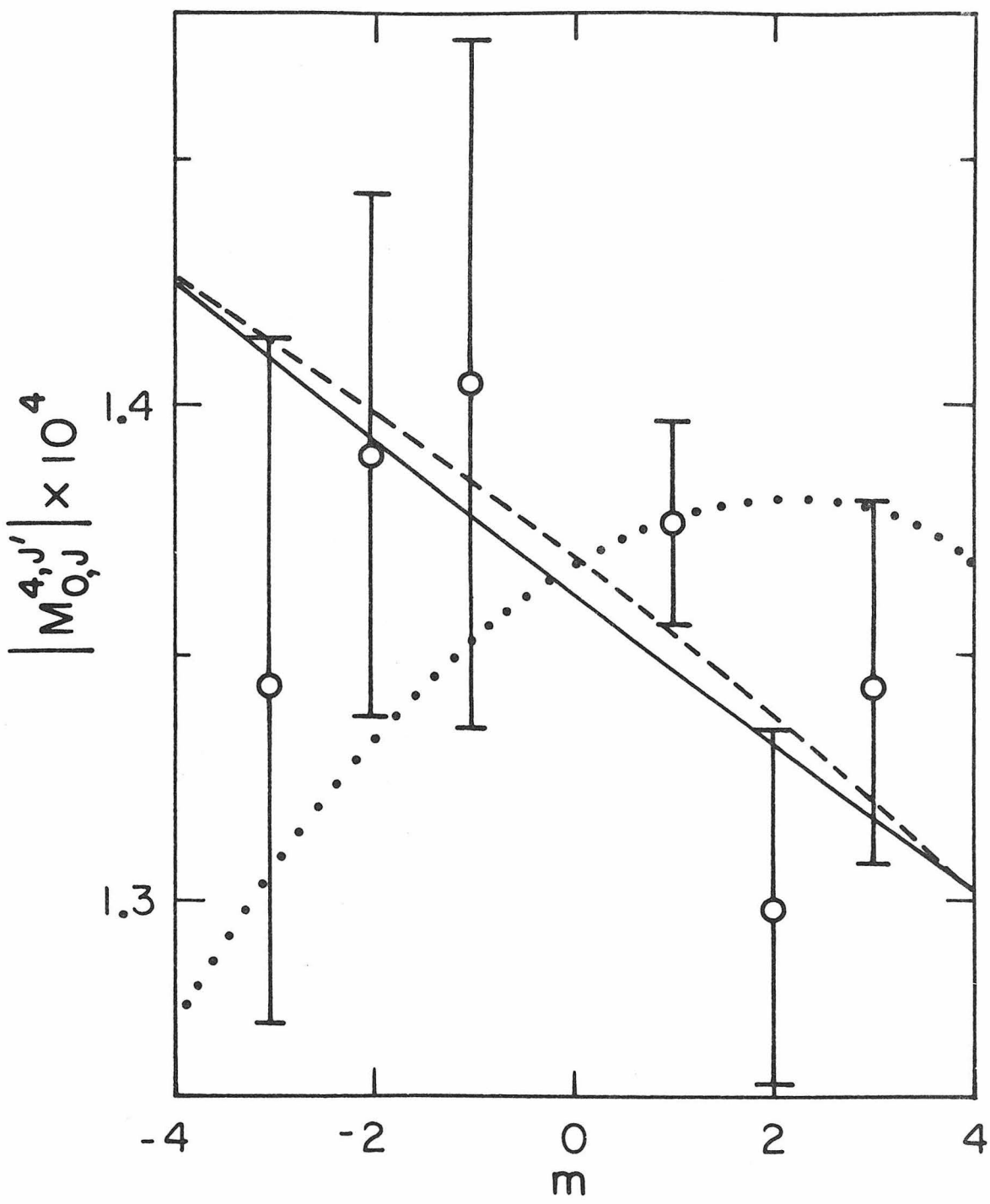

Figure 4.

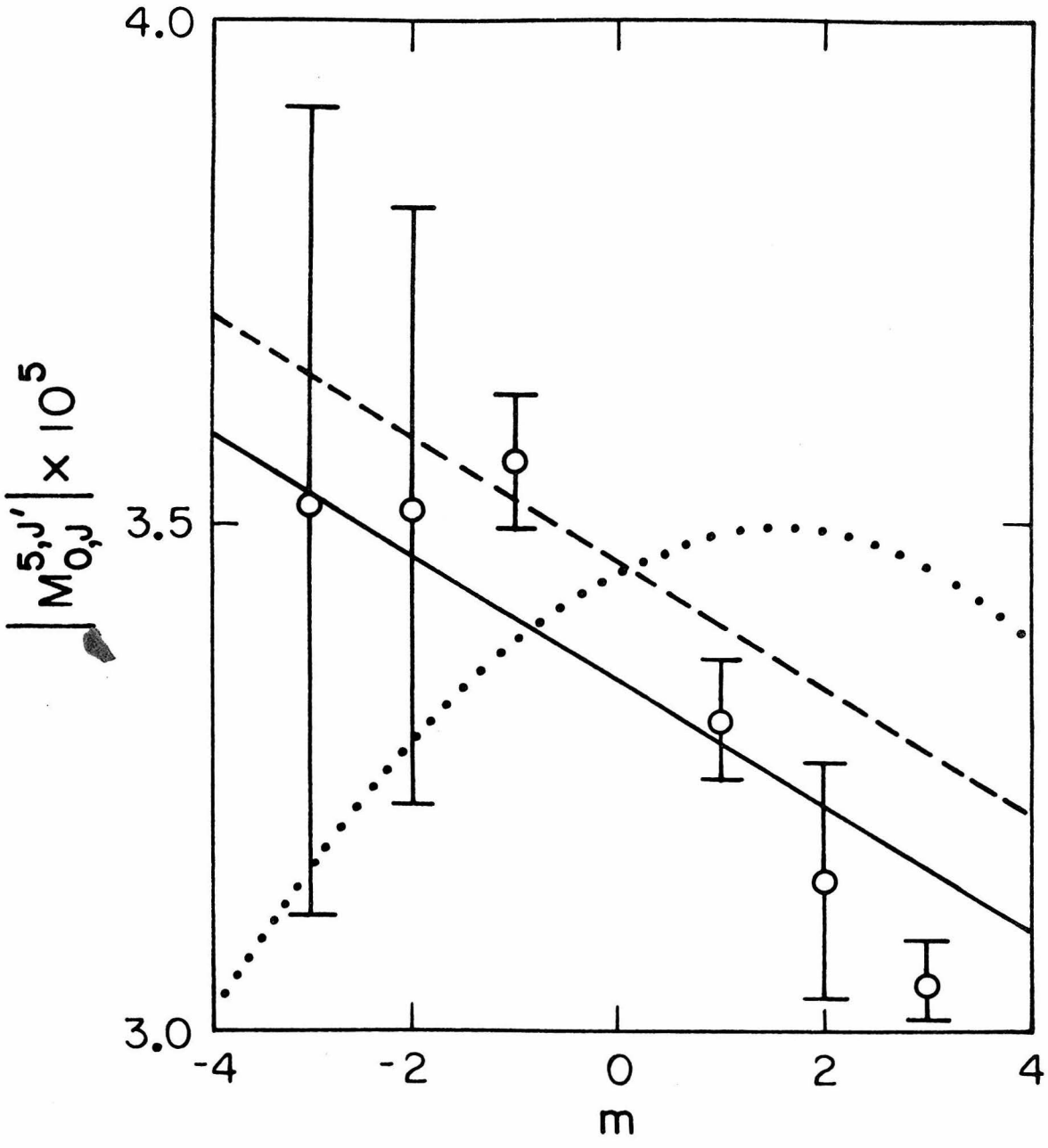

Figure 5.

5. REACTION AND VIBRATIONAL RELAXATION IN HYDROGEN IODIDE

Reaction and vibrational relaxation in hydrogen iodide*

Robert H. Reiner and Aron Kuppermann

Arthur Amos Noyes Laboratory of Chemical Physics,†
California Institute of Technology, Pasadena, California 91125

(Received)

ABSTRACT

Thermal and photochemical decomposition studies were performed on HI. The wavelength of the light used was longer than that required for the production of electronically excited HI. The following results were observed: (1) A small first-order component in the dark (thermal) reaction was detected in addition to the well-known second-order component. (2) The activation energy of the second-order reaction component between 660 and 710 K is 52.9 ± 2.8 kcal/mole as compared with the 44 kcal/mole previously reported. (3) The rate of the HI decomposition was enhanced in the photochemical experiments. However, a kinetic analysis indicated that this enhancement was due to thermal heating of the system by absorption of the light rather than by the reaction of vibrationally excited HI away from thermal equilibrium. (4) Theoretical estimates of vibrational reaction and relaxation rates suggest experimental conditions which could lead to observation of vibrational enhancement of this reaction.

---

* This work was supported in part by a contract (EY-76-S-03-0767) from the U.S. Energy Research and Development Administration. Report Code: CALT-767P4-148.

† Contribution No. 5391.

1. INTRODUCTION

The availability of high intensity tunable dye lasers has made possible the study of chemical reactions of highly vibrationally excited molecules. In addition to elucidating the role of vibrational energy in chemical reactions, [1-5] the monochromaticity of the laser, combined with the narrow bandwidth of the vibrational lines may provide a practical means of isotopic separation. [6, 7]

Except when these studies are made under controlled conditions, such that the reactants are state selected and can only undergo single collisions (as in crossed molecular beams[3]), interpretation of the results is not straightforward. For example, in a typical bulk gas phase experiment, [8, 9] a high intensity chemical or glass laser is focused into a thermostated reaction cell. Reaction rates are then measured as a function of light intensity, concentration of reactants and buffer gases and any other parameters which can help distinguish the effects of thermal heating from those of vibrational excitation. This is not a trivial matter since the average internal state energy of the absorbing molecules may correspond to a temperature many hundreds of degrees higher than the thermostated cell walls. [8] It is quite possible that the vibrationally excited reactants may be collisionally deactivated before reaction with another molecule, resulting in high rotational and translational energies also. Thus an observed rate increase may not be due to vibrational excitation but to heating effects produced by the intense light source needed in the photolysis. Several techniques have been tried, with varying degrees

of success, to eliminate or at least to separate the effects of thermal heating from those of vibrational excitation. Braun et al.[10] used a modulated CO_2 laser to successfully differentiate between vibrational energy and thermal heating when the reaction of vibrationally excited ozone with NO was studied. Bailey et al.[8] analyzed the induction period as a function of laser power in the unimolecular description of ethyl chloride. The results were not conclusive. Yogev and Loewenstein-Benmair[9] had some success analyzing the decomposition of trans-2-butene by comparing the product distributions of photolyzed samples with those in thermal samples.

Hydrogen iodide seems to be a good candidate for producing highly excited vibrational states. It is a diatomic molecule with relatively large vibrational spacing and large electric dipole transition anharmonicity. The activation energy for the thermal reaction

$$2HI \rightarrow H_2 + 2I \qquad (A)$$

is reported to be only 44 kcal/mole.[11-13] A molecular beam study done by J. B. Anderson[14] showing that translational energy by itself is not effective in promoting reaction (A) suggests that vibrational energy plays an important role in this reaction.

If it were possible to produce a sufficient population of $HI^{\dagger}$ (v = 7, 8, or 9), then one could study the vibrationally excited analog of reaction (A),

$$HI^{\dagger} + HI \rightarrow H_2 + 2I\,. \qquad (B)$$

An analysis of the results of such experiments would involve a consideration of reactions (A) and (B) as distinct mechanistic steps. In the next section we describe such an approach. In Section 3 we give the techniques used to perform such experiments, in Section 4 we present the results,and in Section 5 we discuss their meaning and suggest modified conditions under which these experiments should be attempted in the future.

2. KINETIC ANALYSIS

The feasibility of using a multiple quantum transition to pump reaction (B) in the gas phase is now considered. Suppose a vessel containing HI is irradiated with an intense visible light source to induce a transition from the ground state to a high vibrational level of this molecule (λ = 643 nm for a $0 \rightarrow 8$ transition). Observation of increased reaction rate in the photolyzed sample above that in the non-photolyzed sample is a necessary but not a sufficient indication of rate enhancement due to vibrational excitation; a detailed analysis of the reaction kinetics is necessary to determine the effect of vibrational excitation.

Let us assume the following mechanism describes the above experiment:

$$HI + h\nu \rightarrow HI^{\dagger} \qquad (C)$$

$$HI^{\dagger} + HI \rightarrow HI + HI \qquad (D)$$

$$HI^{\dagger} + HI \rightarrow H_2 + 2I \qquad (B)$$

$$HI + HI \rightarrow H_2 + 2I \qquad (A)$$

where $HI^{\dagger}$ stands for a vibrationally excited HI molecule. Assuming the validity of the steady state approximation and that only a small fraction of the incident light is absorbed by the HI, as is the case in the present experiments, one obtains

$$[HI^{\dagger}]_{ss} = \frac{I_0 S_{HI} \ell}{(k_B + k_D)V} \qquad (1)$$

where ℓ is the absorption path length, V is the cell volume, S_{HI} is the

strength for the pumped transition v, k_B and k_D are the rate constants for reactions (B) and (D), and I_0 is the continuum light source intensity per unit frequency. We see that $[HI^\dagger]_{SS}$ is independent of [HI] and therefore reaction (A) is second order in [HI], whereas reaction (B) is first order in this concentration. The rate of H_2 formation is

$$\frac{d[H_2]}{dt} = \tfrac{1}{2}k_B[HI^\dagger][HI] + \tfrac{1}{2}k_A[HI]^2 , \qquad (2)$$

where k_A and k_B refer to the rate constants for HI (plus $HI^\dagger$) disappearances. The effect of reaction (B) is entirely contained in the first-order term in [HI] of the right-hand side of this equation, which may be rewritten as

$$\frac{2}{[HI]}\frac{d[H_2]}{dt} = k' + k_A[HI] . \qquad (3)$$

Equation (3) indicates that a plot of $(2/[HI])(d[H_2]/dt)$ against [HI] should be a straight line which does not pass through the origin. Its slope, k_A, is the thermal rate constant and its intercept, k', is $k_B[HI^\dagger]_{SS}$.

From k_A, an internal reaction temperature may be obtained using the known temperature dependence of reaction (A) from our thermal (dark) experiments. This temperature is more appropriate as a measurement of the bulk gas phase temperature than that measured at the cell walls, due to the large amount of power that is pumped into the cell. The linear intercept of Eq. (3) contains information about the vibrationally excited reaction (B) of interest.

3. EXPERIMENTAL

In preliminary experiments, continuum radiation (suitably filtered to prevent electronic excitation of HI) from a 2.5 kW xenon arc lamp (Hanova 975 C-98) was focused into a photolysis vessel. A continuum source was used because the wavelength of the HI ($v = 0, J \rightarrow v' = 8, J'$) transition was not known within the accuracy needed to tune a dye laser. The vessel, a 10 cm diameter hollow quartz sphere A (see Fig. 1) was gold-plated (bright white gold #10 - Hanova liquid gold). Since the gold coating has a high reflectivity (greater than 0.85 for $\lambda > 640$ nm),[15] this modification increased the optical path by a factor of 50 over a conventional cylindrical photolysis cell of equal volume. The vessel was wrapped with many layers of aluminum foil (overall thickness of about 1 cm) to improve the temperature homogeneity.

This photolysis vessel was mounted in a resistance-heated oven whose temperature was regulated with a platinum resistance thermometer bridge (Hallikainen Thermotrol 1472 A). Temperature was measured with six iron-constantan thermocouples placed into indentations about 1 cm deep distributed around the vessel. Each of the six thermocouples was calibrated against the same mercury thermometer, itself checked at 273.15 K and 373.15 K. The average deviation between the six temperature readings during an experiment was less than 1.0 K. The temperature drift of the vessel during an experiment was less than 0.1 K. A mercury-free vacuum line attached to the vessel was used to transfer the reactants and products to and from bulb A.

A resistance-heated, molten-lead thermostated bath was used for two additional dark experiments. The liquid lead bath was stirred and its temperature regulated to within 0.1 K using the platinum resistance thermometer bridge described above. A second platinum resistance thermometer, NBS calibrated, was used to measure the bath temperature.[16]

Hydrogen iodide (Matheson Gas Products, 98% min. purity) was vacuum distilled three times from an acetone slush bath (180 K), the center one-third fraction being retained after such distillation. Hydrogen iodide pressures were measured using a pressure transducer (Celesco Industries P7D) which had been calibrated against a mercury manometer. Pressures between 0 and 500 torr were measured accurately to 0.1 torr.

After photolysis, HI and I_2 from the reaction mixture were condensed into bulb B using a liquid nitrogen bath. The uncondensed H_2 product was added to a known amount of helium (Matheson, 99.995%) by expansion into bulb C of Fig. 1. The hydrogen and helium parent ion peaks of this mixture were then measured in a mass spectrometer (Consolidated Electrodynamics Corporation, 21-103C) that had been precalibrated with hydrogen and helium mixtures of known composition, similar to that of the unknown mixture prepared on a Saunders-Taylor apparatus. The hydrogen-to-helium ratio could be measured with an accuracy of 2%.

4. RESULTS

According to Eq. (3) a plot of $(2/[HI])(d[H_2]/dt)$ against [HI] should be a straight line with a non-zero intercept. It was found that this was, in fact, this case. Typical plots for a photolyzed and a non-photolyzed sample are shown in Fig. 2. This indicates that the empirical rate law describing the appearance of H_2 is indeed of the form of Eq. (3). The fractional [HI] decomposition in all the experiments reported here was about 2% or less. The results of experiments conducted at various temperatures are summarized in Table I. In addition to the six photolyses and four dark experiments made using the original quartz cell, two experiments (one photolysis, one dark) were performed using a cell to which quartz wool had been added. The quartz wool increased the surface-to-volume ratio of the cell by a factor of about 300.

Column 3 (Table I), labeled T_{wall}, gives the average of the temperature readings of the six thermocouples (or platinum resistant thermometer in experiments 11 and 12). An Arrhenius plot of our k_A values using this temperature is given in Fig. 3, in which the straight line is obtained from a linear regression analysis using the values for experiments 9 through 12. The corresponding second-order thermal rate constant, k_A, is given by $\log k_A(\text{liter mole}^{-1}\ \text{sec}^{-1}) = (13.5_7 \pm 0.9_0) - (52._9 \pm 2._8)\text{kcal}/2.303\ RT$. Indicated also in that figure (but not used in the regression analysis) are points obtained by Sullivan[11a] and Taylor and Crist;[12] these are discussed in detail in Sec. 5.1. The values of T_{gas} given in column 4 are obtained from this straight line as discussed at the end of Sec. 2.

It is apparent from column 5 of Table I that $\Delta T \equiv T_{gas} - T_{wall}$ is clearly greater than zero and significantly greater than any error in the thermocouple measurements. We attribute the large positive values of ΔT to a temperature gradient across the cell wall produced by absorption of light. Using the line strength estimates made elsewhere[17] and the known spectral emission of the light source, we estimated the expected temperature increase in the HI due to absorption of the radiation to be about 0.02 K. This is too small to explain the observed values of ΔT. However, we calculated the temperature gradient across the wall of the reactor, due to absorption of light by the quartz and the gold coating, and obtained an inner wall temperature between 2°K and 12°K higher than that of the outer wall of the reactor. The gas is expected to be in thermal equilibrium with the inner wall.

In columns 6-9 of the table, the results of experiments similar to those displayed in Fig. 2 are presented. A linear regression analysis was performed to find the most probable straight line [Eq.(3)] through the experimental points. σ_{k_A} and $\sigma_{k'}$ are the standard deviations in the slope, k_A and intercept, k'.

When an Arrhenius plot of k', the observed first-order rate coefficient, is made using the observed wall temperature, T_{wall}, linear plots are obtained for both the photolyses and dark reaction results. The corresponding Arrhenius lines seem to differ from each other (see Fig. 4). However, if the corrected gas phase temperature, T_{gas}, is used instead (Fig. 5), the photolyses results are shifted to higher temperatures and the two lines are not as distinct. Linear regression analyses of the points in Fig. 5 yield the following

expressions for the first-order rate constants: $\log k'(sec^{-1}) = (1._0 \pm 1._1) - (22._7 \pm 3._5)$ kcal/2.303 RT and $\log k'(sec^{-1}) = (4._8 \pm 0._5) - (34._5 \pm 1._4)$kcal/2.303 RT for the dark and thermal reactions, respectively. Using both sets of data we obtain the dotted line in Fig. 5 whose equation is given by $\log k'(sec^{-1}) = (4._3 \pm 0._4) - (32._9 \pm 1._3)$kcal/2.303 RT. Since the dotted line (which includes both thermal and photolyzed results) is not significantly different from the solid line (only photolyzed results), we conclude that the rate increase in the photolyzed samples is primarily a thermal heating effect. Vibrational excitation (if any) is smaller than the experimental uncertainty in the measurement of k′.

The source of the linear intercept, k′, is thus far unexplained. In order to obtain more information about it, we performed several blank experiments using empty reaction vessels. These indicated the following behavior.

(a) Even after pretreating a reaction vessel by heating it to a dull red color while maintaining it under diffusion pump vacuum (as recommended by others[12]) hydrogen evolved in a blank experiment conducted immediately thereafter at 711.4 K using that vessel.

(b) The rate of hydrogen evolution from a blank reaction vessel at a given temperature was not constant, decreasing significantly with heating time.

(c) A significant amount of hydrogen evolved from an empty vessel even at room temperature.

(d) The initial rate of hydrogen evolution in these blank experiments accounted for a large fraction of the observed values of k′ (of the order of 25% to 95%).

The meaning of these observations is discussed in the following section.

5. DISCUSSION

5.1 Origin of the first order component of the dark and photolysis experiments

In the previous section we concluded that the empirically observed first-order term, k', was not due to the presence of vibrationally excited $HI^{\dagger}$ as implied by reaction (B) in the mechanism of Section 2. The actual origin of this term for the dark and the photolysis experiments is therefore very puzzling. From the blank experiments described at the end of the previous section, one is tempted to conclude that it is related to the evolution of hydrogen from the quartz walls of the reaction vessel. However, when quartz wool was added to the vessel, thereby increasing the surface to volume ratio by a factor of about 300, k' was unchanged (see results of experiments 7 and 8 of Table I). In addition, similar non-zero intercepts are seen in the thermal data of Crist and Taylor[12] shown in Fig. 6, although they measure the rate of HI disappearance rather than that of H_2 appearance. We obtain from their results, $k' = (1.1_2 \pm 0.1_7) \times 10^{-6}$ sec^{-1} at 667 K and $(2.7_4 \pm 0.8_0) \times 10^{-6}$ sec^{-1} at 699 K. Unfortunately, similar analyses performed on other experimental results[18, 19] are inconclusive because of excessive scatter in those data. In Fig. 7, an Arrhenius plot of k' is displayed for all of these experiments, including our own. As can be seen, they all scatter around a single straight line whose equation is $\log k'\ (sec^{-1}) = (5.1_8 \pm 0.8_5) - (35._6 \pm 2._7)$ kcal/2.303 RT.

While we are not claiming that the gas phase thermal decomposition of HI necessarily has a homogeneous first-order component, it is evident that some previously determined thermal rate constants for this reaction are subject to question. When a second-order rate constant is calculated from a plot of $-(1/[HI])(d[HI]/dt)$ versus $[HI]$, assuming that that plot is a straight line which is forced to pass through the origin, a biased value for the slope of that line will be obtained if that line actually has a non-zero intercept. This is a non-trivial point. If one defines the correct second-order rate constant as the slope of that straight line, the values from the data of Crist and Taylor[13] displayed in Fig. 6 are $(1.8_1 \pm 0.12) \times 10^{-4}$ and $(1.0_4 \pm 0.06) \times 10^{-3}$ liter mole^{-1} sec^{-1} at 667 and 699 K, respectively, whereas by forcing the plots to go through the origin those authors obtain the values $(2.5_9 \pm 0.1_0) \times 10^{-4}$ and $(1.24_2 \pm 0.03_7) \times 10^{-3}$ liter mole^{-1} sec^{-1}, respectively. The differences in the two methods are therefore 43% at 667 K and 19% at 699 K. In the Arrhenius plot of Fig. 3 we have included the two sets of Crist and Taylor points just described. It can be seen that the points obtained without forcing the $-(1/[HI])(d[HI]/dt)$ versus $[HI]$ lines to go through the origin fall closer to the Arrhenius line of Fig. 3, than those obtained forcing those lines to go through the origin. Also included in Fig. 3 are two rate constants obtained by Sullivan[12a] from the reverse reaction and the H_2, I_2-HI equilibrium constant.[20] Sullivan's results are also in better agreement with the Arrhenius line than the reported results of Taylor and Crist. It is also interesting that the activation energy determined from Fig. 3 ($52._9 \pm 2._8$ kcal/mole) is in better agreement

with the high temperature results of Graven[18] (49.2 kcal/mole) than is the result reported by Taylor and Crist[12] (44 kcal/mole). In view of the great importance that thermal reaction (A) and its reverse play in the fundamental aspects of gas phase kinetics, the linear intercept anomaly discussed here should be subject to a further and more detailed experimental investigation.

5.2 Estimation of ϵ_{HI}, k_D and k_B

The mechanism of Section 2 permits us to obtain a theoretical value of k' from a knowledge of the physical properties S_{HI}, k_B, and k_D and the conditions of the experiment contained in I_0 and ℓ. In this section we estimate the values of S_{HI}, k_B and k_D. In the next section appropriate experimental conditions needed to be able to observe k' are determined using the theoretical estimate of this quantity.

Although $S_{HI}(v)$ has not been measured for $v > 3$, it has been estimated in a another paper[17] (where the notation for this quantity was S_0^v). For $v = 8$, for example, we had obtained $S_0^8 \leq 8 \times 10^{-5}$ $atm^{-1}\ cm^{-2}$.

The deactivation rate constant, k_D, is a weighted average of several processes by which the vibrationally excited HI molecule can relax to the ground vibrational state. These processes include collisional deactivation via vibrational-to-translational (V→T) and vibrational-to-vibrational (V→ V) energy transfer. Infrared fluorescence is slow compared to these collisional processes at pressures above 5 torr. Indeed, the Einstein coefficient $A_{0\leftarrow 1}$ of HI(v=1) is 0.038 sec^{-1},[21] and assuming that the radiative lifetime of $HI^{\dagger}(v)$, τ_v, is no smaller than τ_1/v (the value it would have for a harmonic oscillator[22,23]) we conclude that for $v \leq 8$

$$\tau_v \geq \frac{1}{8} (A_{0\leftarrow 1})^{-1} \approx 3.3\ sec^{-1} . \qquad (4)$$

At pressures greater than 5 torr, $HI^{\dagger}(v)$ will undergo more than 4×10^7 collisions during τ_v. Since only 10^5 collisions are needed to

deactivate $HI(v=1)$ [and $HI^{\dagger}(v>1)$ should deactivate faster] fluorescence can be ignored under our experimental conditions.[24]

Collisional deactivation is therefore the important process for $HI^{\dagger}$ relaxation. Deactivation cross sections have been measured for $HI(v=1)$ and $HI(v=2)$.[24-26] They are 0.0038 A^2 and 0.046 A^2, respectively. The relaxation of $HI(v=1)$ in collision with $HI(v=0)$ (by far the dominant species in this system) can proceed only by a $V \rightarrow T,R$ process. $HI(v=2)$ can also relax by a $V \rightarrow V$ transition. The order of magnitude increase in relaxation cross section in going from $v=1$ to $v=2$ shows that the $V \rightarrow V$ process is much faster than the $V \rightarrow T,R$ in HI. This is true in general.[25] The $V \rightarrow V$ transition is therefore assumed to be the dominant relaxation process for $HI^{\dagger}(v>1)$, and one may assume that k_D is of the same order of magnitude as the rate constant, k_E, of the process

$$HI^{\dagger}(v) + HI(v=0) \rightarrow HI(v=1) + HI(v=1) \quad . \qquad (E)$$

If HI were a harmonic oscillator and the perturbing force linear with distance, we would have

$$k_0 \sim k_E(\text{harmonic}) = \frac{v k_F}{2} \quad , \qquad (5)$$

where k_F is the rate constant of the process

$$HI(v=2) + HI(v=0) \rightarrow 2\ HI(v=1) \quad , \qquad (F)$$

which has been previously measured.[26] HI, of course, is not a harmonic oscillator, and therefore Eq. (5) is not strictly valid. Indeed, the $V \rightarrow V$ transfer rate may be significantly slower than that

predicted by this equation since the mechanical anharmonicity of HI prevents reaction (E) from being a resonant energy transfer process.[27] Since a better approximation is not available and neither k_D nor k_E have been measured, we use Eq. (5) nevertheless and obtain $k_D \approx vk_F$.

The temperature dependence of V→V rate constants in general and k_F in particular is not well understood. Bott and Cohen[28] determined that the rate constants for V→V transfer between HF(v = 1) and various diatomic molecules, AB, had temperature dependences of between T^{-1} and T^0, for AB having approximately the same vibrational energy spacing as HF. Ahl and Cool[26] found for HI that $k_F = 8.98 \times 10^7$ and 6.98×10^7 liter mole^{-1} sec^{-1} at 300 and 350 K, respectively. Within the accuracy needed for our calculations we shall assume that in the temperature range 300 K to 690 K, k_F does not exceed its room-temperature value.

The rate constant k_B is more difficult to estimate. The purpose of this experiment was actually to measure it. Using data on k_A an upper bound may be placed on k_B. If vibrational enhancement is important in reaction (A) as Anderson's results suggest,[14] the following simplified mechanism may be proposed for the thermal reaction (A):

$$HI + HI \rightleftharpoons HI^{\dagger}(v) + HI \qquad (G)$$

$$HI^{\dagger}(v) + HI \rightarrow H_2 + 2I \quad . \qquad (B)$$

If reaction (B) proceeds slowly compared to the time required to restore the fast equilibrium G, a Boltzmann distribution

of vibrational states may be assumed. The rate of the dark reaction must be an upper limit to the rate of reaction (B), since additional reaction pathways for H_2 formation are bound to exist, such as the reaction of less vibrationally excited HI or the reaction between two vibrationally excited HI molecules. Therefore,

$$2\,\frac{d[H_2]}{dt} = k_A[HI]^2 \geq k_B[HI][HI^{\dagger}(v)] \quad , \tag{6}$$

from which we obtain

$$k_B \leq k_A \frac{[HI]}{[HI^{\dagger}]} = k_A\, e^{E(v)/RT} \quad , \tag{7}$$

where E(v) is the energy of vibrational state v of HI, the origin of energy measurement being the ground vibrational state.[29] Using our rate data for k_A, we get an upper limit for k_B

$$k_B \leq 10^{13.57} e^{-[52.9 - E(v)\text{kcal}]/RT} (\text{liter mole}^{-1}\,\text{sec}^{-1}). \tag{8}$$

5.3 Conditions necessary for observation of reaction of vibrationally excited HI molecules

From Eqs. (1) and (3) we know that the intercept, k′, of the plot of $\frac{2}{[HI]} \frac{d[H_2]}{dt}$ versus [HI] is given by

$$\lim_{[HI] \to 0} \left(\frac{2}{[HI]} \frac{d[H_2]}{dt} \right) = k' = \frac{k_B}{k_B + k_D} \frac{I_0 S_{HI} \ell}{V} \qquad (9)$$

where k_B, k_D and S_{HI} are functions of the upper vibrational quantum number, v.

The minimum detectable intercept, k'_{min}, can be easily estimated using the approximation to the left-hand side of Eq. (9),

$$k'_{min} \approx \frac{2}{\overline{[HI]}} \frac{[H_2]_{min}}{t_{max}} \quad . \qquad (10)$$

$\overline{[HI]}$ is the value of the lowest [HI] used in the experiments which furnishes k′ [through Eq. (9)] with an acceptable accuracy, $[H_2]_{min}$ is the minimum concentration of H_2 detectable in the analytical system and t_{max} is the maximum practical photolysis time. It should be noted that in order to make k'_{min} as small as possible, $\overline{[HI]}$ should be made as large as possible, but in order to make k′ as accurate as possible $\overline{[HI]}$ should be made as small as possible. These conflicting demands on $\overline{[HI]}$ lead to a compromise in its choice.

Let us define the quantities

$$Q(v) = \frac{I_0 \ell S_{HI}}{V k'_{min}} \tag{11}$$

and

$$X(v) = \frac{k_B}{k_B + k_D} . \tag{12}$$

From Eqs. (9) through (12) we can rewrite the detectability conditions

$$k' \geq k'_{min}$$

as

$$X(v) \geq \frac{1}{Q(v)} \tag{13}$$

For a given set of experimental conditions, the value of Q(v) is uniquely determined, and $1/Q(v)$ is then the smallest value which X(v) can have and still be detected in those experiments. In Fig. 8, the unhatched area represents the part of the two-dimensional configuration space Q(v), X(v) corresponding to a detectable k′ for values of the other parameters which are experimentally achievable with present techniques. Since, by definition, $X(v) \leq 1$, we see that for $Q(v) \leq 1$ no information can be obtained about X(v) from the corresponding experiments. For $Q(v) > 1$, X(v) can be measured only if it exceeds $1/Q(v)$.

The following additional constraint can be imposed on X(v) in view of Eqs. (5), (7), and (12):

$$X(v) = X(v,T) \leq \frac{k_A(T)}{k_A(T) + \frac{v}{2} k_F e^{-E(v)/kT}} . \qquad (14)$$

A series of horizontal lines corresponding to the equality sign in Eq. (14) have been drawn in Fig. 8 for several choices of v and two values of T. In addition, vertical arrows pointed towards the abscissa were drawn labeled LPv corresponding to different values of Q(v) achievable with the Xenon lamp used in these experiments. In addition, two arrows labelled LS v=8 and PO v=4 were drawn for two lasers which are presumably available on the market. The LS v=8 arrow is for a tunable dye laser giving 10^{19} photons/sec and having a 1 cm^{-1} bandwidth,and the PO v=4 is for a parametric oscillator giving 5×10^{16} photons/sec at a 1 cm^{-1} bandwidth. The calculation for the laser light sources was made with appropriate estimations of the individual rovibrational line strengths $S_{0J}^{vJ'}$.

Observation of Fig. 8 shows that no information can be obtained using the Xe light source or the parametric oscillator which is not already contained in Eq.(14). Information can be obtained using the dye laser, if the positions of the rovibrational lines in the 0→8 band can be measured independently.

6. CONCLUSIONS

The kinetic method developed in the present paper permits the separation of the effects of vibrational enhancement of the HI(v) + HI reaction from those due to thermal heating in the vibrational photochemistry of HI, if care is taken to correct for the small first-order component which has been detected in the dark experiments. However, failure to correct for this first-order component produces large inconsistencies in the rate constants and activation energies measured for the second-order reaction. Under the experimental conditions used, the photochemical enhancement observed was entirely due to heating. Theoretical estimates indicate that these experiments should be repeated using a tunable dye laser, after the location of the rovibrational lines is determined by an independent method.

TABLE I. Rate constants for thermal and photochemical experiments.

Exp.	Conditions[a]	T_{wall} (K)	T_{gas}[d] (K)	ΔT[e] (K)	k_A (10^{-4} liter mol^{-1} sec^{-1})	σ_{k_A}[f]	k' (10^{-7} sec^{-1})	$\sigma_{k'}$[f]
1	P	$670._9$	$693._1$	22	8.4	0.6	6.6	1.2
2	P	$650._7$	$674._7$	24	2.8	0.1	2.4	0.3
3	P	$693._1$	$705._9$	13	17.3	0.9	15.5	1.0
4	P	$639._9$	$666._5$	26	1.7	0.2	1.1	0.4
5	P	$653._7$	$659._4$	5	1.1	0.1	2.9	0.2
6	P	$664._0$	$680._7$	17	4.1	0.4	5.5	0.7
7	P[b]	$712._0$	$718._6$	7	34.3	1.7	22.	2.
8	D[b]	$697._9$	-----	---	14.1	0.8	8.5	1.4
9	D	$697._8$	-----	---	9.4	0.4	8.6	0.8
10	D	$668._6$	-----	---	1.8	0.1	4.0	0.3
11	D[c]	$711._{41}$	-----	---	23.2	1.8	9.6	3.4
12	D[c]	$662._{80}$	-----	---	1.5	0.7	4.4	1.5

[a] P denotes photolysis experiments and D (dark) denotes thermal ones.

[b] These experiments were done in presence of quartz wool.

[c] These experiments were performed in a lead bath oven.

[d] These values are calculated from the slopes of the $(2/[HI])(d[H_2]/dt)$ versus $[HI]$ for the photochemical experiments and from the dark experiment rate constants, as explained in text (Section 2).

[e] This is the difference between the values in columns 4 and 3 for the photochemical results.

[f] Standard deviation of the rate constant in preceding column.

REFERENCES

1. M. J. Kurylo, W. Braun, A. Kaldor, S. M. Freund, and R. P. Wayne, J. Photochem. 3, 71 (1974/75).
2. A. Kaldor, W. Braun, and M. J. Kurylo, J. Chem. Phys. 61, 2496 (1974).
3. P. Brooks, J. V. V. Kasper, and T. Odiorne, J. Chem. Phys. 55, 1980 (1971).
4. R. J. Gordon and M. C. Lin, Chem. Phys. Lett. 22, 262 (1973).
5. L. B. Sins, L. R. Dosser, and P. S. Wilson, Chem. Phys. Lett. 32, 150 (1975).
6. D. Arnoldi, K. Kaufmann, and J. Wolfrum, Phys. Rev. Lett. 34, 1597 (1975).
7. R. V. Ambartzumian, Y. A. Gorokov, U. S. Letokhov, and G. N. Makarov, JETP Lett. 21, 375 (1975).
8. R. T. Bailey, F. R. Cruickshank, J. Farrell, D. S. Horne, A. M. North, P. B. Wilmot, and Tin Win, J. Chem. Phys. 60, 1699 (1974).
9. A. Yogev and R. M. J. Loewenstein-Benmair, J. Am. Chem. Soc. 95, 8487 (1973).
10. W. Braun, M. J. Kurylo, A. Kaldor, and R. P. Wayne, J. Chem. Phys. 61, 461 (1974).
11. (a) J. H. Sullivan, J. Chem. Phys. 36, 1925 (1962); (b) ibid. 46, 73 (1967); (c) ibid. 47, 1566 (1967).
12. A. H. Taylor, Jr., and R. H. Crist, J. Am. Chem. Soc. 65, 1377 (1941).

13. Reactions A and B may not be elementary and may be replaced by the elementary steps

$$HI + HI\,(\text{or } HI^{\dagger}) \rightarrow H_2I + I$$

$$I + H_2I \rightarrow H_2 + I_2$$

(see Ref. 12b).

14. S. B. Jaffe and J. B. Anderson, J. Chem. Phys. 51, 1057 (1969).

15. "Liquid Gold Products" Catalogue, Hanovia Division, Engelhand Industries, East Newark, NJ.

16. We thank Dr. J. H. Sullivan of the Los Alamos Scientific Laboratory for the loan of this thermometer.

17. R. H. Reiner and A. Kuppermann, J. Chem. Phys., to be submitted for publication.

18. W. H. Graven, J. Am. Chem. Soc. 78, 3297 (1956).

19. J. C. Blagg and G. M. Murphy, J. Chem. Phys. 4, 631 (1936).

20. Sullivan (Ref. 12a) has shown that the $H_2 + I_2$ reaction (and hence reaction (A), by microscopic reverisbility) is not bimolecular but is a chain reaction. This does not affect our determination of k_A (except as noted in Ref. 13), since the fractional decomposition of HI is less than 2%.

21. G. Ameer and W. Benesch, J. Chem. Phys. 37, 2699 (1962).

22. This is easily derived from the properties of the Hermite polynomials. See, for example, G. Herzberg, Spectra of Diatomic Molecules (D. Van Nostrand Inc., Princeton, NJ, 1950) 2nd ed., p. 82.

23. J. M. Herbelin and G. Emanuel, J. Chem. Phys. 60, 689 (1974).

24. H. L. Chen, J. Chem. Phys. 55, 5551 (1971).

25. Measurements of V → T, R and V → V processes in HCl indicate that V → V reactions occur at least ten times faster than V → T, R. These results are typical of other molecules. See, for example, H. L. Chen, J. Chem. Phys. 54, 4072 (1971).

26. J. H. Ahl and T. A. Cool, J. Chem. Phys. 58, 5540 (1973).

27. M. H. Alexander, J. Chem. Phys. 56, 3030 (1972).

28. J. F. Bott and N. Cohen, J. Chem. Phys. 58, 4539 (1973).

29. If we consider a model for $k_B(v,T)$ in which the pre-exponential factor is independent of v and equal to that of $k_A(T)$ and in which the activation energy, $E_a(v)$, equals $E_a - E(v)$, where E_a is the activation energy of $k_A(T)$, it is easy to see that this model furnishes

$$k_B(v,T) = k_A(T)e^{E(v)/RT}.$$

If such a model were valid, the inequality sign in Eq. (7) could be replaced by an equality

30. Graphic symbols per American Vacuum Society Standard, J. Vac. Sci. Technol. 4, 139 (1967).

FIGURE CAPTIONS

Fig. 1 - Schematic diagram of photolysis cell, oven and vacuum system. Vacuum line graphic symbols are defined in Ref. 30. See text for explanation of figure components.

Fig. 2 - $(2/[HI])(d[H_2]/dt)$ versus $[HI]$. Circles correspond to samples photolyzed at $670._9$ K. Squares label the thermal (dark) results obtained at $668._6$ K.

Fig. 3 - Rate constants k_A versus $1/T$ for the thermal (dark) HI reaction. Triangles are results from the air oven, squares are the ones from the liquid lead temperature bath, solid circles are the results of Taylor and Crist,[12] open circles are these results corrected as indicated in the text, and diamonds are the results of Sullivan.[11a] Error bars indicating one standard deviation are included when larger than symbol size.

Fig. 4 - First-order rate constant k' of Eq. 3 versus $1/T$ where T is the measured wall temperature. Circles represent the photolyses data and squares the thermal (dark) results. The triangle and the hexagon indicate the dark and photolysis results of the increased surface to volume experiments, respectively. Error bars indicate standard deviations.

Fig. 5 - First-order rate constant k' of Eq.(3) versus $1/T$ where T is the gas temperature obtained as indicated in text. See Fig. 4 caption for symbol description. The solid and dashed lines are least squares determinations of the photolysis and thermal results, respectively. The dotted line is the least

squares determination using both sets of results.

Fig. 6 - $-(1/[HI])(d[HI]/dt)$ versus $[HI]$ for the experiments of Taylor and Crist.[12] The circles and squares represent the results of experiments performed at $698._6$ K and $666._8$ K, respectively.

Fig. 7 - First-order rate constant k' of Eq.(3) from several experiments. Square, Ref. 18; circles, Ref. 12 ; diamonds, present thermal results; triangles, present photolysis results (including quartz wool experiments). Error bars indicate standard deviations. Those smaller than symbol size are not shown.

Fig. 8 - X(v) versus Q(v). The unhatched region corresponds to a physically detectable X(v). The arrows into the abscissa, labeled LP (abbreviation for lamp) v = 2-9 are experimentally obtainable Q(v)'s using the xenon arc lamp and the apparatus described in Sec. 3. Arrows labeled LS (abbreviation for laser) v = 8, and PO (abbreviation for parameter oscillator) v = 4 are the Q's obtainable using a dye laser (10^{19} photons/sec) and a parametric oscillator (5×10^{16} photons/sec) to pump the v = 8 and v = 4 states of HI, respectively. The horizontal lines X(v, T) are upper limits on X estimated in Sec. 5.3. For the indicated values of v, solid lines, ———, correspond to T = 690 K, dashed lines, -----, to T = 300 K.

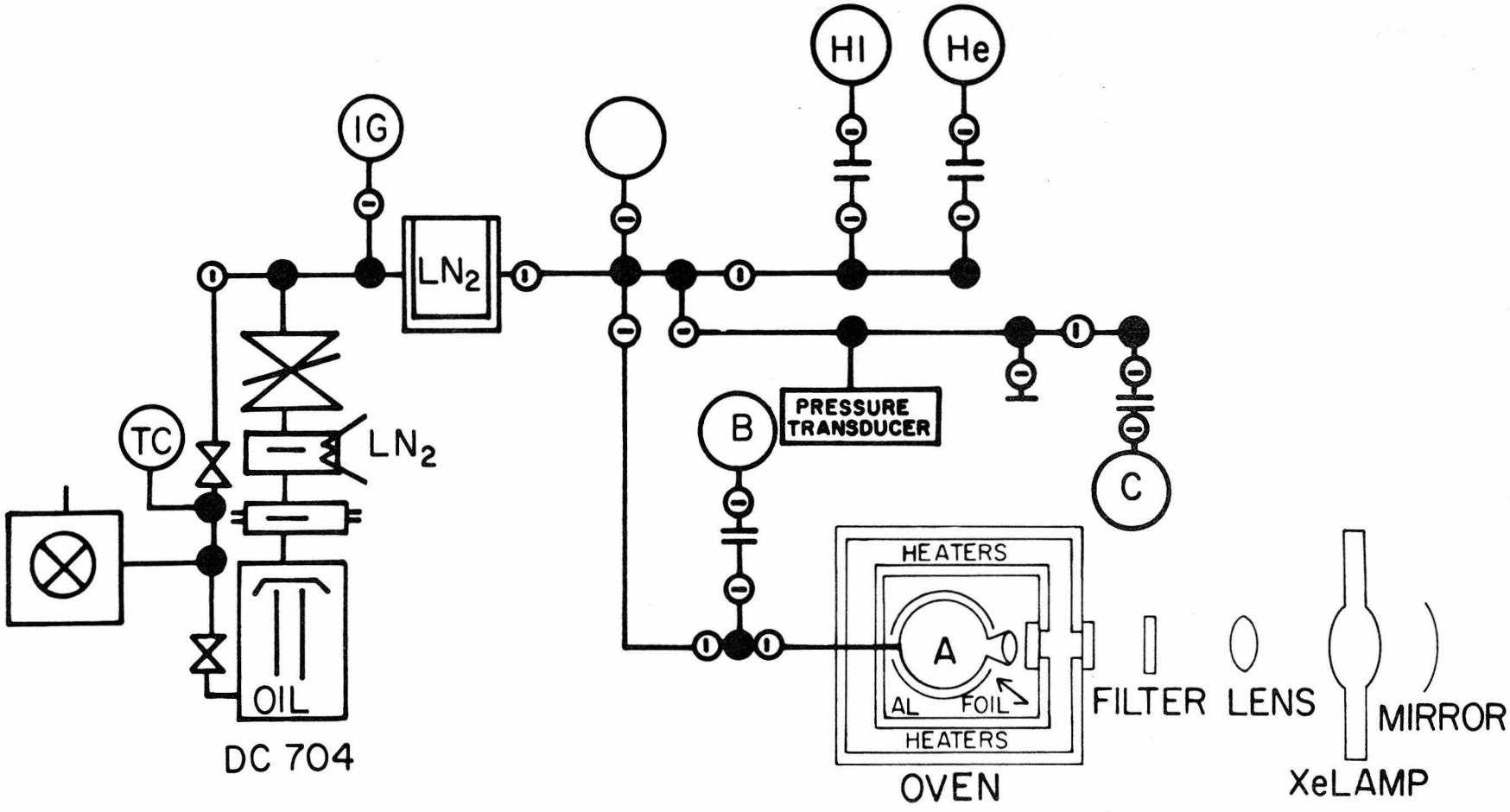
HI
He
IG
LN2
TC
LN2
PRESSURE TRANSDUCER
B
C
HEATERS
A
AL FOIL
HEATERS
OIL
DC 704
OVEN
FILTER
LENS
MIRROR
XeLAMP

Figure 1.

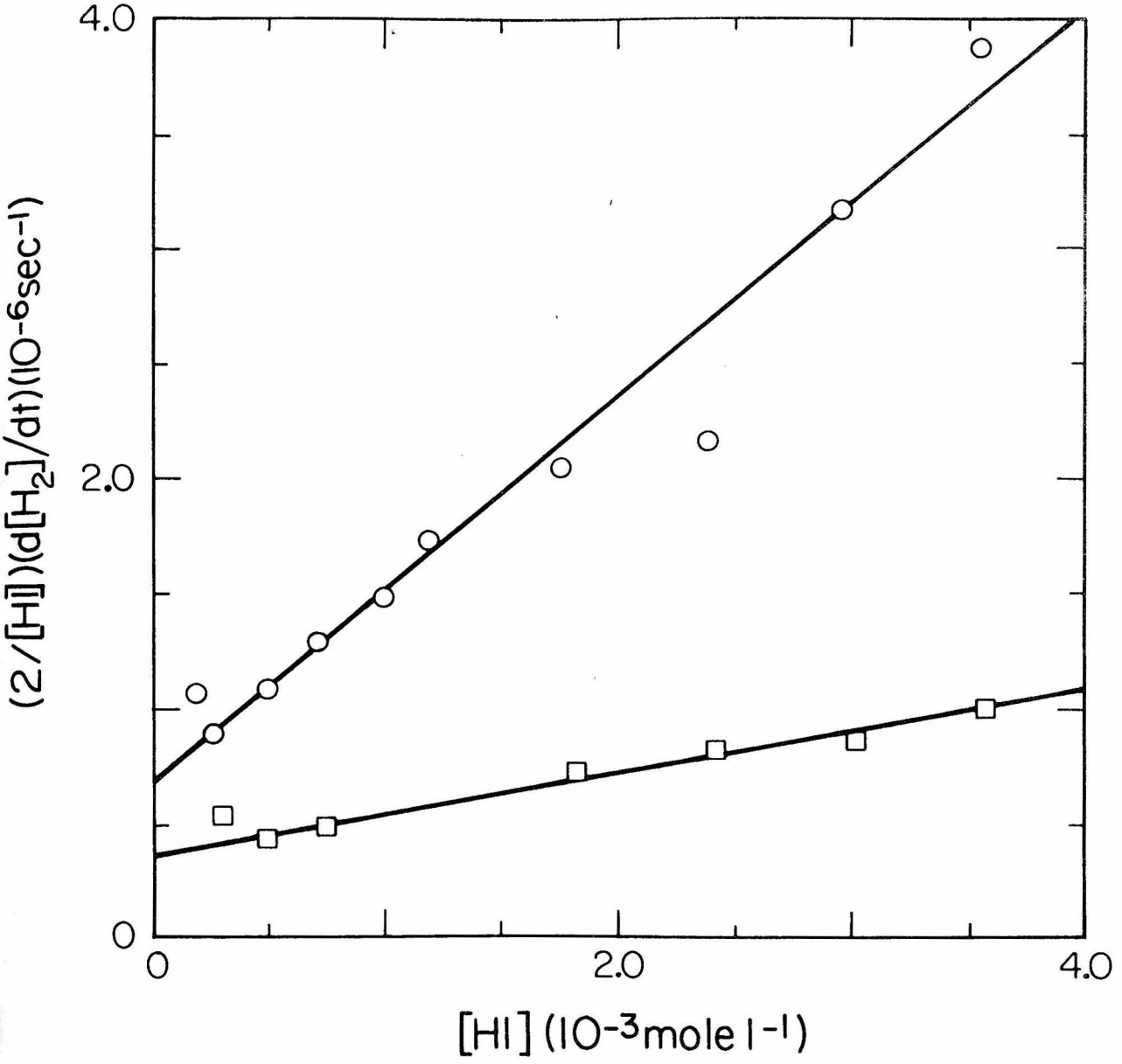

Figure 2.

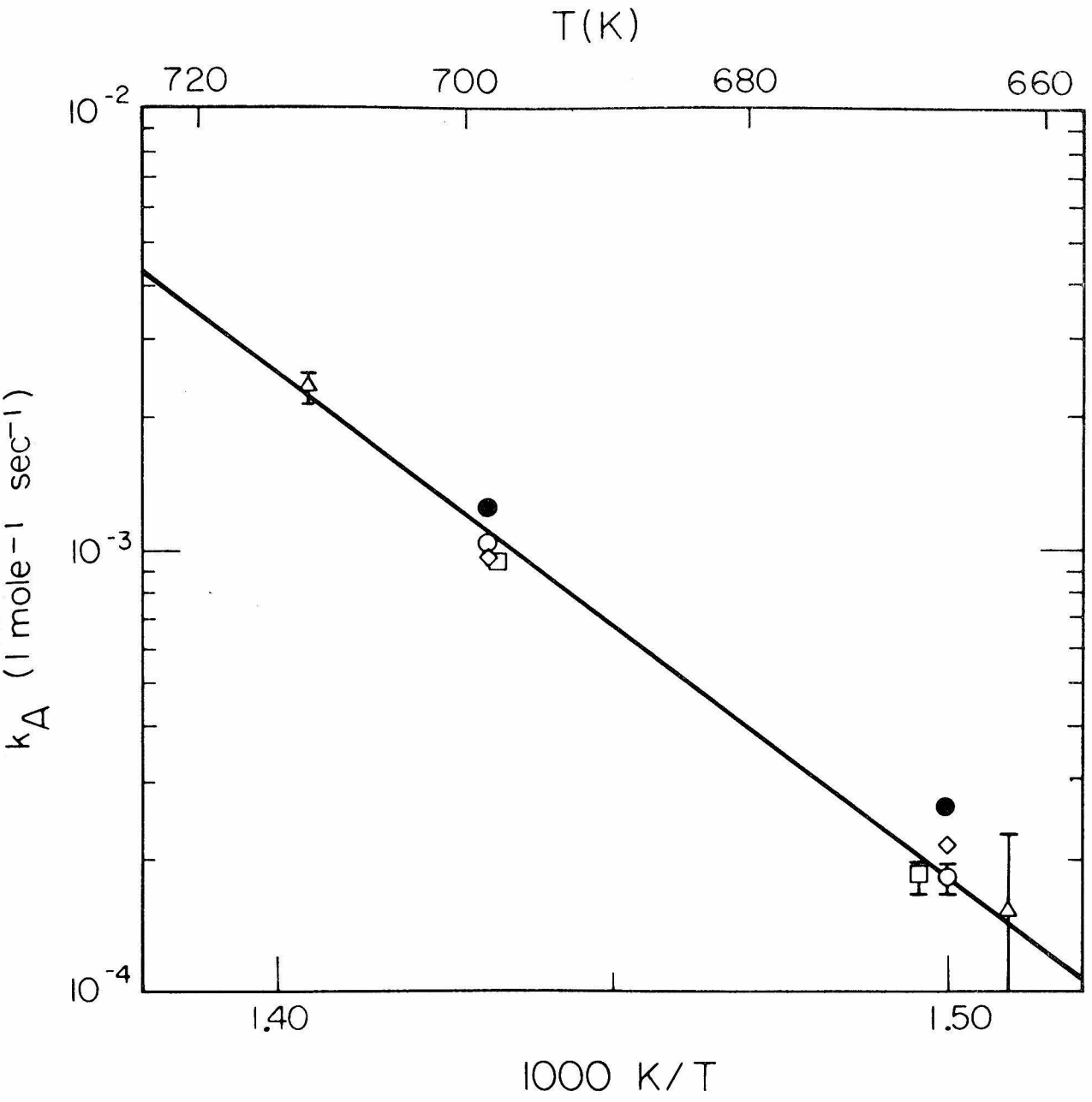

Figure 3.

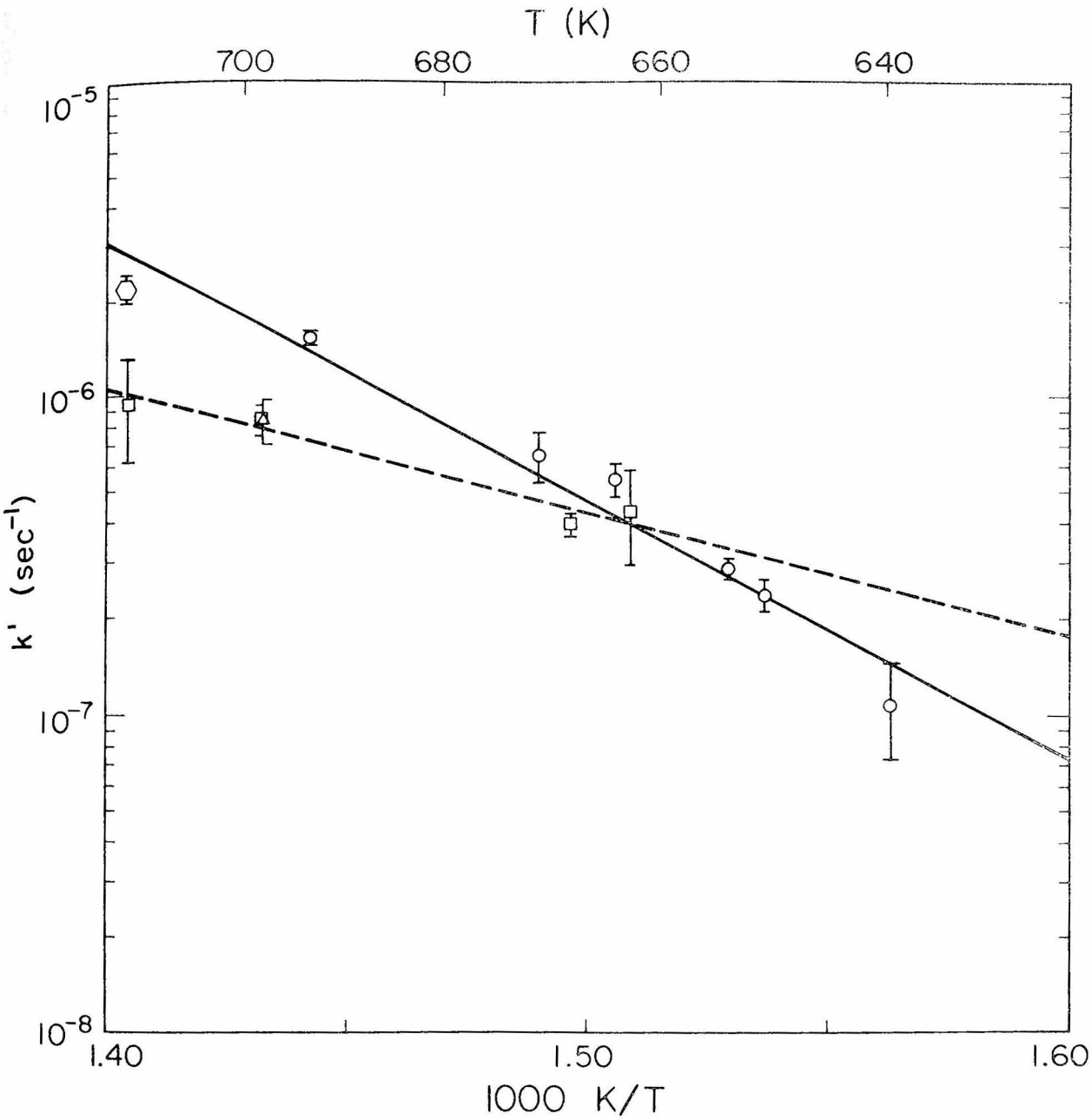

Figure 4.

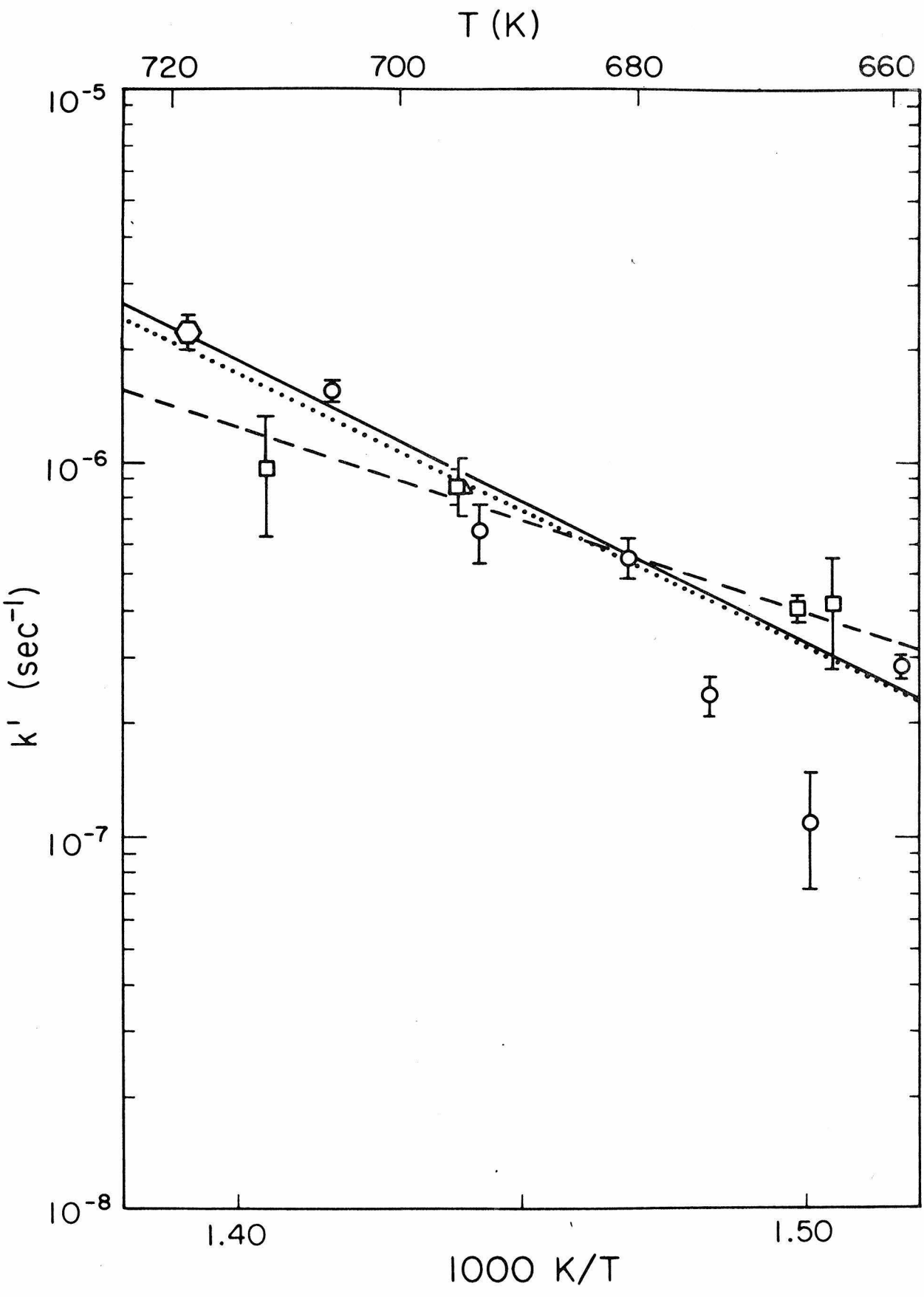

Figure 5.

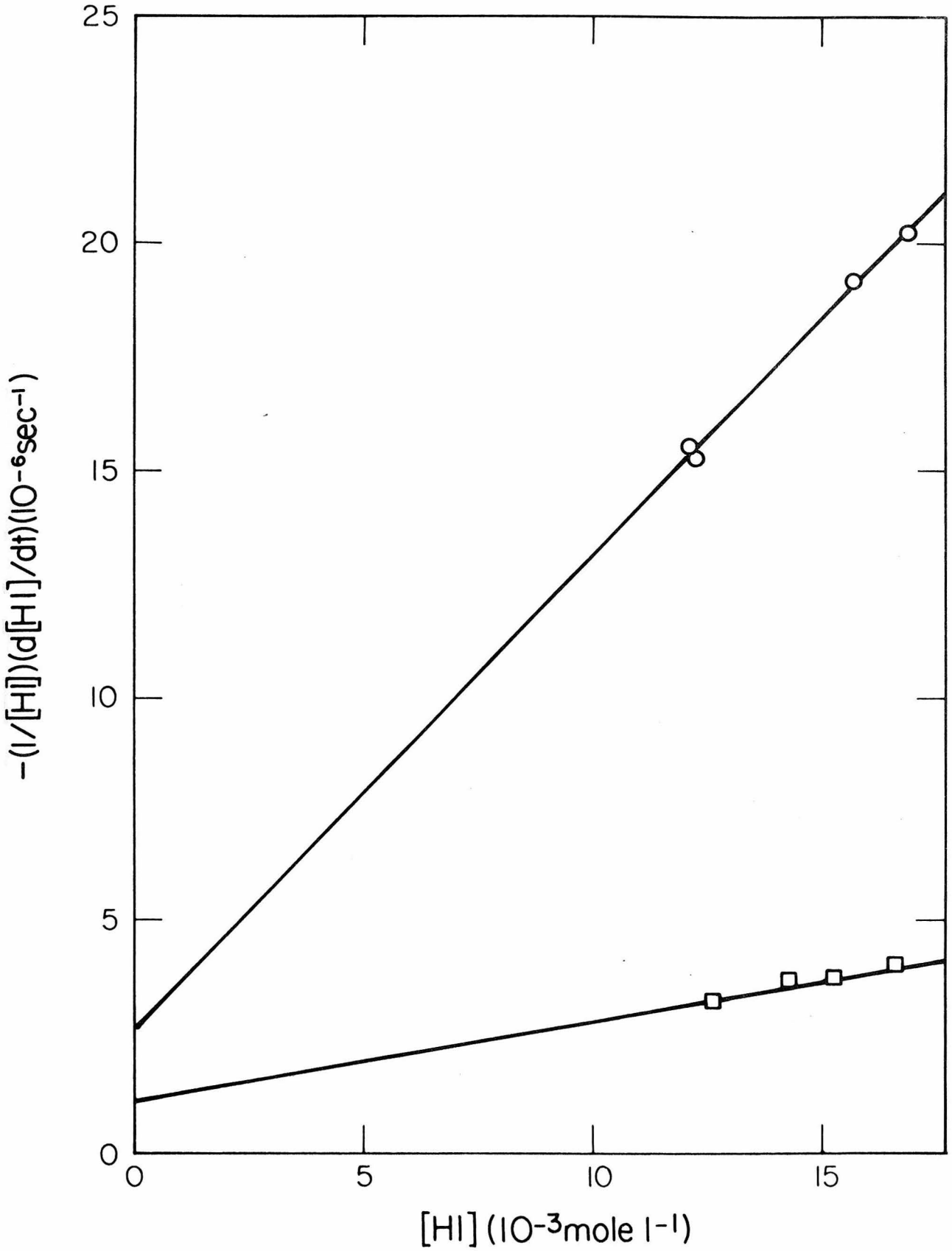

Figure 6.

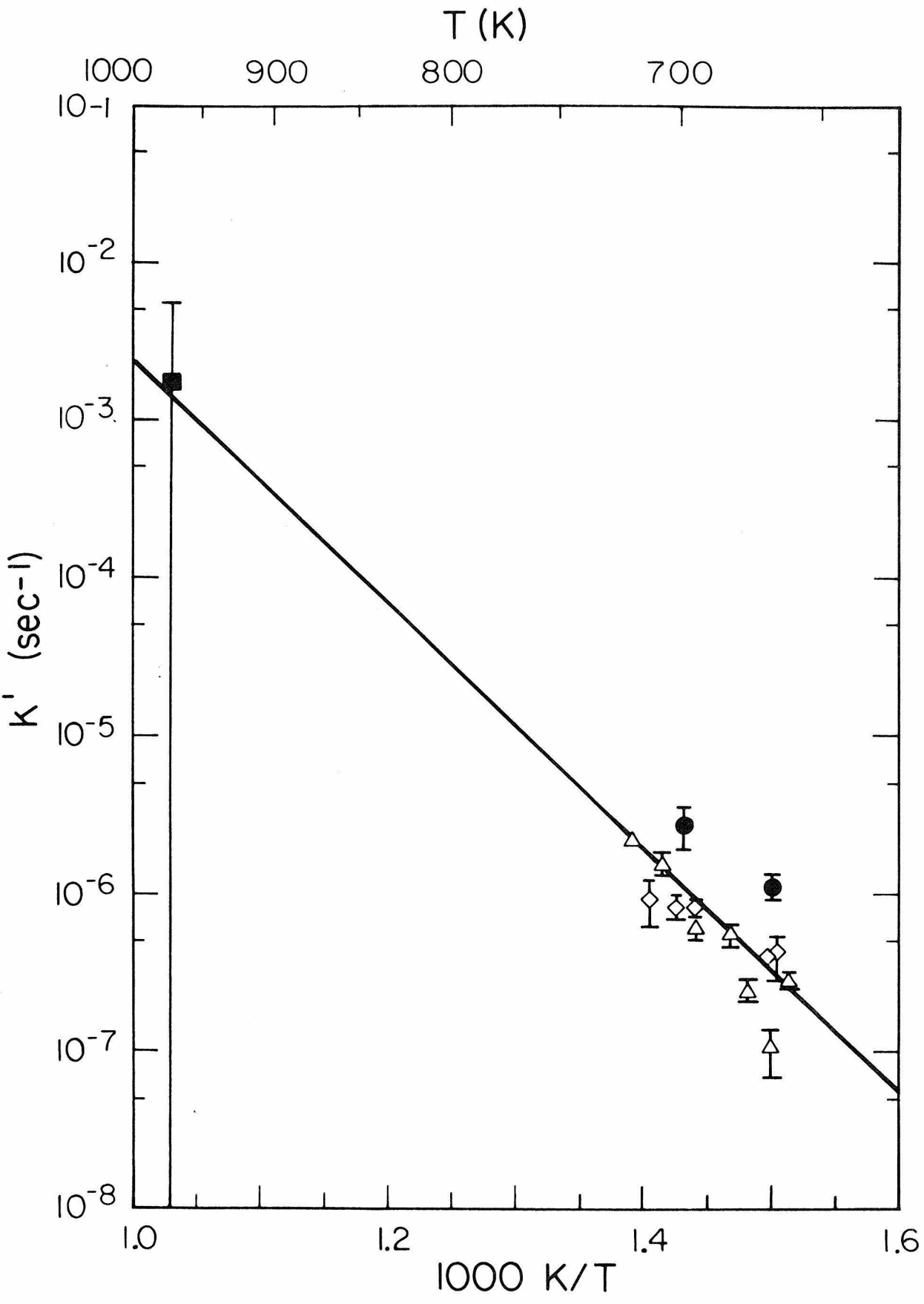
T (K)
1000
900
800
700
10-1
10-2
10-3
10-4
10-5
10-6
10-7
10-8
K' (sec-1)
1.0
1.2
1.4
1.6
1000 K/T

Figure 7.

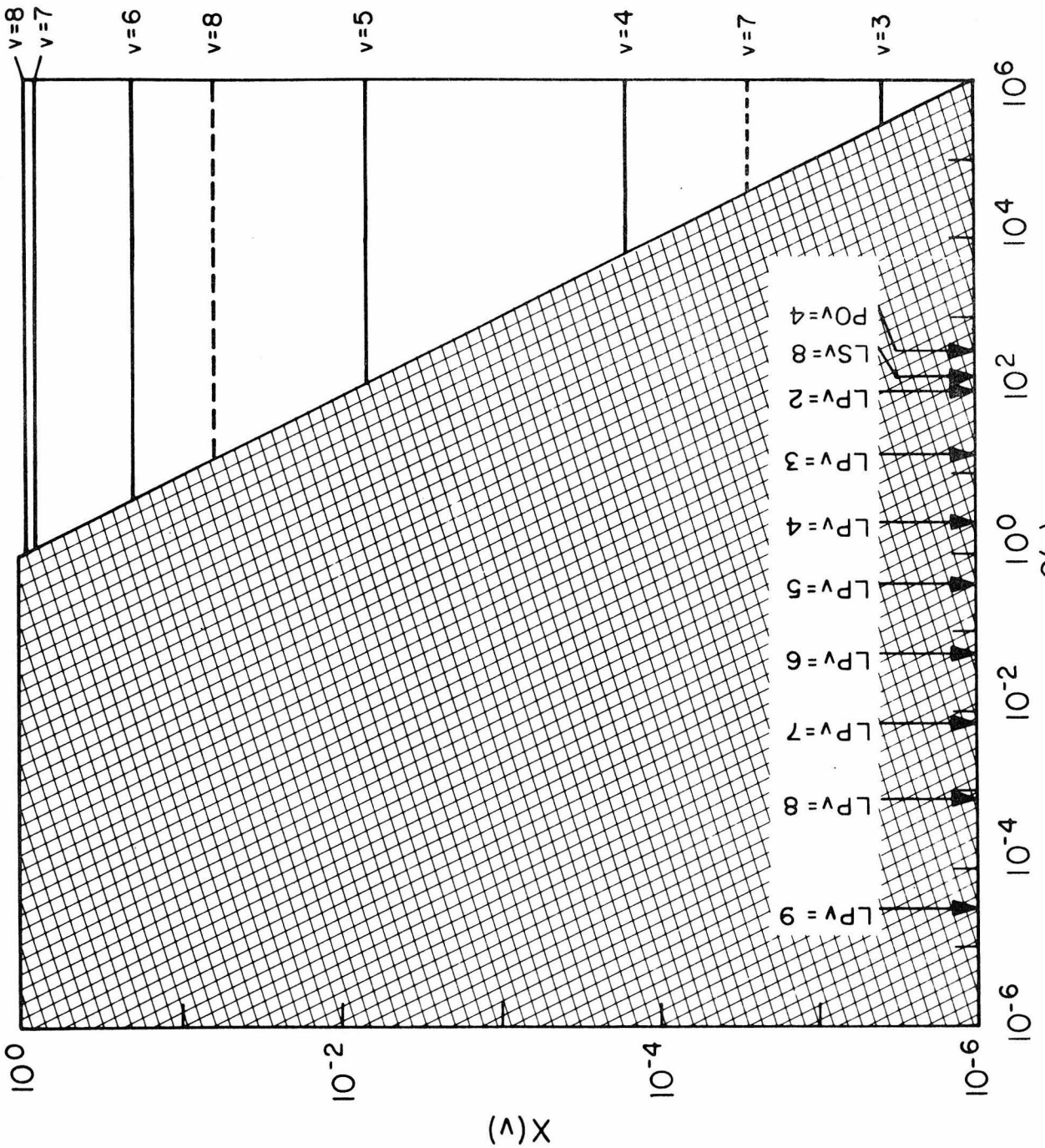
v=8
v=7
v=6
v=8
v=5
v=4
v=7
v=3
LPv = 9
LPv = 8
LPv = 7
LPv = 6
LPv = 5
LPv = 4
LPv = 3
LPv = 2
LSv = 8
POv = 4
X(v)
Q(v)
10^0
10^-2
10^-4
10^-6
10^-6
10^-4
10^-2
10^0
10^2
10^4
10^6

Figure 8.

6. THE PHOTOCHEMISTRY OF IODINE MONOCHLORIDE IN HYDROGEN

The photochemistry of iodide monochloride in hydrogen*

Robert H. Reiner and Aron Kuppermann

Arthur Amos Noyes Laboratory of Chemical Physics,†
California Institute of Technology, Pasadena, California 91125

(Received)

ABSTRACT

The quantum yields of HCl formation in mixtures of ICl and H_2 have been remeasured in order to resolve contradictions present in previous studies. Results indicate that (1) while earlier results are qualitatively correct, the secondary reactions in the ICl-H_2 system are more complicated than previously envisioned, (2) the reported rate constant for the reaction Cl + ICl → Cl_2 + I determined from the photolysis of pure ICl is several orders of magnitude too small, and (3) the reaction ratio of ICl to H_2 with Cl at 298.05°K is 1133. ± 69.

---

* This work was supported in part by a contract (EY-76-S-03-0767) from the U. S. Energy Research and Development Administration. Report Code: CALT-767P4- .

† Contribution No.

1. INTRODUCTION

Early photochemical experiments on hydrogen-iodide monochloride mixtures showed that (1) no hydrogen chloride was produced unless a large excess of hydrogen was present and (2) no hydrogen iodide was ever detected.[1-3] In the first attempt to measure the quantum yield of HCl formation, Φ_{HCl}, Hofer and Wiig[4] suggested the following mechanism to explain their results:

$$ICl + h\nu \rightarrow Cl + I \quad (A)$$

$$Cl + H_2 \rightarrow HCl + H \quad (B)$$

$$H + ICl \rightarrow HCl + I \quad (C)$$

$$Cl + ICl \rightarrow Cl_2 + I \quad (D)$$

$$I + I + M \rightarrow I_2 + M. \quad (E)$$

They postulated that ICl is a much better chlorine atom scavenger than hydrogen and as a result Φ_{HCl} is 2 only at infinite dilution of ICl in H_2. For a H_2:ICl pressure ratio of 19:1, they reported $\Phi_{HCl} = 1.5$ (at 301.2°K).

Later Palmer and Wiig[5] repeated these experiments using slightly different experimental conditions and obtained $\Phi_{HCl} = 0.04$ (at 303.2°K) for the same H_2:ICl ratio. Palmer and Wiig did not discover the reason for the disagreement between the two experiments but suggested that possible reactions of ICl with stopcock grease, or water dissolved on the vessel walls might be responsible. They also speculated that the true value of Φ_{HCl} may lie somewhere between the two reported values.

A question concerning the mechanism postulated by Hofer and Wiig may also be raised. A molecular beam experiment performed by

McDonald et al.[6] has shown that the primary reaction of H and ICl is not reaction (C) but the reaction

$$H + ICl \rightarrow HI + Cl . \qquad (F)$$

When reaction (F) is added to this mechanism, the expression for Φ_{HCl} becomes more complicated (see Discussion).

Since ICl is currently being used as a prototype for laser photochemical isotopic separation studies, the secondary reactions of ICl are of great interest.[7] To help unravel the mechanism of the H_2, ICl system, we have determined Φ_{HCl} as the ICl:H_2 ratio approaches zero. In the next section, experimental apparatus and techniques are described. The results of these experiments are presented in Sec. 3 and are discussed in Sec. 4.

2. EXPERIMENTAL

2.1. Apparatus

Due to the high reactivity of ICl with mercury, stopcock grease and water absorbed on glass walls,[5] special care was taken in the construction of the photolysis vacuum system. The mercury-free vacuum line, shown schematically[8] in Fig. 1, was used to evacuate and transfer gases to the photolysis cell. High vacuum stopcocks (Kontes K 826600-0004) fitted with Teflon plugs and viton O-rings were used to eliminate stopcock grease. Urry-type O-ring joints were substituted for ground glass joints for the same reason. A diaphragm-type transducer (Celesco Industries P7D) was used in place of a mercury manometer for pressure measurements. This vacuum system was routinely evacuated below 10^{-6} Torr.

A 500 ml quartz photolysis cell (25 cm long) was attached to the vacuum line (A, Fig. 1). The cell was positioned so that it could be surrounded by a constant temperature water bath (298.05 ± 0.05°K) during photolysis or in a liquid nitrogen bath (77°K) to condense products.

The light source was a tunable dye laser (Molectron DL-200) pumped by a pulsed nitrogen laser (Molectron UV-400). Coumarin 120 was used in the dye laser to obtain lasing at 426 nm. This light beam was collimated well enough so that its intensity could be measured using a disc calorimeter (Scientech 360001) with an uncertainty of less than 1%. The calorimeter was calibrated internally using a resistance heater which provided an accuracy of ± 3%.

2.2. Procedure

Reagent grade ICl (Eastman 1981) dried over P_2O_5 was pretreated with excess HCl for several hours. The HCl was removed using several freeze-pump-thaw cycles at 215°K and the ICl was distilled once from bulb C to bulb B at 235°K. A known amount of ICl was than added to the photolysis cell by thermostating bulb B at a temperature selected using previously determined vapor pressure data.[9] In this manner ICl was only exposed to glass, quartz, Teflon, and viton. Cell A was then valved closed, the water bath removed, and the cell was cooled to 77°K. A known amount of hydrogen (Matheson 99.9995%) was added to the cell.

The cell was rethermostated at 298.05°K and the mixture photolyzed using 426 nm radiation from the dye laser. Depending on the ICl pressure used, between 13% and 65% of the light was absorbed by the sample. Experimental conditions were chosen so that less than 10% of the ICl was photolyzed. The light intensity was measured just prior to and just after each ten-minute photolysis.

The photolysis cell and traps D and E were cooled to 77°K. The hydrogen was then slowly pumped out of cell A. The remaining products and reactant were recondensed into the cell. An isopentane slush bath (113°K) was placed at trap E and the HCl collected at bulb B (using liquid N_2). All the operations just described were performed with room lights off. Experiments using known amount of HCl in H_2, ICl mixtures showed that the procedure was quantitative, i.e., none of the HCl was lost.

In preliminary experiments, a known amount of CO_2 was added to the HCl in bulb B. The area of the parent ion peaks of HCl and CO_2 were

then measured in a mass spectrometer (Du Pont 21-492B) which had been precalibrated with hydrogen chloride and carbon dioxide mixtures of known composition. Later, it was discovered that concentration of HCl could be determined more accurately by measuring its pressure using the transducer.

3. RESULTS

The results of ten photolyses and seven blank experiments are summarized in Table I. Evidently there is a slow thermal (dark) reaction of H_2 and ICl which is, perhaps, catalyzed by the photolysis vessel surface. Shown in Fig. 2 is the amount of HCl produced by this reaction plotted versus H_2 pressure for [ICl] = 3.87 Torr. These four blanks indicate that the amount of HCl produced decreases as the $[H_2]$ increases. The least squares straight line fitted to these points is also displayed. Since the nature of the reaction responsible for production of HCl in these blank experiments is unknown, use of this straight line fit is arbitrary. The scattering of the blank experiments about this straight line may be due to limitations on the accuracy of the experimental technique or failure of this straight line to describe the behavior of the dark reaction. However, in most of the photolyses, the dark reaction produces less than a 20% change in the quantum yield, making the scattering of the blank experiments in Fig. 2 unimportant.

This can be seen by looking at the results of the seven photolyses of 3.87 Torr of ICl shown in Fig. 3. The abscissa in this figure is $[ICl]/[H_2]$, the ordinate is $(\Phi_{HCl})^{-1}$. The crosses are the results using the uncorrected quantum yields, the open squares are the same results corrected by subtracting the HCl produced from the thermal reaction. The error bars on the corrected results were determined using the average deviation of the blank experiments about the straight line in Fig. 2. (Error bars smaller than plotting symbols are not shown.) These error bars illustrate the importance of the scatter in the blank experiments; when the thermal reaction does not change Φ_{HCl}

significantly, the error bars are small, and when the thermal reaction does change Φ_{HCl} significantly, the error bars are large. Also shown in Fig. 3 (open circles) are the corrected results of three photolyses of 0.74 Torr of ICl. In these three experiments the error bars and the uncorrected results lie beneath the plotting symbols.

The solid line having a slope of 566. ± 34 and intercept 0.69 ± 0.04 shown in Fig. 3 is the weighted least squares fit of all ten photolyses. (Fitting the data to a straight line is justified in the next section.) Each point was assigned a weight inversely proportional to the magnitude of its error bars. The data fit this line remarkably well except for the three points having large error bars. Although these three points appear to indicate nonlinear behavior in the plot of $(\Phi_{HCl})^{-1}$ versus $[ICl]/[H_2]$, we have little confidence in them and none of the mechanisms that describe these reactions predicts nonlinear behavior (see Sec. 4.2).

In Fig. 4a,b we have displayed the previous results of Palmer and Wiig[5] to compare the quality of their data with ours.

4. DISCUSSION

4.1. Quantum yields and reaction rate constants

Our results are in qualitative agreement with both those of Palmer and Wiig[5] and Hofer and Wiig.[4] That is, as $[ICl]/[H_2]$ decreases, Φ_{HCl} increases. Their mechanism, reactions (A)-(E), predicts that

$$(\Phi_{HCl})^{-1} = \tfrac{1}{2} + \frac{k_D}{2k_B}\frac{[ICl]}{[H_2]} \quad , \qquad (1)$$

assuming steady state [Cl] and [H]. From Palmer and Wiig's results at 303.2°K and 313.2°K, reciprocal quantum yields falling in the hatched region of Fig. 3 are predicted at 298.1°K. The agreement is remarkably good (considering the reproducibility of Palmer and Wiig's results) and indicates that Hofer and Wiig's quantum yields are approximately a factor of 40 high.

If, however, the previously reported values of k_B[10] and k_D[11] are substituted in Eq.(1), the dashed line shown in Fig. 3 is obtained. The slope of this line is 1.48×10^{-2}, 4.6 orders of magnitude lower than observed. This discrepancy indicates that either the Hofer-Wiig mechanisn is incorrect or the literature values for k_B and k_D are seriously in error.

In Sec. 4.2 we shall see that while the Hofer-Wiig mechanisn is incomplete, proposed revisions in the mechanism do not change the slope of the line of $(\Phi_{HCl})^{-1}$ versus $[ICl]/[H_2]$.

Similarly, the rate constant k_B has been studied by several researchers[10,12,13] using a variety of experimental techniques, and it is correct to within at least a factor of three.

However, the rate constant for reaction (D) reported by Christie, Roy, and Thrush[11] is subject to considerable question. First, the rate constant $k_{D'}$ for the analogous reaction

$$Cl + BrCl \rightarrow Cl_2 + Br \qquad (D')$$

is 3.9 orders of magnitude higher than the value for k_D reported by Christie et al.[14] This great difference is surprising since both reactions are exothermic and ICl and BrCl have almost equal bond energies. Second, a semi-empirical estimate of k_D[15] is 3.1 orders of magnitude higher than the value reported by Christie et al. Finally, a preliminary experiment using reaction (D) as a chlorine atom scavenger in the photochlorination of carbon monoxide[15] estimated $k_D \sim 1.9 \times 10^9$ ℓ mol^{-1} sec^{-1} or 3.8 orders of magnitude higher than that reported by Christie. On the basis of these three self-reinforcing results, a 3-4 orders of magnitude disagreement in the Christie estimate of k_D is indeed possible, necessitating an independent determination of this rate constant.

4.2. Mechanism

As we mentioned in Sec. 1, the results of molecular beam experiments[6] suggest that reaction (F) be included in the Hofer-Wiig mechanism reactions (A)-(E). We also wish to examine other reactions that may be important in this system. In addition to reactions (A)-(F), we may have:

$$M + Cl + Cl \rightarrow Cl_2 + M \qquad (G)$$

$$H + I_2 \rightarrow HI + I \qquad (H)$$

$$H + Cl_2 \rightarrow HCl + Cl \qquad (I)$$

$$Cl + I_2 \rightarrow ICl + I \qquad (J)$$

$$Cl + HI \rightarrow HCl + I \qquad (K)$$

$$HI + \begin{Bmatrix} ICl \\ Cl_2 \end{Bmatrix} \rightarrow HCl + \begin{Bmatrix} I_2 \\ ICl \end{Bmatrix} . \qquad \begin{matrix} (L) \\ (L') \end{matrix}$$

While not much data are available for these reactions, our experimental conditions allow us to make some important simplifications.

We might expect that $k_H \sim k_I \sim k_C$, allowing us to ignore reactions (H) and (I) if $[\overline{I_2}] \approx [\overline{Cl_2}] \ll [\overline{ICl}]$ (where $[\overline{A}]$ is defined as the average concentration of species A during an experiment). Under our experimental conditions, $[\overline{Cl_2}] \sim [\overline{I_2}] < 0.03\,[\overline{ICl}]$, allowing us to neglect reactions (H) and (I), at least as a first-order approximation. Similarly, we expect that $k_J \sim k_D$, allowing us to neglect reaction (J) since $[\overline{I_2}] \ll [\overline{ICl}]$.

Assuming the steady state approximation is valid for [Cl] and [H], using reactions (A)-(G), (K), and (L) we obtain

$$[H]_{SS} = \frac{k_B[H_2]}{(k_C + k_F)[ICl]}\,[Cl]_{SS} \qquad (2)$$

$$[Cl]_{SS} = \frac{I_0 \epsilon \ell [ICl] + k_F[ICl][H]_{SS}}{k_B[H_2] + k_D[ICl] + k_G[Cl]_{SS}[M] + k_K[HI]} \qquad (3)$$

$$[Cl]_{SS} = \frac{I_0 \epsilon \ell [ICl] + \dfrac{k_F k_B}{(k_C + k_F)}\,[H_2][Cl]_{SS}}{k_B[H_2] + k_D[ICl] + k_B[M][Cl]_{SS} + k_K[HI]} \qquad (4)$$

$$[Cl]_{SS} = \frac{I_0 \epsilon \ell\,[ICl]}{\dfrac{k_B k_C}{(k_C + k_F)}\,[H_2] + k_D[ICl] + k_G[M][Cl]_{SS} + k_K[HI]} . \qquad (5)$$

We now wish to show that reaction (G) may be ignored. A condition sufficient for us to ignore reaction (G) in Eq.(5) is

$$k_G[M][Cl]_{SS} \ll \frac{k_B k_C}{(k_C + k_F)}[H_2] \tag{6}$$

or

$$k_G[Cl]_{SS} \ll \frac{k_B k_C}{(k_C + k_F)} , \tag{7}$$

since $[M] \approx [H_2]$ in all of our experiments. We define

$$[Cl]^0_{SS} \equiv \frac{I_0 \epsilon \ell [ICl]}{\frac{k_B k_C}{(k_C + k_F)}[H_2]} . \tag{8}$$

From Herschbach's experiments[6] we know that $\frac{k_C}{k_C + k_F} \approx 1/4$. Using the reported value for k_B[10] and typical experimental conditions for I_0, ϵ, ℓ, $[ICl]$, and $[H_2]$, we find that $[Cl]^0_{SS} \leq 1.5 \times 10^{-7}$ mol ℓ^{-1}. From the corresponding iodine and bromine rate constants[16] we estimate $k_G \sim 3.1 \times 10^9 \sec^{-1}\ell^2\text{mol}^{-2}$. Therefore,

$$k_G[Cl]^0_{SS} \sim 4.4 \times 10^2 \ell\,\text{mol}^{-1}\sec^{-1} \ll \frac{k_C k_B}{k_C + k_F} \sim 2.1 \times 10^6 \ell\,\text{mol}^{-1}\sec^{-1}. \tag{9}$$

Since all concentrations and rate constants are non-negative numbers,

$$[Cl]_{SS} \leq [Cl]^0_{SS} , \tag{10}$$

making Eq.(7) valid. Reaction (G) may be ignored and Eq.(5) becomes

$$[Cl]_{SS} = \frac{I_0 \epsilon \ell [ICl]}{\frac{k_B k_C}{(k_C + k_F)}[H_2] + k_D[ICl] + k_K[HI]} . \tag{11}$$

Reaction (K) and reactions (L) or (L′) are included to explain the observation that no appreciable amount of HI has been detected in reaction products of this system.[2,3] Since either reaction (or both) may be responsible for the removal of HI from the system, we shall examine both possible mechanisms in detail.

Using the steady state hypothesis for [HI] we see that in the first possible mechanism, reactions (A)-(F) and (K):

$$[HI]_{SS} = \frac{k_F[ICl]}{k_K} \frac{[H]_{SS}}{[Cl]_{SS}} = \frac{k_B k_F [H_2]}{k_K(k_C + k_F)} \quad . \tag{12}$$

Assuming that all the HI reacts, the rate of HCl production is

$$\frac{d[HCl]}{dt} = k_B[Cl]_{SS}[H_2] + k_C[H]_{SS}[ICl] + k_F[H]_{SS}[ICl] \tag{13}$$

$$= k_B[H_2][Cl]_{SS} + (k_C + k_F)[ICl] \left\{ \frac{k_B}{(k_C + k_F)} \frac{[H_2]}{[ICl]} [Cl]_{SS} \right\} \tag{14}$$

$$= 2k_B[H_2][Cl]_{SS} \tag{15}$$

$$= \frac{2k_B[H_2] I_0 \epsilon \ell [ICl]}{k_B \left(\frac{k_C}{k_C + k_F} \right) [H_2] + k_D[ICl] + k_K[HI]_{SS}} \tag{16}$$

$$= \frac{2k_B I_0 \epsilon \ell [ICl]}{k_B \left(\frac{k_C}{k_C + k_F} \right) + k_D \frac{[ICl]}{[H_2]} + \frac{k_B k_F}{(k_C + k_F)}} \quad . \tag{17}$$

The quantum yield of HCl production, Φ_{HCl}, is

$$\Phi_{HCl} = \frac{d[HCl]/dt}{I_0 \epsilon \ell [ICl]} \tag{18}$$

$$\Phi_{HCl} = \frac{2k_B}{k_B + k_D \frac{[ICl]}{[H_2]}} = \frac{2}{1 + \frac{k_D}{k_B} \frac{[ICl]}{[H_2]}} \quad . \tag{19}$$

Equation (19) is the same expression for Φ_{HCl} that was obtained from the Hofer-Wiig mechanism, Eq.(1).

In the second possible mechanisn [reactions (A)-(F), (L)], Eqs. (13), (14), and (15) are still valid. However, now k_K goes to zero and Eq.(16) becomes

$$\frac{d[HCl]}{dt} = \frac{2k_B I_0 \epsilon \ell [ICl]}{\frac{k_B k_C}{k_C + k_F} + k_D \frac{[ICl]}{[H_2]}} \quad . \tag{20}$$

The quantum yield for HCl formation is

$$\Phi_{HCl} = \frac{2}{\frac{k_C}{k_C + k_F} + \frac{k_D}{k_B} \frac{[ICl]}{[H_2]}} \tag{21}$$

or

$$(\Phi_{HCl})^{-1} = \tfrac{1}{2} \left(\frac{k_C}{k_C + k_F} \right) + \tfrac{1}{2} \frac{k_D}{k_B} \frac{[ICl]}{[H_2]} \tag{22}$$

The important point in comparing Eqs.(19) and (21) is that no matter what becomes of the HI, the slope of the plot of $(\Phi_{HCl})^{-1}$ versus $[ICl]/[H_2]$ is the same, $\frac{1}{2} k_D/k_B$. Thus the arguments concerning k_D and k_B made in Sec. 4.1 are valid regardless of which mechanism is correct.

The intercepts predicted by each mechanism are quite different, however. If reaction (K) is responsible for the removal of HI, the intercept is $\frac{1}{2}$ as in the Hofer-Wiig mechanism. If, however, reaction (L) is responsible for the removal of HI, the intercept should be $\frac{1}{2}\left(\frac{k_C}{k_C+k_F}\right)$, which Herschbach estimates to be $\frac{1}{8}$. These intercepts correspond to extrapolated quantum yields of 2 and 8, respectively. As shown in Fig. 3, we obtained $\Phi_{HCl} = 1.45$ at infinite dilution of ICl in H_2. While it is quite possible that our estimate is 38% low (corresponding to $\Phi_{HCl} = 2$), it is very improbable that our result is off by 450% (if $\Phi_{HCl} = 8$). This, coupled with the good agreement of our results with those of Hofer and Wiig [based on the validity of Eq.(1)], indicate that reaction (K) is responsible for the removal of HI and that reactions (A)-(F) and (K) correctly describe the behavior of this system.

This result indicates that HI is a much better Cl atom scavenger than ICl. Although no experimental information is available for k_K, Mok and Polanyi[17] have estimated its activation energy to be 0.2 kcal. Comparing this activation energy with the value of 2.35 kcal estimated for k_D[15] and assuming that both reactions have the same pre-exponential factor, we see that $k_K/k_D \sim 38$ at 298°K. This is consistent with our mechanism.

TABLE I. Quantum yields for HCl formation, Φ_{HCl} for the photolysis of iodine monochloride in hydrogen at 298.05 °K.

Exp.	Conditions[a]	$[H_2]$ (Torr)	[ICl] (Torr)	$[H_2]/[ICl]$	Photons-absorbed (einsteins)	[HCl] (Torr)	Φ_{HCl} (uncorrected)	Φ_{HCl} (corrected)
1	B	5.894(2)	3.87	1.60(2)	--	7.87(-3)	--	--
2	B	9.691(2)	3.87	2.63(2)	--	4.76(-3)	--	--
3	B	2.228(2)	3.87	6.04(1)	--	1.10(-2)	--	--
4	P	9.711(2)	3.87	2.63(2)	5.34(-6)	7.34(-2)	0.380	0.361
5	P	7.817(1)	3.87	2.12(2)	5.60(-6)	6.83(-1)	0.338	0.306
6	P	5.953(2)	3.87	1.61(2)	6.66(-6)	6.41(-2)	0.266	0.229
7	P	4.080(2)	3.87	1.11(2)	6.05(-6)	4.78(-2)	0.218	0.165
8	P	1.060(2)	3.87	2.87(1)	5.43(-6)	1.87(-2)	0.095	0.015
9	P	2.102(2)	3.87	5.70(1)	5.14(-6)	2.92(-2)	0.157	0.080
10	P	1.349(2)	3.87	3.66(1)	5.16(-6)	1.97(-2)	0.106	0.023
11	B	1.264(2)	3.87	3.43(1)	--	1.87(-2)	--	--
12	B	9.102(2)	0.74	1.23(3)	--	5.93(-3)	--	--
13	B	1.044(3)	0.74	1.41(3)	--	3.99(-3)	--	--
14	B	4.955(2)	0.74	6.70(2)	--	7.09(-3)	--	--
15	P	6.063(2)	0.74	8.19(2)	1.18(-6)	2.84(-2)	0.664	0.494
16	P	6.748(2)	0.74	9.12(2)	1.19(-6)	4.24(-2)	0.988	0.823
17	P	1.067(3)	0.74	1.44(3)	1.10(-6)	4.08(-2)	1.031	0.905

[a] P denotes photolysis experiments and B (blank) denotes thermal experiments.

REFERENCES

1. G. K. Rollefson and F. E. Lindquist, J. Am. Chem. Soc. 52, 2793 (1930).
2. D. P. Mellor and T. Iredale, Nature 127, 93 (1931).
3. S. E. Ashler and W. West, Nature 127, 308 (1931).
4. L. J. E. Hofer and E. O. Wiig, J. Am. Chem. Soc. 67, 1441 (1945).
5. G. G. Palmer and E. O. Wiig, J. Am. Chem. Soc. 74, 2785 (1952).
6. J. D. McDonald, P. R. LeBreton, Y. T. Lee, and D. R. Herschbach, J. Chem. Phys. 56, 769 (1972).
7. S. Datta, R. W. Anderson, and R. N. Zare, J. Chem. Phys. 63, 5503 (1975).
8. Graphic symbols per American Vacuum Society Standard, J. Vac. Sci. Tech. 4, 139 (1967).
9. C. Y. Calder and W. F. Giavque, J. Phys. Chem. 69, 2443 (1965).
10. D. D. Davis, W. Braun, and A. M. Bass, Int. J. Chem. Kinetics 2, 101 (1970).
11. M. I. Christie, R. S. Roy, and B. A. Thrush, Trans. Faraday Soc. 55, 1149 (1959).
12. W. H. Rodebush and W. C. Klingelhoefer, J. Am. Chem. Soc. 55, 130 (1933).
13. P. G. Ashmore and J. Chanmugan, Trans. Faraday Soc. 49, 254 (1953).

14. M. I. Christie, R. S. Roy, and B. A. Thrush, Trans. Faraday Soc. 55, 1139 (1959).

15. W. G. Burns and F. S. Dainton, Trans. Faraday Soc. 48, 52 (1952).

16. H. B. Palmer and D. F. Hornig, J. Chem. Phys. 26, 98 (1957); D. Bunker and N. Davidson, J. Am. Chem. Soc. 80, 5085 (1958).

17. M. H. Mok and J. C. Polanyi, J. Chem. Phys. 51, 1451 (1969).

FIGURE CAPTIONS

FIG. 1. Schematic diagram of the experimental apparatus. Symbols are described in Ref. 8.

FIG. 2. Pressure of HCl as a function of H_2 pressure for blank experiments. The experiments were performed using [ICl] = 3.87 Torr at 298.05°K. The solid line is a least squares fit to the points.

FIG. 3. Reciprocal quantum yield, $(\Phi_{HCl})^{-1}$, as a function of $[ICl]/[H_2]$ at 298.05°K. The crosses are the raw quantum yields where [ICl] = 3.87 Torr; the open squares are the same results corrected using the blank experiments; the open circles are the corrected quantum yields where [ICl] = 0.74 Torr (uncorrected quantum yields at [ICl] = 0.74 Torr fall underneath the open circles). Error bars displayed reflect the uncertainty in the determination of the dark reaction rate (error bars smaller than plotting symbols are not displayed). The solid line is the weighted least squares determination of the corrected photolyses, with each point is assigned a weight inversely proportional to the magnitude of its error bars. The hatched region is the quantum yield predicted by Palmer and Wiig;[5] the dashed line is predicted using Eq.(1) and previously reported values of k_B and k_D.

FIG. 4. (a) Reciprocal quantum yields of HCl as a function of $[ICl]/[H_2]$ obtained by Palmer and Wiig[5] at 303.2°K. Open and solid circles refer to micro- and macro-runs, respectively (see Fig. 3, Ref. 5). The solid line is the best fit of the data of Palmer and Wiig. (b) Results of Palmer and Wiig at 313.2°K.

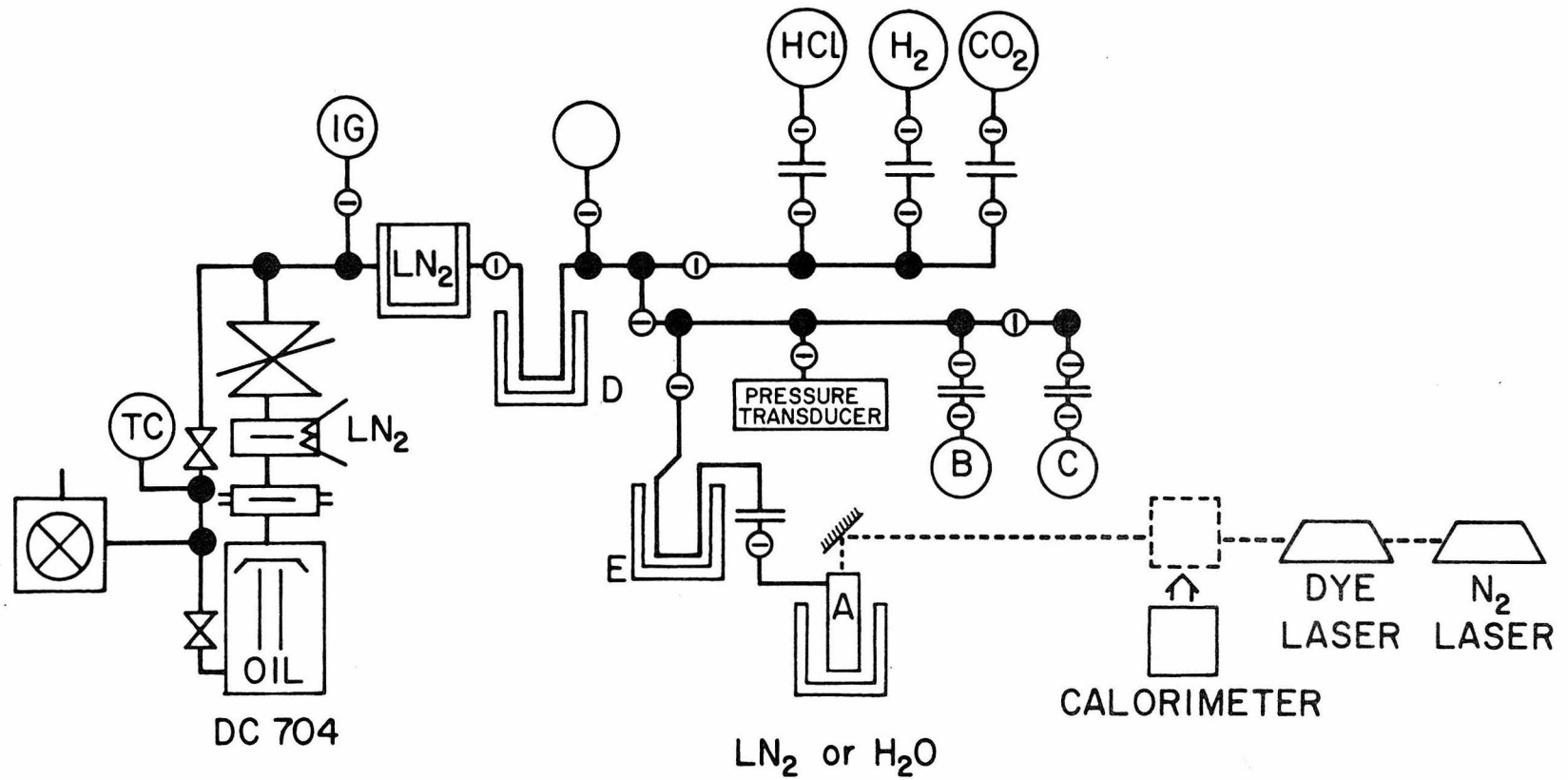
HCl
H_2
CO_2
IG
LN_2
D
TC
LN_2
PRESSURE TRANSDUCER
B
C
E
A
DYE LASER
N_2 LASER
CALORIMETER
OIL
DC 704
LN_2 or H_2O

Figure 1.

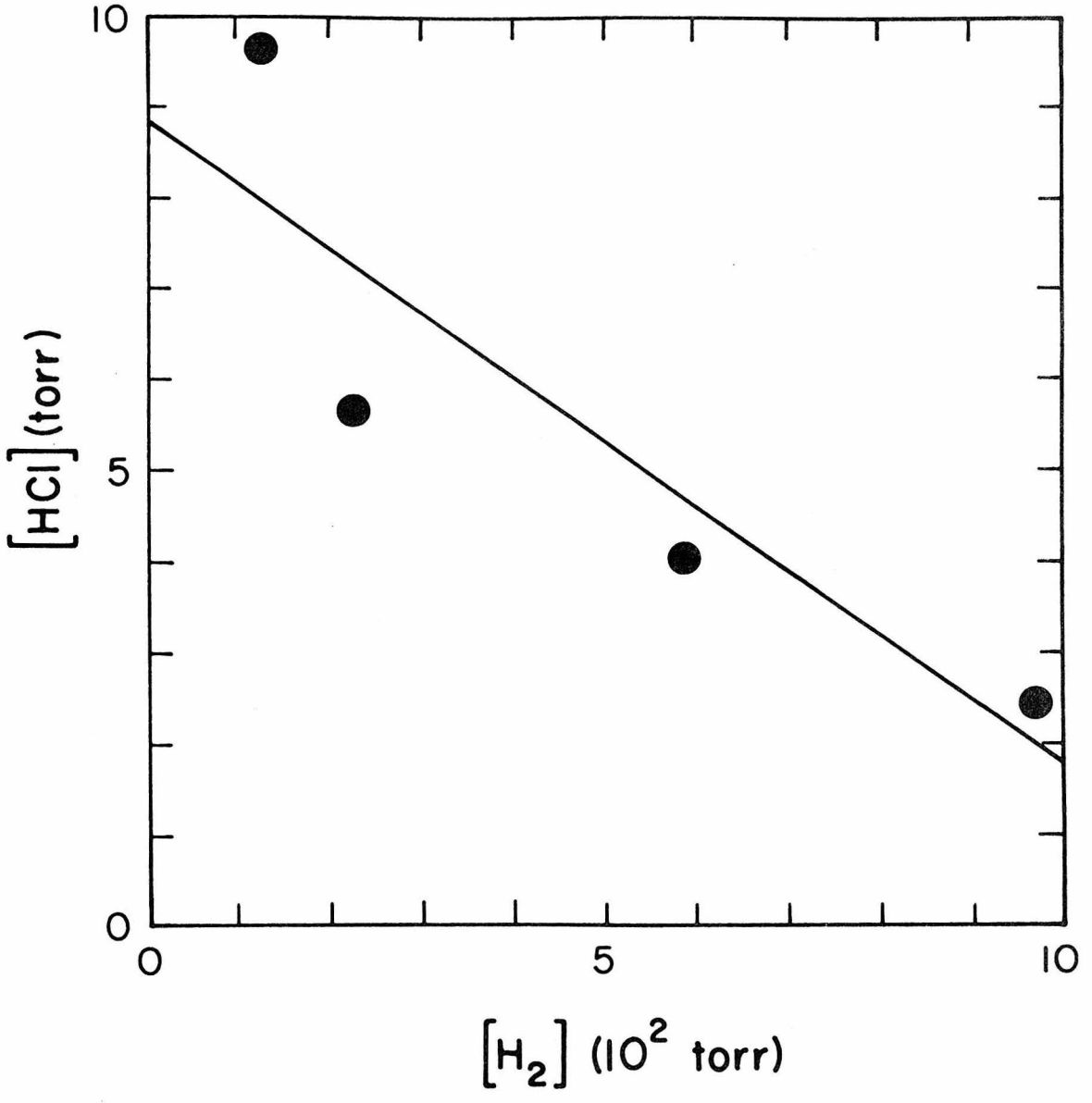

Figure 2.

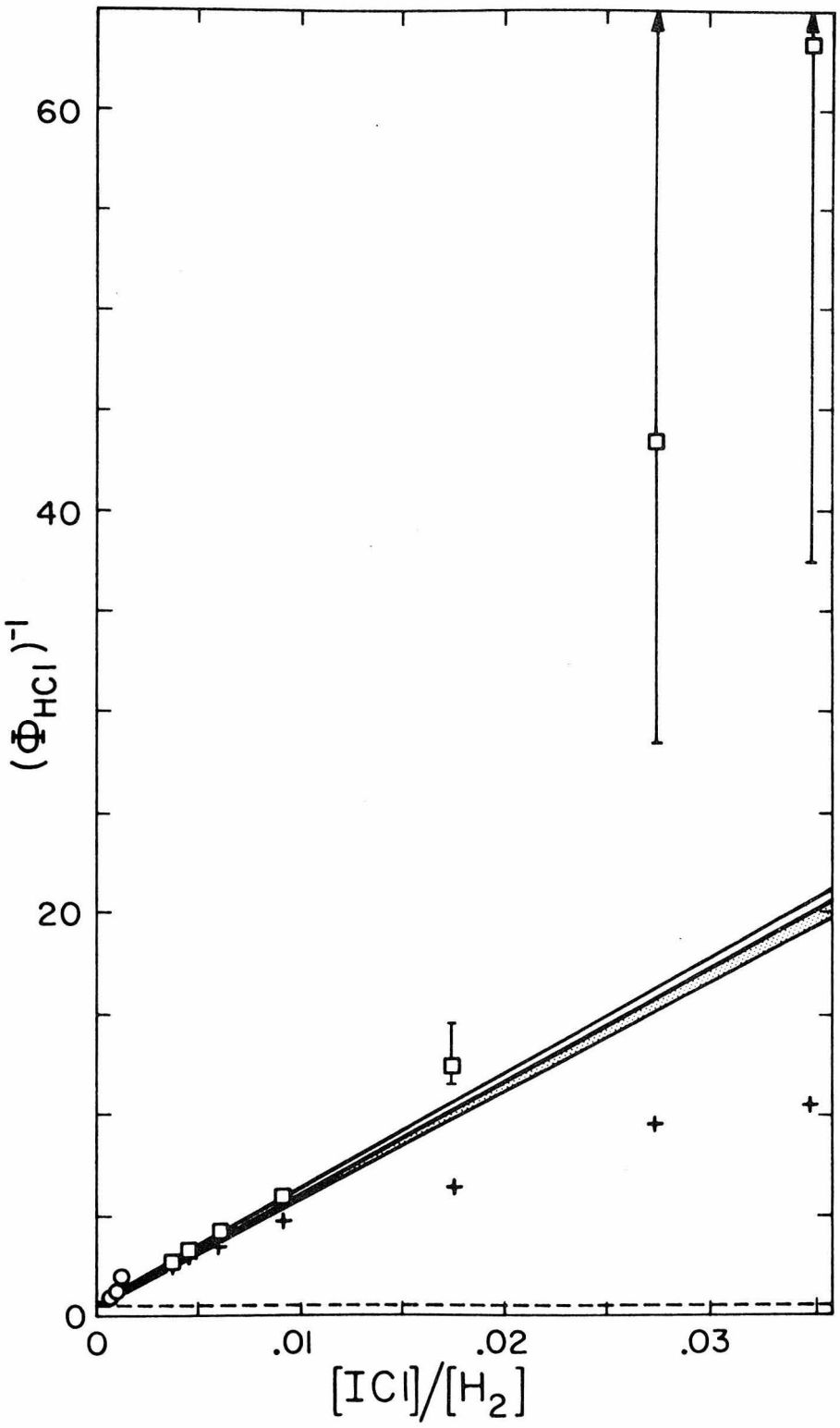

Figure 3.

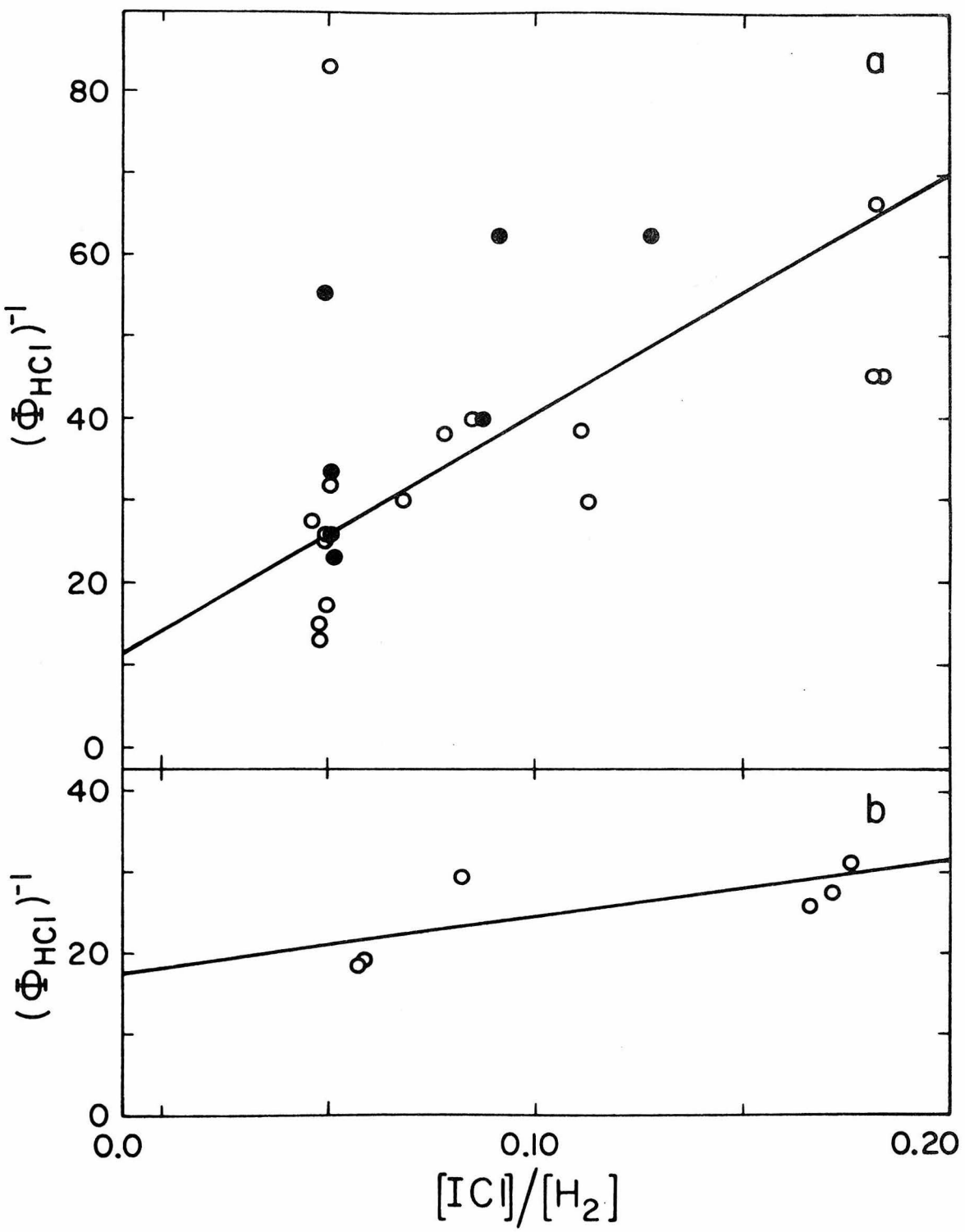

Figure 4.

Proposition I: DETECTION OF HYDROGEN HALIDE VIBRATIONAL ENERGY LEVELS USING INDUCED FLUORESCENCE

Abstract: It is proposed that the vibrational energy levels in the ground electronic state be located using laser induced vibrational fluorescence. From these levels, experimental potential-energy curves are constructed for comparison with ab initio results.

An accurate internuclear potential-energy curve for a diatomic molecule can be constructed from the experimental vibrational energy levels using the RKR method.[1] Of particular interest is the behavior of the potential-energy curve near the dissociation limit of the molecule. This region of the curve is poorly described by empirical potential energy functions such as the Morse potential.[2] In order to use the RKR method to construct this portion of the potential energy curve it is necessary to measure the high vibrational levels near the dissociation limit of the molecule. Unfortunately these energy levels are not always easy to obtain.

The vibrational energy levels of the ground state of a molecule are usually determined by absorption spectroscopy or by emission spectroscopy. While absorption spectroscopy provides a convenient measurement of the fundamental vibrational band, measurement of the vibrational overtones by absorption becomes increasingly difficult, since the band strength of these transitions falls off drastically as the change in

vibrational quantum number, Δv, increases. Absorption, therefore, is not a good means of locating the highest vibrational levels in the ground state of a molecule.[3,4] In emission spectroscopy this problem is avoided since the transition probabilities are determined by the Franck-Condon factors rather than vibrational matrix elements.[5] For any molecule having a low lying bound electronic state, emission spectra provide a convenient means of determining all the vibrational energy levels of the ground electronic state.

Unfortunately many diatomics do not have any low lying bound electronic states and therefore no discrete emission to the ground electronic state is observed. The hydrogen halides are such molecules. Except for HF, where chemiluminescence has provided the location of vibrational bands for $v \leq 9$,[6] the only measurement of the ground state vibrational levels has been made by infrared absorption. As a result, only with great difficulty have the fifth vibrational overtones of HCl, HBr and HI been determined.[7,8]

Since higher vibrational levels are of importance in the construction of the RKR potential, it is proposed that they be measured experimentally using a laser induced vibrational fluorescence technique. In this technique a tunable dye laser would be used to excite a hydrogen halide into a high vibrational state of the ground electronic state. The infrared fluorescence from this state would be measured as the frequency of the dye laser is changed. When the frequency of the dye laser is resonant with a vibrational transition, an increase in fluorescence is observed.

The advantage of detecting fluorescence rather than detecting absorption is directly related to the power of the light source used. In absorption spectroscopy, the success of an experiment is dependent upon the fraction of light absorbed. To obtain the 10 to 90 percent absorption required for the experiment, one increases the concentration and path length of the sample. Even using high pressure, multiple-pass cells[9], there are practical limits to the strength of a vibrational transition which can be measured. For the hydrogen halides this limit is reached for $\Delta v \leq 6$. In fluorescence, however, the critical quantity is not the fraction of light absorbed but number of photons emitted. The number of photons emitted is proportional to the intensity of the light source used. Therefore, the sixth order of magnitude increase in light intensity obtainable using a laser rather than a black body source is a significant advantage.

As an illustration consider the $\Delta v = 8$ band of HI. Using the transition moments calculated previously, we estimate the line strength of a rovibrational transition in this band to be $\leq 8.7 \times 10^{-7} atm^{-1} cm^{-2}$. To obtain ten percent absorption, an effective optical path (concentration x path length) of 1.2×10^{6} cm atm is needed. This requires a very large cell. However, using a commercially available dye laser[10] having an intensity of 10^{18} photons/sec and a bandwidth of .5 cm^{-1} and an optical path of 50 cm atm we would estimate that 3×10^{13} photons/sec would be absorbed. Under these conditions 10^{7} photons/sec would be emitted. This signal could easily be detected using a commercially available InAs detector.[11]

References

1. M. McClintock, W. Demtröder and R. N. Zare, J. Chem. Phys. 51 5509 (1969).
2. I. N. Levine, Molecular Spectroscopy (John Wiley and Sons, Inc., New York, New York, 1975), p. 161.
3. See papers 3 and 4 of this thesis.
4. In HCl, for example, the intensity of the second overtone of HCl is 500 times weaker than the fundamental transition. See W. S. Benedict, R. Herman, G. E. Moore and S. Silverman, J. Chem. Phys. 26 1671 (1957).
5. I. N. Levine, Ref. 2, pp. 302-303.
6. E. S. Fishburne, K. N. Rao, J. Mol. Spectrosc. 19 203 (1966).
7. Pascal Bernage, Pierre May and Rene Houdart, Compt. Rend. 278 235 (1974).
8. D. H. Rank, B. S. Rao and T. A. Wiggins, J. Mol. Spectrosc. 17 122 (1965).
9. J. U. White, J. Opt. Soc. Am. 32 285 (1942).
10. "Laser Products" Catalog, Spectra-Physics, Mountain View, Calif. 94042.
11. "Infrared Detectors" Catalog, Santa Barbara Research Center, Goleta, Calif. 93017.

Proposition II: GAS PHASE POLARIZATION MEASUREMENTS OF METALLIC ACETYLACETONATES

Abstract: It is proposed that the total polarization, P_T, of various metal acetylacetonates be measured in the gas phase in order to study the magnitude of their atomic polarization. An improved technique for the measurement of P_T using a quartz resonator is proposed which provides three orders of magnitude more sensitivity than the traditional method. This would make gas phase measurements feasible and eliminate errors in P_T due to induced polarization.

Dipole moment measurements are of considerable importance in physical chemistry. In addition to giving information about molecular structure, dipole moments can be used to test ab initio bonding calculations.

The general procedure for determining permanent moments is the heterodyne beat method.[1,2] For gases, this method is very reliable. A molecule's total molar polarization, P_T, is measured by determining its dielectric constant using a standard capacitor. P_T is the sum of the orientation polarization P_0, the atomic polarization, P_A, and the electronic polarization, P_E:

$$P_T = P_0 + P_A + P_E \quad .^3 \qquad (1)$$

The orientation polarization, P_0, is related to the dipole moment μ

through the Debye equation

$$P_0 = \frac{4\pi N\mu^2}{9kT} \qquad (2)$$

where N is Avogadro's number and k is Boltzmann's constant.[4] P_E and P_A are induced effects caused by the electric field of the capacitor. P_0 is temperature dependent, while P_E and P_A are not. Thus, determining P_T at various values of T will yield μ.

Unfortunately many molecules of interest are not gases over a wide enough temperature range to use the above procedure. The method used for gas phase determinations of μ (i.e., plotting P_T versus 1/T) cannot be used for solutions since (1) the temperature range between the melting point and boiling point of the solvent is too small to get an accurate slope determination, and (2) the solute-solvent interactions are usually temperature dependent. Several treatments, like that of Halverstadt and Kumler[5] have been developed to determine P_T of a solute in a nonpolar solvent.

In order to find P_0 in a solution, P_A and P_E must be determined by other measurements. P_0, P_A and P_E respond to changes in the applied field at different rates. It takes 10^{-6}sec for orientation polarization to follow a changing electric field, from 10^{-12} to 10^{-14}sec for atomic polarization, and 10^{-15}sec for electronic polarization. If P_T could be measured as a function of electric field frequency, then P_0 could be determined directly.

Unfortunately, it is not yet possible to perform such an experiment. The usual experimental procedure is to determine P_T (as in the

gas phase method) by measuring the dielectric constant at 1 MHz. The electronic polarization is then determined by measuring the visible refractive index, n, of the solution using

$$\varepsilon_{\nu} = n^2 \tag{3}$$

where ν is the frequency used to determine n. If P_A is small, then

$$P_T - P_E = P_0 + P_A \simeq P_0 \quad . \tag{4}$$

For small molecules the atomic polarization has been shown to be less than 5% of P_E.[7] However, when P_A is not small Eq. (4) leads to large errors in P_0. One such example is the metal acetylacetonates.

In 1938, Finn, Hampson and Sutton[8] measured the electronic and molar polarizations of various metal acetylacetonates:

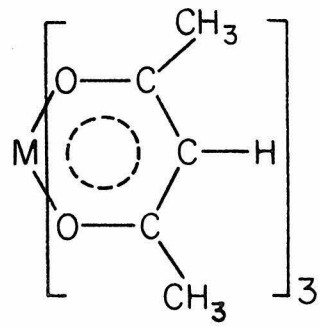

and found that $(P_T - P_E) \sim 30$ cm^3. Since the ligands are symmetrically attached to the metal atom, this result was quite puzzling.

After they ruled out several possible explanations for this phenomenon, such as incomplete chelation, specific solvent effects, or slow thermal bending of the ring, there remained two probable explanations for their results. Either the compounds had an abnormally

high values of atomic polarization or else the molecules were not completely symmetrical as previously postulated.

X-ray diffraction studies[9] of various metal acetylacetonates showed that although the ligand portion of the ring was planar, the oxygen-metal-oxygen plane was about 20° out of coplanarity with the ligand in the solid state.[10] (One exception is $Fe(AcAc)_3$ which is completely planar.)

This lack of symmetry in the solid state led Nelson and White[11] to postulate that the molecules possessed a permanent dipole moment. From vector analysis they concluded that the compounds should possess a permanent dipole moment, μ_T, where

$$\mu_T = \mu_L \sqrt{3} \sin 20° \quad . \tag{5}$$

Here μ_L is the moment of the ligand.

This postulated permanent moment caused by bending of the rings does not explain why the symmetrical $Fe(III)(AcAc)_3$ should have a dipole moment. Nor does the fact that a compound is bent in the solid state (in order to fit into a crystal lattice) mean that the compound is bent in solution.[12]

Such considerations as the above led DeCarlo and co-workers to the other conclusion--namely that the nonzero values of (P_T-P_E) were due to atomic polarization. Their temperature studies showed that (P_T-P_E) was independent of temperature, a fact not normally true for molecules with dipole moments. DeCarlo[13] and others[14] found that dielectric values determined in the microwave region showed losses that

would be predicted if the substances exhibited atomic polarization. (At this frequency one would expect that the molecule could reorient itself to the changing electric field by binding or by distorting its electron cloud. Yet the permanent dipoles could not reorient themselves by flipping over--since this is a slow process.)

This controversy could easily be resolved if it were possible to measure gas phase polarizations of these compounds. Unfortunately, the vapor pressure of these metal acetylacetonates is too small to use the heterodyne beat method. When Coop and Sutton[15] attempted to measure P_T in the gas phase, high temperatures were required to obtain sufficient vapor pressures for the measurement. At these temperatures, the metal acetylacetonates decomposed during the experiments, making the results inconclusive.

The heterodyne beat method is not sensitive enough to changes in capacitance to measure polarizations of compounds with small vapor pressures. It is therefore proposed that polarizations be measured by monitoring the frequency of a capacitor in parallel with a thermostated quartz resonator. This technique would be three orders of magnitude more sensitive to changes in capacitance than the heterodyne beat method. The quartz crystal is a very stable (high Q) resonator. It is equivalent to the LCR circuit shown below:[16]

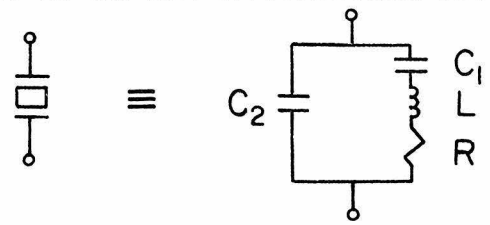

The resonance frequency, ω_0, of such a circuit is given by

$$(\omega_0 L - \frac{1}{C\omega_0})(1 + \frac{C_1}{C_2} - \omega_0^2 C_2 L) - R^2 \omega_0 C_2 = 0 \quad . \tag{6}$$

To a good approximation this circuit is a parallel LCR circuit whose resonance frequency is given by

$$\omega_0 \simeq \frac{1}{\sqrt{L\ C_2}} \tag{7}$$

If this circuit is placed in a temperature controlled environment, $\Delta\omega_0/\omega_0 \sim 10^{-11}$. [17] If an external capacitor, C_3, is placed in parallel with the quartz crystal, the resonance frequency, ω_0, changes. The new resonance frequency, ω_0, is given by Eq. (6) with the quantity (C_2+C_3) substituted for C_2. Using Eq. (7) with (C_2+C_3) substituted for C_2 we find that

$$\frac{\Delta\omega_0}{\omega_0} \simeq -\frac{1}{2}\frac{\Delta C_3}{C_3} \quad . \tag{8}$$

A change in C_3 of 2 parts in 10^{11} changes ω_0 by 1 part in 10^{11}. If this combination of quartz crystal and C_3 were used in an oscillator, the frequency change in this oscillator would be sensitive to changes in C_3 of two parts in 10^{11}. Actually it is only possible to measure a frequency to 2 parts in 10^9 using a commercially available frequency counter. [18] Thus, using this counter it should be possible to measure C_3 to 4 parts in 10^9. If C_3 is the standard capacitor used to measure P_T of an unknown substance, we have increased the detection sensitivity

by 3 orders of magnitude over the conventional heterodyne beat method (where $\Delta C/C \sim 10^{-6}$, see Ref. 2).

This increase in sensitivity in the detection of P_T (or $\Delta C/C$) means that for the metallic acetylacetonates, lower vapor pressures may be used to determine P_T. This would decrease the temperatures needed to measure P_T by about 100C, temperatures where these compounds are thermally stable, allowing one to make reliable gas phase measurements.

References

1. F. Daniels, J. Williams and D. Bender, Experimental Physical Chemistry (McGraw-Hill, New York, 1962).
2. D. Shoemaker and C. Garland, Experimental Physical Chemistry (McGraw-Hill, New York, 1967), p. 295.
3. C. P. Smyth, Dielectric Behavior and Structure (McGraw-Hill, New York, 1955).
4. H. Thompson, J. Chem. Ed. 66 (1966)
5. I. F. Halverstadt and W. D. Kumler, J. Am. Chem. Soc. 64 2988 (1942).
6. C. Smyth, op. cit., p. 53.
7. J. Van Vleck, The Theory of Electric and Magnetic Susceptibilities (Oxford, London, 1932), pp. 45-54.
8. A. Finn, G. Hampson and L. Sutton, J. Chem. Soc. (London), 1254 (1938).
9. E. C. Lengafelter, Coord. Chem. Rev. 1 151 (1966).
10. R. Nelson and C. White, J. Phys. Chem. 73 3439 (1969).
11. R. Nelson and C. White, ibid.
12. In fact, as pointed out by DeCarlo, the 20° angle reported by Lengafelter is 0° within experimental error of the measurement.
13. E. N. DeCarlo, R. E. Stronski and C. E. Varga, J. Phys. Chem. 73 3433 (1969).
14. S. Dasgupta and C. Smyth, J. Amer. Chem. Soc. 89 5532 (1967).
15. I. Cook and L. Sutton, J. Chem. Soc. (London) 1269 (1938).
16. H. V. Malmstadt, C. G. Enke and S. R. Crouch, Electronic Measurements for Scientists (W. A. Benjamin Inc., Menlo Park, Ca. 1974), p. 780.

17. "Electronic Instruments and Systems" Catalog, Hewlett-Packard, Palo Alto, Ca., p. 275.

18. Hewlett-Packard, ibid, p. 238.

Proposition III: THE PHOTOLYSIS OF IODINE MONOCHLORIDE

Abstract: It is proposed that the photolysis of ICl be reinvestigated in order to measure the rate constants for the reactions

$$Cl + ICl \rightarrow Cl_2 + I \qquad (A)$$

and

$$Cl + I_2 \rightarrow ICl + I \quad . \qquad (B)$$

Although reaction (A) was previously studied by photolysis of ICl,[1] evidence exists suggesting that the rate constant so determined is in error. Chlorine isotope separation using laser photodissociation of ICl is one practical reason for the current interest in these reactions.

Christie, Roy and Thrush[1] photolyzed iodine monochloride in order to determine the rate constant k_A for the reaction:

$$Cl + ICl \rightarrow Cl_2 + I \quad . \qquad (A)$$

They assumed that the following mechanism described the photolysis of ICl:

$$ICl + h\nu \rightarrow I + Cl \qquad (C)$$

$$Cl + ICl \rightarrow Cl_2 + I \qquad (A)$$

$$I + I + M \rightarrow I_2 + M \qquad (D)$$

$$I + Cl + M \rightarrow ICl + M \qquad (E)$$

$$Cl + Cl + M \rightarrow Cl_2 + M \quad . \qquad (F)$$

Using the steady state hypothesis for [I] and [Cl], they derived an expression for $[I_2]$. By monitoring the $[I_2]$ produced during the photolysis of ICl, Christie and co-workers determined k_A.

Unfortunately, their value of k_A is four orders of magnitude smaller than that observed by Palmer and Wiig[2] and ourselves[3] in the photolysis of codine monochloride in hydrogen. It is also several orders of magnitude smaller than the value obtained by Burns and Dainton from the photolysis of Cl_2 in CO. The value of k_A obtained by Christie, Roy and Thrush is therefore suspect. Since it is highly unlikely that their experimental technique would lead to errors of this magnitude, the likely culprit is the reaction mechanism they used.

One problem in these halogen atom-molecule reactions is that there are significant thermal reactions occurring. Christie et al. found that a dark reaction, dependent on the surface area of the vessel, occurred which consumed I_2, probably

$$Cl_2 + I_2 \rightarrow 2ICl \quad . \qquad (G)$$

Another problem in these systems is that many rate constants of possible secondary reactions have not been measured, making it difficult to estimate their importance. For example, the reaction

$$Cl + I_2 \rightarrow ICl + I \qquad (B)$$

was not included in the mechanism of Christie. The rate constant, k_B,

has never been measured, however Benson[5] speculates that it has no activation energy. If he is correct then k_B is approximately 50 times greater than k_A (at 300K) and must be included in the ICl mechanism.

The choice of which reactions to include or exclude from a mechanism, measuring the appearance of disappearance of one reaction component, then using that mechanism to determine rate constants, can lead to enormous errors if the mechanism is incorrect.

In this spirit, it is proposed that the photolysis of ICl be reinvestigated by monitoring three reaction components: I_2, Cl_2 and ICl. By monitoring three components rather than one, the stoichiometry of the proposed mechanism may be checked. If, for example, a reaction which consumed I_2 occurred that was not included in the proposed mechanism, the time dependence of $[I_2]$ would not be correct.

Using reactions A-G as an <u>ansatz</u> for the proposed mechanism of the ICl photolysis, we obtain the following behavior for the concentrations of the three reaction components in the steady state approximation.

$$[\dot{Cl}_2] = k_A[Cl]_{ss}[ICl] + k_F[Cl]_{ss}^2 - k_G[Cl_2][I_2] \qquad (1)$$

$$[\dot{ICl}] = -I_0\varepsilon\ell[ICl] - k_A[Cl]_{ss}[ICl] + k_E[I]_{ss}[Cl]_{ss}[M]$$
$$+ k_B[Cl]_{ss}[I_2] + 2k_G[Cl_2][I_2] \qquad (2)$$

$$[\dot{I}_2] = k_D[I]_{ss}^2[M] = k_G[I_2][Cl_2] \qquad (3)$$

where $[I]_{ss}$ and $[Cl]_{ss}$ are the respective steady state concentrations of iodide and chlorine atoms, I_0 is intensity of the photolysis source,

ε is the extinction-coefficient of ICl, and ℓ is the optical path length of the beam.

Equations (1), (2) and (3) may be simplified by the proper choice of experimental conditions (low pressure and low intensity) so that k_F $k_F[Cl]_{ss} \ll k_A[ICl], k_B[I_2]$. Under these conditions reaction (F) may be neglected. (This assumption must be checked after these quantities have been determined). We also suspect that $[Cl]_{ss} \ll [I]_{ss}$, since Cl is removed by reactions (A), (B), (E) and (F), while I is only removed by reactions (D) and (E). Since we expect that $k_D \sim k_E$,[1] if $[Cl]_{ss} \ll [I]_{ss}$ reaction (E) may be ignored. (This assumption must also be checked later). Neglecting reactions (E) and (F), the steady state concentrations of chlorine and iodine are:

$$[Cl]_{ss} = \frac{I_0\, \varepsilon\ell[ICl]}{k_A[ICl] + k_B[I_2]} \tag{4}$$

and

$$[I]_{ss}^2 = \frac{I_0\varepsilon\ell[ICl] + (k_A[ICl] + k_B[I_2])[Cl]_{ss}}{k_D[M]} \tag{5}$$

or

$$[I]_{ss} = \left(\frac{2I_0\varepsilon\ell[ICl]}{k_D[M]}\right)^{1/2} . \tag{6}$$

Equations (1), (2) and (3) now simplify yielding:

$$\dot{[Cl_2]} = \frac{k_A[ICl]I_0\varepsilon\ell[ICl]}{k_A[ICl] + k_B[I_2]} - k_G[Cl_2][I_2] \tag{7}$$

$$\dot{[ICl]} = -2I_0\varepsilon\ell[ICl] + 2k_G[Cl_2][I_2] \tag{8}$$

$$[I_2] = 2I_0\varepsilon\ell[ICl] - k_G[Cl_2][I_2] \quad . \tag{9}$$

If we measure $[I_2]$, $[Cl_2]$ and $[ICl]$ as functions of time, we can determine $[\dot{Cl}_2]$, $[\dot{ICl}]$ and $[\dot{I}_2]$. With these quantities and $I_0\varepsilon\ell$ we can use Eqs. (7), (8) and (9) to find k_A, k_B and k_G. Since I_0, k_E and k_F are known[6,7] the validity of the neglected reactions (E) and (F) may be determined.

In order to measure $[I_2]$, $[ICl]$ and $[Cl_2]$ continuously during the photolysis, a three-photon beam experiment is proposed. The photon beam used to measure $[ICl]$ is the same one used to photolyze the sample with $\lambda \simeq 425$ nm. A low power HeNe laser ($\lambda = 633$ nm) can be used to monitor $[I_2]$. A second low intensity light beam ($\lambda \simeq 340$ nm) can be used to measure $[Cl_2]$. One problem here is that the beam used to measure $[Cl_2]$ will dissociate the chlorine molecule. Therefore, the experiment proposed should be repeated several times as the intensity of the beam used to monitor $[Cl_2]$ is varied. The correct results are then obtained as the limit of zero intensity of this beam is taken.

References

1. M. I. Christie, R. S. Roy and B. A. Thrush, Trans. Faraday Soc. 55 1149 (1959).
2. G. G. Palmer and E. O. Wiig, J. Amer. Chem. Soc. 74, 2785 (1951).
3. R. H. Reiner and A. Kuppermann, paper 6, this thesis.
4. W. G. Burns and F. S. Dainton, Trans. Faraday Soc. 48 52 (1952).
5. S. W. Benson, F. R. Cruickshank and R. Shaw, Int. J. Chem. Kinetics 1 29 (1969)
6. K. E. Russell and J. Simons, Proc. Roy. Soc. A217 271 (1957).
7. R. L. Strong, J.C.W. Chein, P. E. Graf and J. E. Willard, J. Chem. Phys. 26 1287 (1957).

Proposition IV. ABSOLUTE ELASTIC DIFFERENTIAL ELECTRON IMPACT CROSS SECTIONS OF SINGLET AND TRIPLET METHYLENE

ABSTRACT

It is proposed that the absolute electron impact differential cross sections (DCS) of singlet and triplet methylene be obtained using an electron impact spectrometer equipped with a molecular beam sample source and an UV light source. Using the light source to photolyze ketene (CH_2CO) both CH_2 radicals and CO are produced. The absolute DCS of CH_2 may be obtained using the previously determined absolute DCS for CO, since $[CO] = [CH_2]$. The elastic DCS can then be used to obtain the absolute inelastic DCS of CH_2.

Trajmar and coworkers have obtained absolute differential cross sections (DCS) for elastic scattering for a number of stable molecules.[1,2,3] Their method involves measuring the elastic DCS for the molecule of interest relative to that of He. The absolute elastic DCS is obtained by normalizing the relative results to measured absolute elastic DCS of He.[4,5,6] From the absolute elastic DCS of a molecule, absolute inelastic cross sections may be easily obtained by measuring inelastic to elastic intensity ratios.

While this method works for stable molecules whose pressure in a gas reservoir can be measured (see Eq. (16) reference 1), it is of no

use in measuring absolute DCS of transient species whose concentrations are unknown. If a molecule is produced in an electric discharge, microwave discharge, or by photon absorption in the sample beam prior to interaction with the electron beam, it is difficult if not impossible to determine its concentration.

In order to measure the absolute elastic DCS of two such transient molecules, singlet and triplet methylene (CH_2) the following novel experiment is proposed. Using an experimental apparatus similar to that of Trajmar (see fig. 1, ref. 1), we propose photolyzing a ketene (CH_2CO) target beam prior to the interaction of the target beam with the incident electron beam. The photolysis source can be either a continuum source (argon arc lamp--suitably filtered) or a near UV laser. For a typical target beam flux, on the order of 10^{18} photons/sec are needed for a one pass absorption to produce a ten percent dissociation.[7] The ketene photodissociates to produce CO in the $^1\Pi$ state and singlet or triplet methylene (depending on the photolysis wavelength; at 270 nm one obtains only $^1CH_2$).[8] In the low pressure of the beam (10^{-4}torr) during the short flight time between the photolysis source and the electron beam (10^{-4}sec), the $^1\Pi$ state of CO would radiate to the $X^1\Sigma^+$ state (lifetime $\sim 10^{-7}$sec)[9] but the methylene would not have time to react or relax. The electron beam would be scattering off a mixture of ketene and equal quantities of CO and CH_2. Using the energy loss spectra of this mixture, the relative quantities of CO, CH_2 and CH_2CO can be determined, since energy loss spectra of pure CO [10] and pure CH_2CO [11] are known. Analysis of energy loss spectra of this mixture also yields the energy

loss spectra of methylene. The contribution of CH_2 to the elastic scattering may be determined by subtracting the contributions of CO and CH_2CO at each angle. This relative elastic DCS for CH_2 yields the absolute DCS when normalized to the absolute DCS of CO (which is obtained using Trajmar's procedure).

Photolysis at 270 nm yields exclusively singlet methylene.[8] By varying the photolysis frequency one obtains mixtures of singlet and triplet methylene. Using the above procedure, it is possible, in principle, to obtain spectra of both states of methylene. In practice this may be difficult because the background noise may be large. By using very long data acquisition period (> 24 hrs) the signal-to-noise ratio can be improved.

The absolute elastic and inelastic DCS of CH_2 are of spectroscopic interest because of the importance of this radical in atmospheric photochemistry, interstellar space and organic reactions. Once the absolute elastic DCS of CH_2 has been obtained, it should be possible to use this same procedure to obtain the DCS of other species produced by any photodissociation which also produces CH_2.

References

1. S. K. Srivastava, A. Chutjian and S. Trajmar, J. Chem. Phys. 63 2659 (1975).

2. S. K. Srivastava, A. Chutjian and S. Trajmar, J. Chem. Phys. 64 1340 (1976).

3. S. K. Srivastava, S. Trajmar, A. Chutjian and W. Williams, J. Chem. Phys. 64 2767 (1976).

4. D. Andrick and A. Bitsch, J. Phys. B 8 393 (1975).

5. R. W. Labahn and J. Callaway, Phys. Rev. A 2 366 (1970).

6. J. W. McConkey and J. A. Preston, J. Phys. B 8 63 (1975).

7. W. M. St. John III, R. C. Estler and J. P. Doering, J. Chem. Phys. 61 763 (1974).

8. G. B. Porter, J. Am. Chem. Soc. 79 827 (1957).

9. J. C. Calvert and J. N. Pitts, Photochemistry (John Wiley & Sons, London, 1966), pp. 174,222.

10. J. K. Rice, Ph.D. thesis, California Institute of Technology, 1969, p. 316.

11. R. P. Frueholz, W. M. Flicker and Aron Kuppermann, Chem. Phys. Lett. 38 57 (1976).

Proposition V. KINETIC FLOW SYSTEM ELECTRON SPIN RESONANCE MEASUREMENTS OF ATOMIC CHLORINE AND BROMINE REACTIONS IMPORTANT IN THE STRATOSPHERE

ABSTRACT

It is proposed that the rate constants for the reaction of Cl and Br with molecules present in the stratosphere be measured using an electron spin resonance (ESR) spectrometer mounted in a fast flow system. These rate constants are important for modeling of chlorine and bromine catalyzed removal of ozone from the stratosphere and therefore of significant environmental interest.

Chlorine atoms, produced by photolysis of CF_2Cl_2, CF_3Cl and $CFCl_3$ in the upper atmosphere have been of significant environmental interest recently because of the possible chain reaction which would remove ozone

$$Cl + O_3 \rightarrow ClO + O_2 \quad (1)$$

$$ClO + O \rightarrow Cl + O_2 \quad (2)$$

[1-9]

Similarly, bromine atoms, produced by the photolysis of bromofluorocarbons (used in fire extinguishers, etc.) may participate in similar ozone destroying chain reactions.

In order to effectively model chemical reactions of the upper atmosphere and to determine the seriousness of the problem of ozone depletion, rate constants for potential Cl and Br scavenger reactions

which would terminate these chains, must be measured.[10] Roland has postulated that the primary path for Cl removal is by reaction with hydrogen containing species to form HCl.[11] Similarly, we would expect that Br could be removed by these same compounds to form HBr.

The most abundant species in the stratosphere containing hydrogen are H_2O, CH_4, H_2, H_2O_2, HNO_3, HO_2 and OH. Some of these reactions such as

$$Cl(Br) + H_2 \rightarrow HCl(Br) + H \qquad (3)$$

$$Cl(Br) + CH_4 \rightarrow HCl(Br) + CH_3 \qquad (4)$$

have been measured previously by a variety of methods.[12,13] However, even in the well studied reactions, disagreement in reported rate constants by factors of three is common and by an order of magnitude is not unusual. It would therefore be of environmental interest to obtain experimental rate constants for these reactions of Cl and Br atoms using a more reliable technique.

The fast flow kinetic reactor, equipped with an ESR spectrometer, has been used by several authors to measure absolute rate constants of several reactions of the form A + BC where A is a free radical (usually an atom) and BC is a stable molecule (not necessarily a diatomic). There are two important advantages of this technique for obtaining absolute rate constants over more conventional methods such as photochemistry, flash photolysis and thermal chemistry. First, erroneous contributions to rate constants resulting from heterogeneous reactions of the free radical are easily separated.[17] Second, absolute concentrations

of the free radical can be obtained directly by interpretation of the ESR spectrum.[18,19] These two features of the ESR flow technique eliminate the primary sources of error present in previous determinations of atom-molecule reactions.

It is therefore proposed that the reactions of chlorine and bromine atoms with the various stable molecules containing hydrogen present in the upper atmosphere be measured using this technique. The theoretical expressions relating [Cl] and [Br] in the ESR cavity to the ESR spectrum have been derived previously.[20] The experimental apparatus used previously[17] is adequate to study reactions of Cl and Br with any of the stable molecules listed above (CH_4, H_2, H_2O, H_2O_2, HNO_3). By modifying the apparatus to include a second microwave discharge cavity (see Fig. 1 of Ref. 17) it should be possible to produce a second free radical and thereby allow one to measure free radial + free radial reaction rates. This may make possible the experimental measurement of reactions such as

$$Cl + HO_2 \rightarrow HCl + O_2 \qquad (5)$$

References

1. M. J. Molina and F. S. Rowland, Nature (London) 249 810 (1974).
2. M. J. Molina and F. S. Rowland, Geophys. Res. Lett. 1 309 (1974).
3. F. S. Rowland and M. J. Molina, AEC Report No. UCI-1974-1, Sept. 1974; to be published in Rev. Geophys. Space Phys.
4. R. S. Stolarski and R. J. Cicerone, Can. J. Chem. 52 1610 (1974).
5. P. Crutzen, Can. J. Chem. 52, 1569 (1974).
6. S. C. Wofsy and M. B. McElroy, Can. J. Chem. 52 1582 (1974).
7. R. J. Cicerone, R. S. Stolarski, and S. Walters, Science 185 1165 (1974).
8. P. Crutzen, Geophys. Res. Lett. 1, 205 (1974).
9. S. C. Wofsy, M. B. McElroy, and N. D. Sze, Science 187 545 (1975).
10. F. S. Roland and M. J. Molina, J. Phys. Chem. 80 2049 (1976).
11. M. J. Molina and F. S. Rowland, J. Phys. Chem. 79 667 (1975).
12. D. D. Davis, W. Braun, and A. M. Bass, Int. J. Chem. Kinetics 2 101 (1970).
13. W. H. Rodebush and W. C. Klingelhofer, J. Am. Chem. Soc. 55 130 (1933).
14. A. A. Westenberg and N. de Haas, J. Chem. Phys. 50 707 (1969).
15. J. M. Brown and B. A. Thrush, Trans. Faraday Soc. 63 630 (1967).
16. M. J. Kurylo and R. B. Timmons, J. Chem. Phys. 50 5076 (1969).
17. A. A. Westenberg and N. de Haas, J. Chem. Phys. 46 490 (1966).
18. A. A. Westenberg and N. de Haas, J. Chem. Phys. 40 3087 (1964).
19. It should be pointed out that although the free radical concentration can be determined from the ESR spectrum, the method, while

straightforward, is not trivial. Westenberg (Ref. 18) for example, has derived an expression relating the number of atoms in the ESR cavity, N_A, with area under the ESR spectrum. See Eq. (11) of Ref. 18.

20. A. A. Westenberg, J. Chem. Phys. 43 1544 (1965).